Faculdade de Engenharia da Universidade do Porto

Departamento de Engenharia Mecânica

Design of a rear axle transmission test rig

Filipa Coelho Brandão Pinto em11119@fe.up.pt

Master's Degree Dissertation presented to

Faculdade de Engenharia da Universidade do Porto

Supervisors

Dr. Fernando Gomes de Almeida
Associate Professor of FEUP

Dr. Jorge Humberto O. Seabra
Full Professor of FEUP

Porto, 2016

LaTeX
FEUP-U.PORTO
Filipa Coelho Brandão Pinto
2016

Acknowledgments

Foremost, I would like to express my sincere gratitude to my supervisors Prof. Gomes de Almeida and Prof. Seabra for giving me their continuous support, patience, motivation, enthusiasm and immense knowledge helped me in all the time of research and writing of this thesis.

I would like to thank my parents: Regina and Jorge for giving me the opportunity to study and for supporting me in all my pursuits throughout my life. I appreciate all of their continuous support and advices throughout my academic and personal journey.

I would like to thank André Guimarães for giving me his patience, support and knowledge in most of my graduating time.

My time at FEUP was made enjoyable in large part due to the many friends that became a part of my life. I am grateful for the time spent on extracurricular activities like sports and parties as well as leisure time.

Abstract

Vehicle fuel economy relies on different variables like mechanical transmissions. The rear axle is one of the main sources of power loss in the transmission, and hence represents an area where improvements can have a significant impact on the overall vehicle fuel economy. Improvements at the component level include applying higher efficiency lubricants.

In this purpose, CETRIB (Unidade de tribologia, vibrações e manutenção industrial) has interest in manufacture a test bench to evaluate these losses with different types of lubricants with different torques and temperature conditions.

This study describes the mechanical and automation designs of a rear axle transmission test rig.

Objectively, this test rig measures the torque applied at the differential propeller shaft and the torque at the drive shafts. With this values, it is possible to calculate the torque losses during the transmission.

A BMW 318d Saloon was used as a reference to this research because it represents the rear-axle transmissions niche market, diesel engines are an increasingly popular choice amongst european consumers and its engine power is within the average of 2015 passenger cars registrations. Its powertrain was characterized and the power and torque requirements of the test bench were consequently mapped.

Two types of drive systems were discussed: hydraulic drive system and electrical drive system. Considering this application, the electrical drive system was considered the most appropriated due to its efficiency compared to the hydraulic systems for the same power ranges.

Some components were selected, particularly: synchronous motors, drives, line module, torque transducers and couplings while others were designed during this work.

A mechanical structure was also designed.

Finally, apart from the selection of a power architecture and the correspondent choice of the necessary components for its implementation, an automation system architecture was designed based on LabView using a Profinet network to integrate all the components like a PLC and analog data acquisition modules.

Resumo

A economia de combustível de um veículo depende de diversas variáveis tais como transmissões mecânicas.

O diferencial é uma das maiores fontes de perda de potência na cadeia de transmissão existente num veículo e, portanto, representa uma área onde possíveis desenvimentos podem causar impactos positivos para a economia de combustível e consequente menor emissão de CO_2 para a atmosfera.

Com este propósito, o CETRIB (Unidade de tribologia, vibrações e manutenção industrial) tem interesse em construir uma banca de ensaios onde consiga medir estas perdas de potência nos diferenciais utilizando diferentes tipos de óleos lubrificantes, sujeitando o diferencial a diferentes cargas e temperaturas de funcionamento.

Este estudo descreve a conceção mecânica e de automação de uma banca de ensaios para diferenciais traseiros.

Objectivamente, esta banca mede o binário aplicado no veio de accionamento do diferencial e o correspondente binário transmitido aos semi-eixos. Com estes valores torna-se possível calcular as perdas de potência que ocorreram na transmissão diferencial.

A berlina BMW 318d foi utilizada como referência deste estudo dado que a BMW é uma marca que apenas fabrica carros com tração traseira, o gasóleo é o combustível em voga na EU e potência do automóvel encontra-se dentro da média da potência dos automóveis na EU em 2015. Todo o seu *powertrain* foi caracterizado e dessa forma foi possível mapear os requisitos de binário e potência de accionamento do diferencial para executar os testes de laboratório.

Foram discutidos dois tipos de sistemas de accionamento: hidráulico e eléctrico, sendo que o eléctrico foi considerado o mais apropriado para esta aplicação devido à sua melhor eficiência face ao accionamento hidráulico para a mesma gama de potência.

Foram selecionados componentes para possibilitar a medição da perda de potência. A destacar: motores síncronos, amplificadores de potência para os respectivos motores, fonte de alimentação, transdutores de binário e acoplamentos. Foram também modelados outros componentes, como patas para fixação dos motores, acoplamentos, entre outros.

Foi efectuado o projecto da estrutura mecânica que visa acoplar todos os componentes seleccionados.

Finalmente, para além da concepção da arquitectura de potência e escolha dos componentes necessários à sua implementação, foi também concebida a arquitetura do sistema de automação, baseada em LabView, utilizando uma rede Profinet para integrar os diferentes componentes como um PLC e módulos de aquisição de dados analógicos.

Contents

List of Figures

List of Tables

Nomenclature

Symbol	Description
F_x	Tractive effort
R_a	Aerodynamic resistance
R_g	Gradient resistance
R_r	Rolling resistance
M	Vehicle's mass
C_d	Drag coefficient
A_f	Projected area of vehicle in the direction of the travel
ρ	Volumetric mass density of air
v	Vehicle speed
C_r	Rolling resistance coefficient
p_t	Tyre pressure
r_{min}	Minimum turning radius
t	Distance between two rear wheels
i	Final drive ratio
v_{out}	Outer wheel speed
v_{in}	Inner wheel speed
D_{out}	Outer diameter of the tyre
T_1	Propeller shaft torque
T_2, T_3	Torque at each drive shaft
n_2,n_3	Angular speed of each drive shaft

n_1	Angular speed of propeller shaft
P_{M1}	Propeller shaft power
P_{M2}, P_{M3}	Drive shaft power
P_{loss}	Power loss in the differential transmission
P_{in}	Measured power applied into the differential
P_{out}	Output measured power of the differential
M_1	Machine that plays the role of of gearbox
M_2, M_3	Machines that play the role of wheels
q_v	Hydraulic secondary unit flow
$P_{q_{max}}$	Hydraulic drive power with maximum flow
p	Operating pressure of hydraulic secondary unit
η_t	Total efficiency of an A4VSO variable pump
P_{supp}	Power supplied
η_2	Efficiency of converting electrical energy into mechanical energy
η_3	Line module efficiency
η_4	Drive+ electric motor efficiency
$J_{1_{eq}}$, $J_{2_{eq}}$, $J_{3_{eq}}$	Mass moment of inertia felt by machines M1, M2 and M3 respectively
M_t	Twisting moment
G	Shear modulus
θ	Angle of twist
K	Fraction of the polar moment of inertia

Chapter 1

Introduction

1.1 Facts about automobile industry

Europe is one of the largest producers and sellers of passenger cars.

More than 70% of journeys are made by car resulting in automobile being the largest source of mobility in Europe [1].

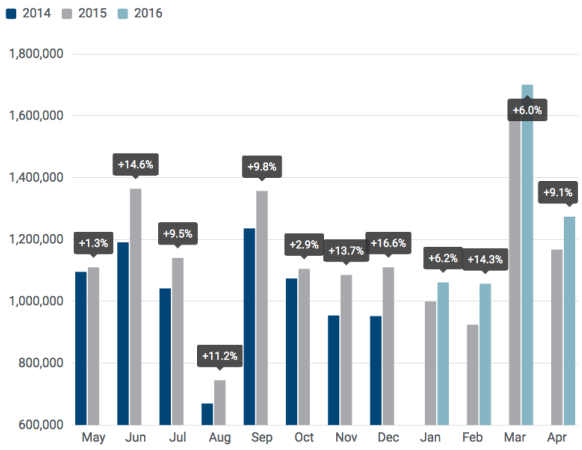

Figure 1.1: New passenger car registrations in the EU

Registrations during April 2016 grew by 9.1% compared to April 2015, see figure 1.1. This is the highest result in volume terms since April 2008, just before the economic crisis hit the automotive industry. From January to April 2016, new passenger car registrations increased by 8.5%, totaling more than 5 million units.

As shown in figure 1.2, most cars on EU roads have an internal combustion engine. So, power losses in rear-wheel-drive configurations keeps to be a focus in current researches because this configuration gives worse efficiency due to mechanical losses in the transmission [2].

In spite of most of passengers cars in Western Europe having a petrol engine, figure 1.3 discloses that Diesel engines are an increasingly popular choice amongst

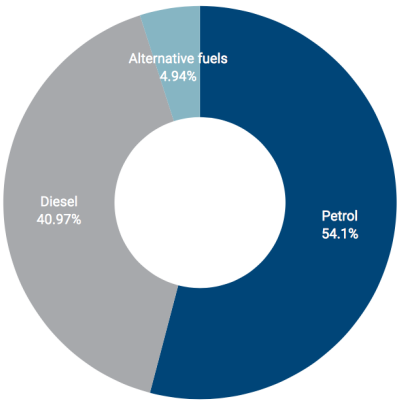

Figure 1.2: Passenger car fleet by fuel type

consumers with over half now opting for this type of powertrain.

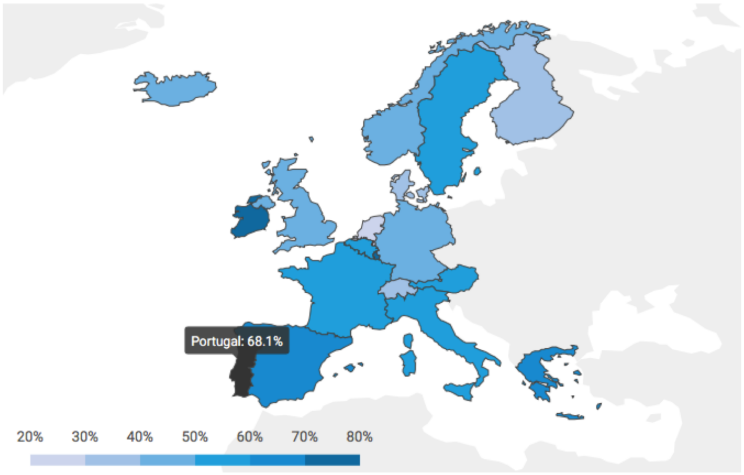

Figure 1.3: Share of Diesel in New Passenger Cars in 2015

Figure 1.4 shows that European cars have become progressively more powerful over the last twenty years [3].

The most relevant passengers cars brands of European market that produce rear axle transmission cars are BMW and Mercedes-Benz [4, 5].

However, the class A, B and CLA marketed by Mercedes-Benz have front-wheel-drive configurations while BMW only have rear-wheel-drive configurations in all commercialized models.

Considering that the main goal of this study is the project and automation design of a rear differential test rig, the BMW 318d Saloon is used as a reference to this

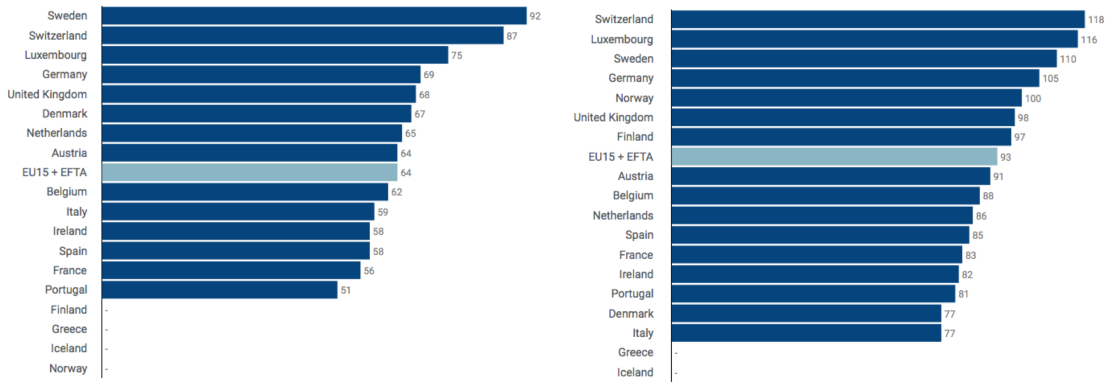

(a) 1995 (b) 2015

Figure 1.4: New passenger car registrations by engine power

research. It can represents this niche market (rear-axle transmission): it has a maximum engine output power of a $105kW$ which value is closed to the power engine average of the Western European passengers cars, and it has a Diesel engine which represents the European market trend [6].

1.2 CO_2 emissions from new passenger cars in the EU

The growing need for improved fuel economy is also a global issue due to the relationship between reduced fuel consumption and reduced CO_2 emissions [7].

Presently, vehicles with internal combustion engines are by far the most popular choice of powertrain. However, concern for the environment has led to policy targets on carbon emissions both globally and at EU level, and the EU is committed to a 20% reduction in CO_2 emission levels by 2020 compared to the level in 1990 [8].

In transport section, this is being achieved by encouraging greater emphasis on increasing the efficiency of existing means, like the differential. The higher the processes inefficiencies, the higher will be the CO_2 emissions.

Climate change is a global challenge which demands collective action and international cooperation. The automotive sector is playing a leading role, embracing its responsibility to reduce CO_2 emissions from vehicles and production, this sector faces continuously tightening legislation to improve fuel efficiency and reduce emissions [8, 7].

Laboratory tests ensure that cars comply with EU limits for both CO_2 and pollutant emissions, before they are put on the market. This lab tests are called driving cycles. The main objective to create this kind of tests was to estimate emissions of air pollutants from road vehicles and reduce them. All conditions for vehicle set-up,

testing and the handling of test results for cars are defined by EU law. By this way, a standard regulation has to be respected by all car manufactures and other players. Additionally, it allows for a repeatable procedure which enables customers to compare emissions between different car models.

As there is no 'one' real-world fuel consumption value, only figures measured in lab tests using standardized cycles allow customers to make comparisons between vehicles in terms of their CO_2 emissions and fuel consumption [9].

1.3 Driving cycles

A driving cycle is a fixed "vehicle speed profile" which allows an emission test to be conducted under specific conditions. Driving cycles are usually defined in terms of vehicle speed and time [10].

As in European Union, in America and Japan, emission tests are required by law. Light-duty vehicles are tested using a power-absorbing chassis dynamometer. In these tests, a trained driver has to follow the driving cycle on the chassis dynamometer, and a 'driver's aid' is provided to ensure that the driven cycle is as close as possible to the defined cycle.

Depending on the speed profile and load, cycles can be divided in two groups:

- "steady-state" cycles:
- "transient" cycles.

The "steady-state" cycles have a sequence of a constant speed and torque. In transient cycles, the vehicle speed and engine load are continuously changing [10].

1.3.1 New European Driving Cycle

In the European Union, the NEDC (New European Driving Cycle) is the most popular and is used today to measure car emissions driving cycle. It is a "transient" cycle which includes two sub-cycles: an urban, ECE, repeated four times; and one extra-urban sub-cycle, EUDC, presented in figure 1.5.

The main characteristics of this cycle are:

- Total distance: 11 016.13 m;
- Driving time: 1180 s;
- Maximum speed: 120.09 km/h;
- Avarage speed: 42.34 km/h.

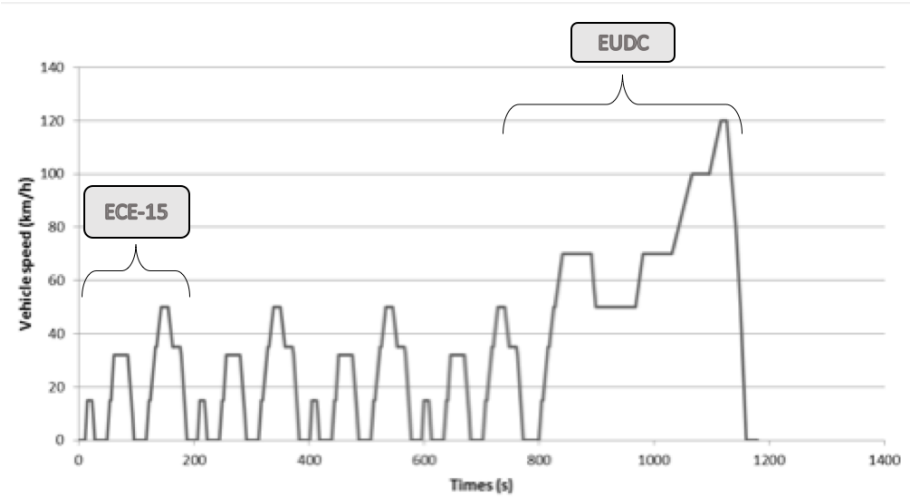

Figure 1.5: New European Driving Cycle

This driving cycle has periods of constant speed and acceleration which bears little relation to real driving profiles on the road.

With this kind of variations in speed, the engine has a better performance and in consequence, emits less polluting gases than a real-world cycles, that are generally much more transient than stylized cycles such as the NEDC.

The NEDC was developed to represent the typical usage of car in Europe. However, nowadays the industry recognizes and has stated consistently that the current NEDC test cycle is outdated. As it was designed in the 1980's and deployed from the 1990's, NEDC does not account for many new technologies in today's cars that have a strong effect on fuel consumption [9].

1.3.2 Worldwide Harmonized Light Vehicles Test Procedure

Because of the shortcomings of the current car emissions test, the automotive industry is actively contributing to the development of the new global test cycle, called the Worldwide Harmonized Light Vehicle Test Procedure (WLTP) [9].

This new test cycle will include higher speeds, more dynamic and representative accelerations and decelerations, and stricter vehicle set-up and measurement conditions than the NEDC like tyre pressure, gear shift strategy for manual transmission vehicles, warm-up, etc. As all these elements will make the WLTP test more accurate than the current lab test, it will provide a better reflection of today's drive situation [11].

The Worldwide Harmonized Light-duty Test Cycle is presented on figure 1.6.

Table 1.1 quantifies the main descriptive parameters of NEDC and WLTC driving cycles.

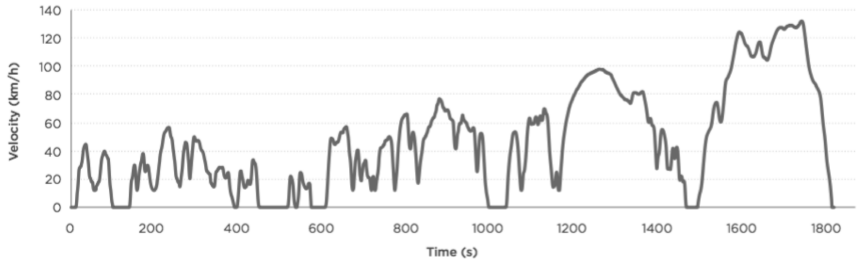

Figure 1.6: Worldwide Harmonized Light-duty Test Cycle

Table 1.1: Descriptive parameters of the driving cycles NEDC and WLTC

	Units	NEDC	WLTC
Duration	s	1180	1800
Distance	km	11.03	23.27
Average velocity	km/h	33.6	46.5
Max. velocity	km/h	120	131.3
Durations			
Constant driving	s	476	66
Acceleration	s	247	789
Deceleration	s	178	719
Shares			
Constant driving		40.3%	3.7%
Acceleration		20.9%	43.8%
Deceleration		15.1%	39.9%

1.3.3 Common Artemis Driving Cycles

The Common Artemis Driving Cycles (CADC) are chassis dynamometer procedures developed within the European Artemis (Assessment and Reliability of Transport Emission Models and Inventory Systems) project, based on statistical analysis of a large database of European real world driving patterns [12].

These cycles include not only urban and rural driving conditions but also motorway. The motorway cycle has two variants with maximum speeds of 130 and 150 km/h.

This cycle is defined by several parameters: speed average, stop frequency, driving time duration among others as presented in figure 1.7.

The main descriptive parameters of Artemis driving cycle are:

- Total distance: 50 886.36 m;
- Driving time: 3143 s;

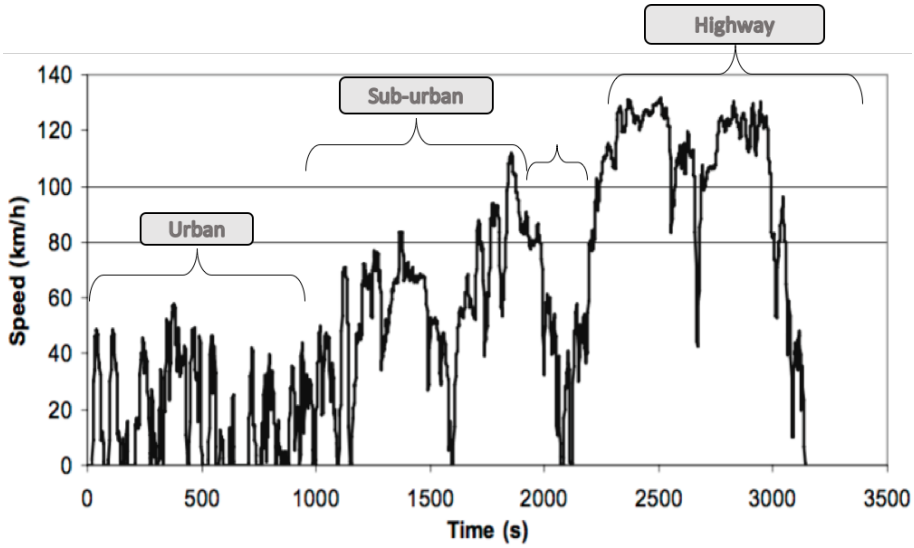

Figure 1.7: Artemis URM130

- Number of stops: 20;
- Maximum speed: 130 km/h-150km/h;
- Average speed: 58.3 km/h.

This Artemis cycle, as WLTC, has got a more realistic drive profile and because of that is another start-point for this study.

1.4 Tractive effort

The tractive effort, F_x is the force required to move forward a vehicle.

The tractive resistance is defined by the opposing force that the tractive effort must overcome to create movement. The tractive resistance is composed by two categories: the steady-state resistance and the dynamic resistance. The steady-state resistance occurs when the vehicle is moving through at constant velocity. It can be divided in three resistances:

- Aerodynamic resistance, R_a: Depends on the size and shape of the vehicle and increases with the square of air velocity;
- Gradient resistance, R_g: Depends on the slope of the road and the weight of the vehicle;

- Rolling resistance, R_r: Depends on type of road pavement, vehicle's weight, tyres and vehicle speed.

The dynamic resistance occurs in addition to the steady-state resistance when the vehicle is accelerating or braking and is caused by the vehicle's inertia [13].

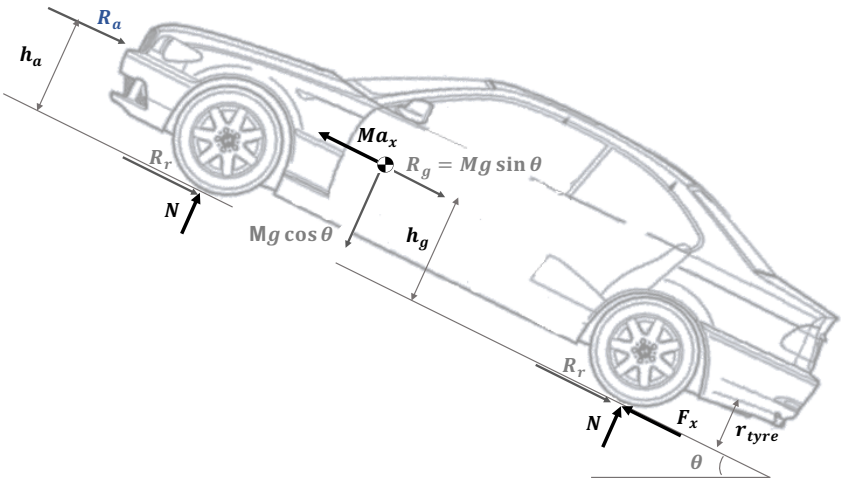

Figure 1.8: Forces acting on a vehicle when in movement

Figure 1.8 presents a vehicle's free body diagram, where the forces described above are presented in their point of application.

Assuming the vehicle's moves along the xx direction, the Newton's second law establishes that,

$$\sum F_x = Ma_x \tag{1.1}$$

$$F_x = R_a + R_g + R_r + Ma_x \tag{1.2}$$

The equation (1.2) defines the tractive effort, F_x, where M is the vehicle's mass.

1.4.1 Aerodynamic resistance

Under moderate to higher speeds, the aerodynamic resistance has a preponderant effect on the vehicle's power requirements as this force increases with the square of the speed [14].

Usually it is expressed as,

$$R_a = \frac{1}{2} C_d A_f \rho v^2 \tag{1.3}$$

where,

- C_d is the drag coefficient;
- A_f is the projected area of the vehicle in the direction of travel;
- ρ is the volumetric mass density of the air;
- v is the vehicle speed relative to the wind.

1.4.2 Gradient resistance

The gradient resistance is the force that relates to the pavement road slope and the weight of the car. This force is applied in the center of gravity of the vehicle [15].

It is defined as,

$$R_g = Mg\sin\theta \tag{1.4}$$

1.4.3 Rolling resistance

The rolling resistance of tires is mainly consequence of the tyre deformation when rolling. It also arises from friction between the tyre and road, the resistance due to air circulating inside and outside the tyre [14].

This force is defined as [16],

$$R_r = C_r Mg\cos\theta \tag{1.5}$$

where the rolling resistance coefficient of a pneumatic tire C_r, in a dry surface is calculated as [16],

$$C_r = 0.005 + \frac{1}{p_t}(0.01 + 0.0095\Big(\frac{v}{100}\Big)^2) \tag{1.6}$$

where p_t is the tyre pressure in $[bar]$, and v is the vehicle speed in $[km/h]$.

1.5 Research scope

Vehicle fuel economy relies on many different variables, such as vehicle's weight, aerodynamics, engine, driveline, rolling resistance, transmissions and accessory load.

As shown in figure 1.9, an internal combustion engine loses energy through process inefficiencies, thermal loses, and friction loses. A vehicle's drivetrain loses energy mainly by friction in the gears and bearings. Only about $13 - 25\%$ of the fuel

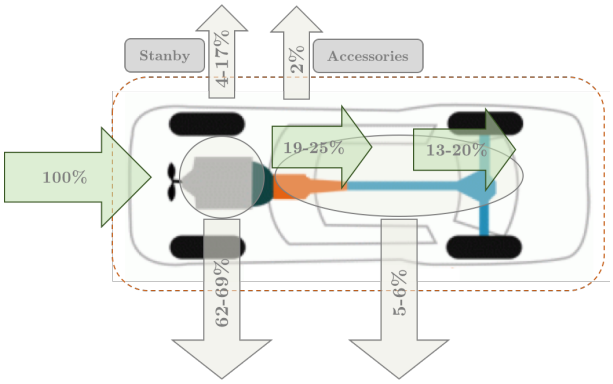

Figure 1.9: Energy flows for a late-model mid-size passenger car

chemical energy is actually used to move the vehicle at a required speed together with running useful ancillary equipment, like the air conditioning [16].

For both urban and highway driving, the mechanical energy that does make its way through the driveline to turn the wheels is consumed by three greatnesses: aerodynamic drag, rolling resistance, and braking. Braking consumes momentum from the vehicle, which must be replenished by acceleration [16].

Braking is a major consumer of mechanical energy during urban driving. In contrast, aerodynamic drag consumes relatively more energy during highway driving since this resistive force rises with vehicle speed.

Improvements at the component level include the use of higher efficiency lubricants. Historically, reducing oil viscosity has resulted in improved fuel economy. However, lower viscosities can lead to reduced lubricants films, which may fail to hold up under higher temperatures and heavy loading associated with axle operations [16].

The rear axle is one of the main sources of power loss in the transmission, and hence represents an area where lubricant improvements can have a significant impact on the overall vehicle fuel economy. The fluid development challenge is to bridge the gap between fuel economy and operating temperature control [7].

1.6 Axle efficiency test rigs

After a research of the state of the art, namely, in SAE (Society of Automotive Engineers) technical papers, it was possible to verify some topologies of the axle efficiency test rigs utilized in several studies.

In 1980 a test stand was developed in order to evaluate the axle efficiency. Figure 1.10 shows a layout diagram of the equipment utilized in a axle box test bench. In there, an automotive engine, equipped with a three mode proportional electronic

speed control governor, is used as the main power source. The power from the engine is transferred to the rear axle pinion through a four-speed manual transmission and a driveshaft equipped with a rotary transformer, strain gage type, torque sensor.

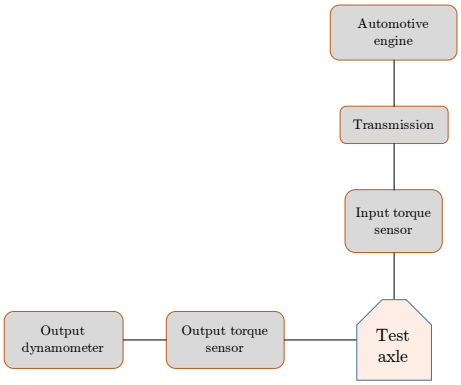

Figure 1.10: Axle box test bench diagram - differential gears locked

The test axle's differential gears are locked in order to allow all power to be transferred through one axle shaft.

A second torque sensor is mounted on this shaft which is coupled to a dynamometer equipped with an automatic load controller [17].

Figure 1.11 presents an outline of an axle efficiency test rig, were the axle is equipped with a thermocouple mounted into the housing. The test rig is also equipped with torques transducers that are capable of providing accurately measures, as well as load cells which measure the force applied into the driveshafts by the dynamometer [18].

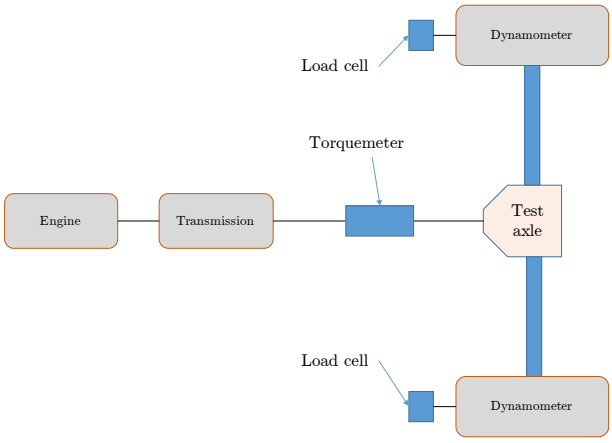

Figure 1.11: Axle box test bench diagram - differential gears unlocked

1.7 Thesis outline

Chapter 1: *Introduction* has presented a brief introduction about automobile industry and its impact in CO_2 emissions. To measure these emissions, the laboratory tests were also presented. It is also presented the state of the art of rear axle transmissions test benches.

Chapter 2: *Powertrain characterization* according to the automobile industry study made in previous chapter, an BMW 318d was taken as an input data of the present study and its powertrain was characterized. The power and torque requirements are defined on the basis of the laboratory test as well as speed, torque and temperature data accuracy according to CETRIB specifications.

Chapter 3: *Power architecture* A numerical comparison between the electrical power input when using test bench with breaking architecture or a drive system with energy recovery test bench is made. Also two solutions of drive systems with energy recovery: electrical drive systems and hydraulic secondary control drive systems are discussed. The power flow between several conditions of rear axle transmissions (acceleration, deceleration and curve) is defined.

Chapter 4: *Components selection* In order to accomplish the accuracy requirements imposed by CETRIB and the power and torque needful for executing the tests, in this chapter all the components needed to achieve the main goal are selected: electric motors (motor modules, line module and control unit), torque transducers, couplings, a PLC and analog modules for doing the data acquisition.

Chapter 5: *Mechanical design* Is presented an overview of the final mechanical solution design for integrate the components selected in previous chapter. Its assembly is described as well as the development of some parts designed. The mechanical solution is validated taking into account the main efforts applied into it.

Chapter 6: *Automation project design* Two types of control architecture are discussed, both based on LabView software.

Chapter 7: *Conclusion and future works* presents the conclusions of this thesis as well as purposes future works.

Chapter 2

Powertrain characterization

As said before, the BMW 318d Saloon is used as a reference for this project.

In this section the engine and the driveline (gearbox and differential) will be characterized to predict power and torque requirements at the wheels.

2.1 Types of power transmission systems

The power transmission system or powertrain may have three different configurations: front-wheel drive, rear-wheel drive or four-wheel drive, figure 2.1 [19, 20].

As shown in figure 2.2 the vehicle is composed by: the engine, the clutch, the gearbox, the propeller shaft, the universal joints, the differential, the drive shafts and the tyres.

The major advantage of four-wheel to rear-wheel drive is that it spreads the road loads of the vehicle across all four tyres. In a rear-wheel drive vehicle, the rear wheels do the driving while the front wheels are used for the steering duties [21]. The BMW 318d Saloon is equipped with a rear-wheel-drive power transmission configuration [6].

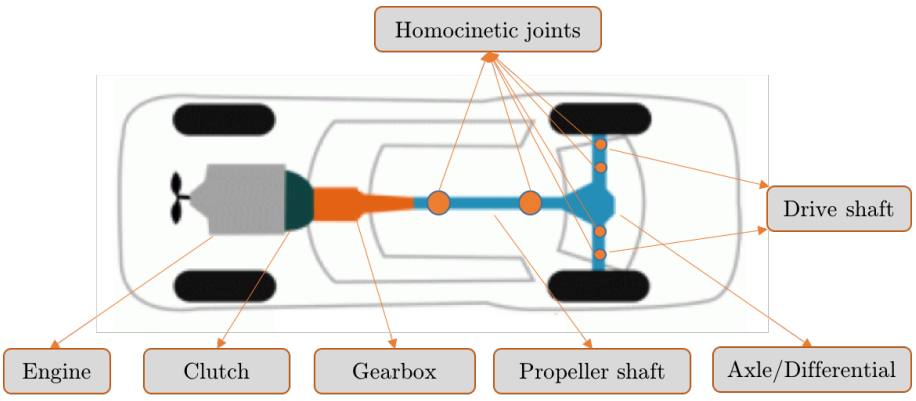

Figure 2.2: A possible vehicle powertrain components of a rear-wheel-drive configuration

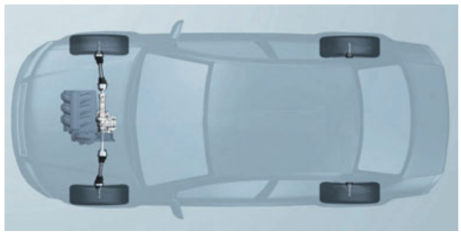

(a) Front-wheel-drive configuration

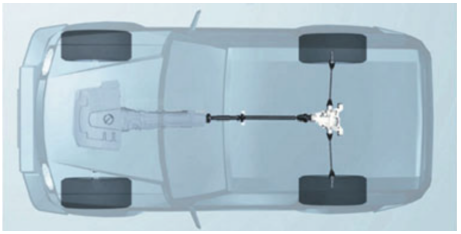

(b) Rear-wheel-drive configuration

(c) Four-wheel-drive configuration

Figure 2.1: Main types of power transmission systems

2.2 Engine

Torque and power are different measurements of the engine performance, with torque referring to the engine's ability to create turning power and power being the ability of the engine to do work over a period of time [21].

The Diesel engine of the vehicle considered in this work has 2.0 liter capacity and 4 cylinders [6].

The engine torque over the engine's speed range, as presented in figure 2.3, is variable. It delivers a maximum torque of 320 Nm between 1750 up to 2550 rpm [6].

The power delivered by the engine can be calculated in the basis of the indicated power or brake power. The indicated power is the power actually produced in the cylinder. The brake power is the power measured at the crankshaft.

The curve commonly starts to increase with the crankshaft speed and about the seven-eighths of the speed range reaches the maximum power value, and starts to

decrease, as shown in figure 2.3. The decline in power at the upper speed range is mainly due to the short time available for inducing fresh charge into the cylinders at very high speeds.

The engine torque and power are detailed in table 2.1 [6].

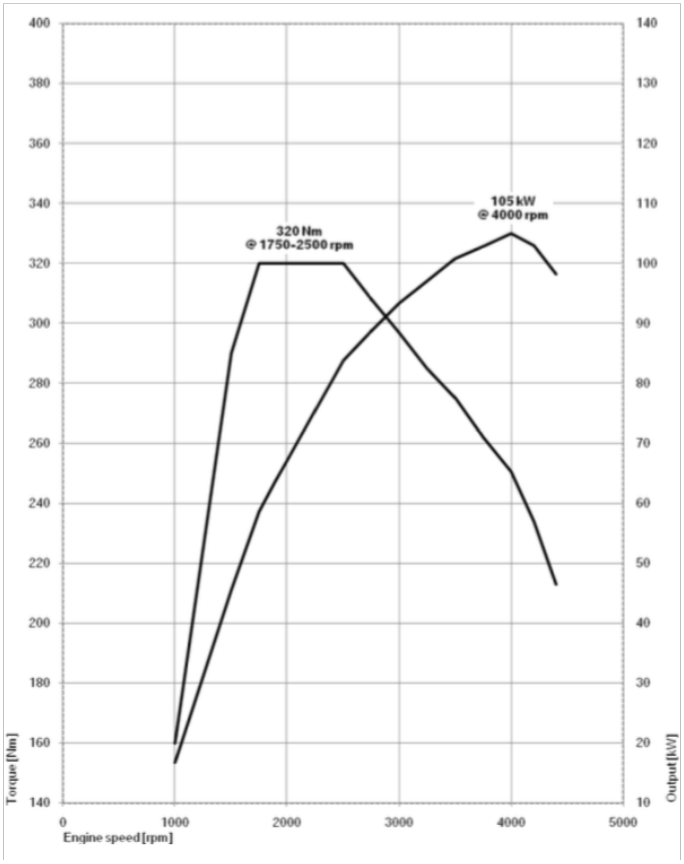

Figure 2.3: Torque and power characteristic curves of BMW 18d

Table 2.1: BMW 318d engine characteristics

Engine		
Cylinders/valves	-/-	4/4
Capacity	cm^3	1995
Stroke/bore	mm/mm	90/84
Max output power	kW	105
Max torque	Nm/rpm	320 1750-2500
Compression ratio	: 1	16.5

2.3 Driveline

The driveline is composed by the gearbox, the propeller shaft and joints, the differential and joints, the drive axes and the tyres. They take the engine power and deliver it to the wheels [21].

2.3.1 Gearbox

The internal combustion engine has many advantages: like high power to weight ratio, reasonable good efficiency and energy storage. However, this kind of engine has also some disadvantages:

- no torque generation at zero speed;
- maximum power only on a small speed range at a certain speed also, figure 2.3;
- fuel consumption is dependent on operating conditions (torque, speed and temperature) on the working point of the engine.

At the maximum engine power and vehicle road speed, the *ideal traction hyperbola*, $F_{Z,Aid}$ and the effective traction hyperbola, $F_{Z,Aid}$ can be calculated as:

$$F_{Z,Aid} = \frac{P_{max}}{v}$$

$$F_{Z,Ae} = \frac{P_{max}}{v}\eta_{tot}$$

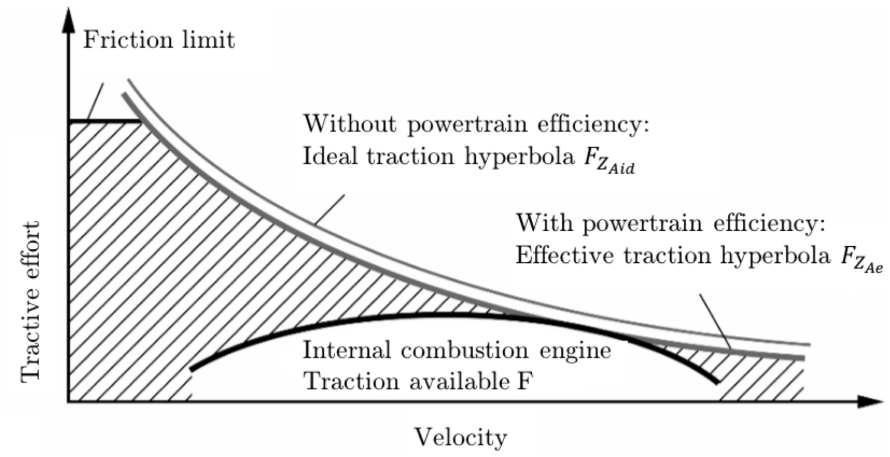

Figure 2.4: Ideal and effective traction hyperbola; A typical traction profile available in a internal combustion engine.

The maximum traction between tyres and road is limited by the friction limit.

As shown in figure 2.4, the shaded area cannot be used without a gearbox. This output converter adapts the characteristic of the combustion engine as closely as possible to the ideal of the traction hyperbola.

The gearbox and the gear ratios values adapt engine traction curve to the correspondent traction as presented in figure 2.5 [15].

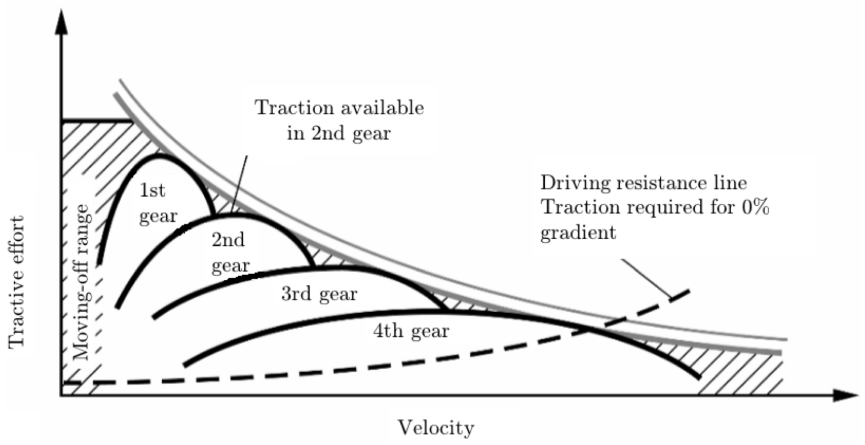

Figure 2.5: Traction diagram of a 4-speed gearbox.

There are three main groups of gearboxes: manual, automatic, which includes the dual clutch (DCT) and lastly, the continuously variable transmissions (CVT). Manual gearboxes require the driver to be continuously selecting the most appropriate gear ratio. The automatic gearboxes are able to make the selection in an automatic way. The driver just has to select which direction to follow [13]. DCT is an automated manual transmission which uses two separate clutches, one of each odd and even gear sets [22]. CVT have now become more popular because provide improved economy and lower emissions. This type of gearbox don't have steps in between gear changes [13].

The BMW 318d under analysis is equipped with a 6-speed manual gearbox. The correspondent gear ratios are shown in table 2.2 [6].

Table 2.2: BMW 318d Saloon Gearbox ratios

	Gearbox ratios
I	4.002
II	2.109
III	1.396
IV	1.000
V	0.781
VI	0.668

Using the torque characteristic shown on figure 2.3 and dividing each point's for the gear ratios (table 2.2), the traction curve available in BMW 318d series can be defined as presented in figure 2.6.

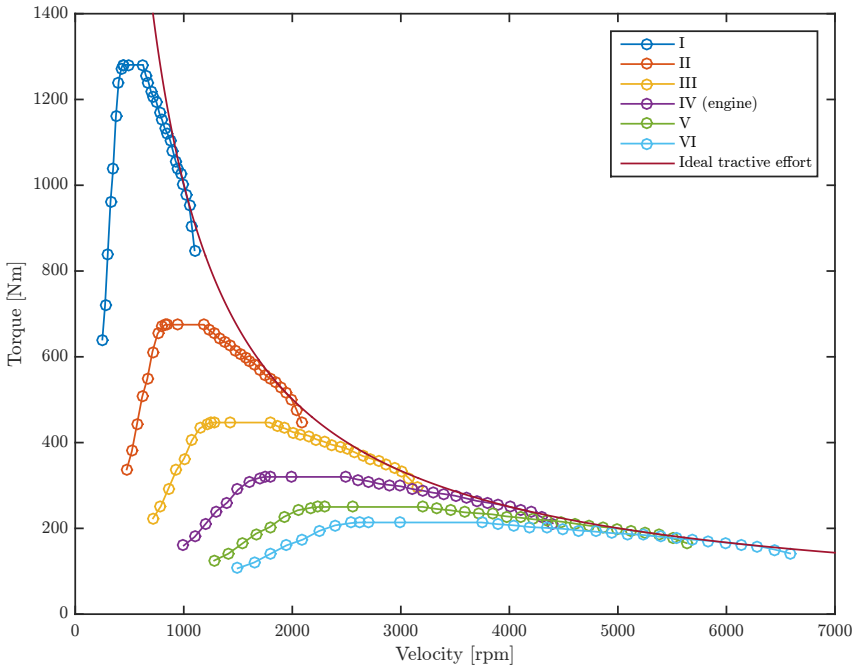

Figure 2.6: Traction effort available on BMW 318d

2.3.2 Final drive

The final-drive gears, also designated as axle box or differential, are used in the transmission system for redirecting the drive from the gearbox or propeller shaft through 90° and to provide a permanent gear reduction between the engine and the

driving road-wheels. The final-drive gears may be directly or indirectly driven from the output gearing of the gearbox [19, 20].

Indirectly driven final drives are used at the rear of the vehicle. The final drive gears may be bevel or worm gears.

The geometry of bevel gears can be approximated by two friction cones: the crown wheel and the pinion, figure 2.7a. There are three main types of bevel gears: spur, spiral and hypoid.

The spur bevel gears are cheap to produce and mechanically more efficient. However are noisy when meshed. The spiral bevel gears (or helical bevel gears) are used to reduce the noise generated by the spur bevel gears, figure 2.7b.

In passenger cars, hypoid gears are usually used. In this case the bevel drive pinion engages above the axial center of the crown gear, as shown in figure 2.7c.This offset is always placed below to give a lower propeller shaft and a reduction in the tunnel height. This offset makes the diameter of the bevel drive pinion larger, and the crown gear can be smaller for the same load than in helical bevel gears. The increased sliding friction between the tooth flanks contributes substantially to reducing noise [15].

Worm gears are now rarely used, mainly because of their extremely low efficiency.

2.3.3 The need for final-drive differential gearing

A given turning circle of a vehicle may be defined as the average circumferential distance moved by the vehicle with the driver's steering-wheel held at same point to one side of the central straight-ahead position. In actual fact, the paths followed by the inner and outer road-wheels will be slightly different.

Figure 2.8 shows that the outer wheels will have a larger turning radius than the inner wheels about some common center. This means that the outer wheels will travel a greater distance than the inner ones. To make this happen at the same time, the outer wheels have to rotate faster than the inner ones.

The differential mechanism included in the axle box or differential allows the wheels to rotate at different speeds, but still maintains **the same torque into both wheels** [19].

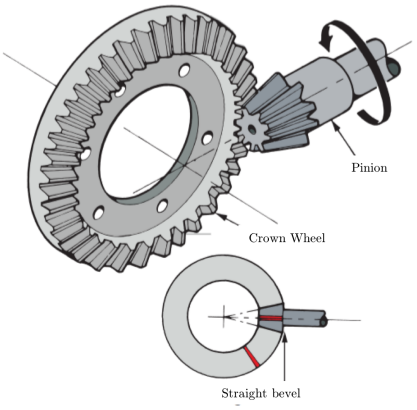

(a) Straight bevel gears

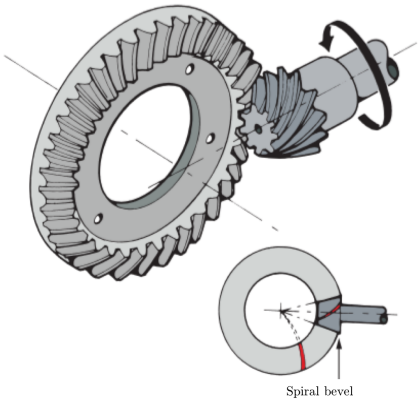

(b) Spiral bevel gears

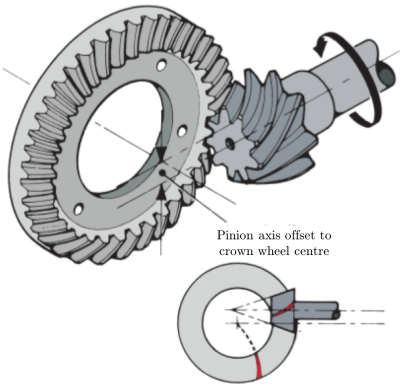

(c) Hypoid bevel gears

Figure 2.7: Types of bevel gears

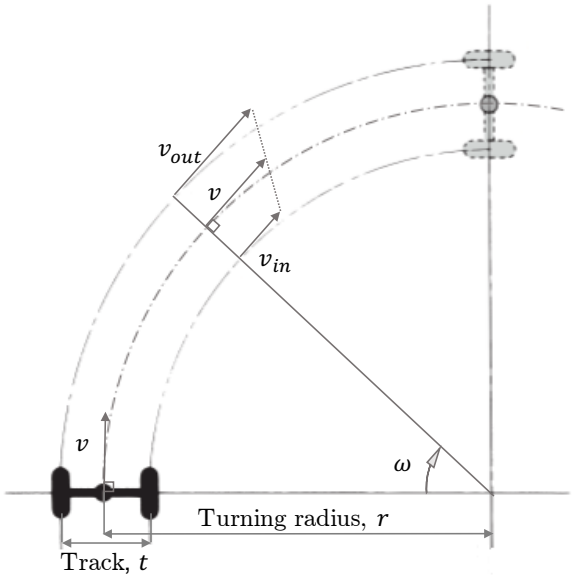

Figure 2.8: The need for differential

There are different types of differentials:

- open differentials;
- lock differentials;
- limited slip differentials;
- torsen limited slip differentials.

The most common type is the open differential because it's the most inexpensive, has the light weight and provides lower maintenance.

The main disadvantage of the open differential is that the engine power follows the path of the least resistance, which means that in case of one wheel has lower traction than the other, for example, when slips in a ice pavement, the other wheel will not have torque enough to move the vehicle forward. The other types of differentials are used in order to solve this problem.

A locking differential may provide increased traction compared to a standard/open differential by restricting each of the two wheels on an axle to the same rotational speed without regard to available traction or differences in resistance seen at each wheel. The LSD (limited slip differential), as its name suggests allows for some difference in angular velocity of the output shafts, but imposes a mechanical limit on this disparity.

The BMW 318d under analysis has an open differential and the corresponding final drive ratio, i, is 3.231 [6]. The traction curve at the wheels is presented below in figure 2.9.

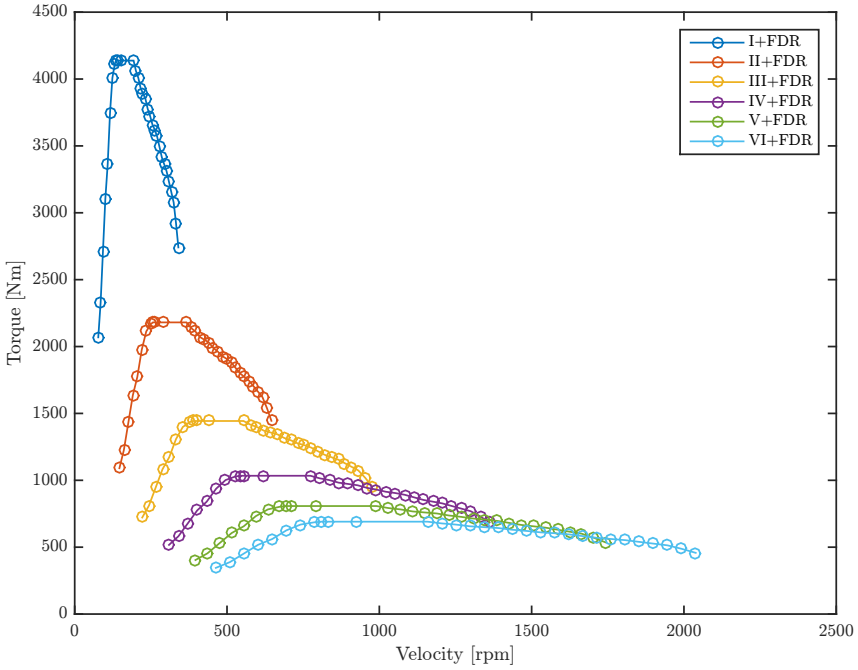

Figure 2.9: Traction effort available on BMW 318d wheels

Knowing the vehicle velocity, v,the minimum turning radius, r_{min} and the wheel track, i.e., the distance between two road wheels on the same axle, t, it is possible to evaluate the maximum speed difference between the outer and the inner wheels.

According to figure 2.8, the vehicle speed is defined as,

$$v = wr \tag{2.1}$$

thus,

$$v_{out} = wr_{out}$$

$$v_{in} = wr_{in}$$

where r_{out} and r_{min} are defined by,

$$r_{out} = r + t/2 \tag{2.2}$$

$$r_{in} = r - t/2 \tag{2.3}$$

Defining ε as,

$$\varepsilon = \frac{v_{out} - v_{int}}{v_{out}} \times 100 \tag{2.4}$$

$$\varepsilon = \frac{t}{\frac{r_{min}+t}{2}} \tag{2.5}$$

Using equation (2.4) with $r_{min} = 11.3/2m$ and $t = 1.582m$ [6],

$$\varepsilon = 24.567\%$$

So, in the case of BMW 318d, the wider gap between the outer and inner wheels rotations speeds has a value of 24.567%, i.e., the inner wheels rotates 24.567% less than the outer wheels.

2.4 Real BMW E46 differential

As the goal of the present study is to design a rear axle transmission test rig, having a real rear differential is a crucial point because with it, the main dimensions may be known (in order to design a mechanical structure) as well as its inertia.

The college had a BMW E46 (produced between 1998 to 2006) of a 320d differential, and based on the purpose exposed above, it was disassembled, see figure 2.10, and its inertia was calculated.

The references of each differential component are presented on table 2.3.

Table 2.3: Reference of differential components

Component	Brand	Ref.
Drive shafts bearings	FAG	H01298_T29
Propeller shaft bearings		
next to the pinion	KOYO	HM 801310
	KOYO	HM 88542
Drive shafts seals	BMW	1214 323 CFW 2 44-90.1 10/15
Propeller shaft seals	BMW	1214 666 ACM RECHTS KACO DSS 45 10/14 RTD F01 101
Crown wheel		H47 YKB 946 0622

The differential pinion has, in this case, 14 teeth and the crown wheel 43. So this particular final drive ratio i is $i = 43/14$, $i = 3.07$.

Measuring the dimensions and mass of the all moving components, the correspondent polar mass moment of inertia in x (axis of the propeller shaft) and y axis (axis of the drive shafts), J_x and J_y, respectively, was calculated. The index of the terms presented in equations 2.6 and 2.8 are referred in figure 2.11.

$$J_x = J_1 + \frac{J_3 + J_4 + J_5 + 2 \times (J_6 + J_2)}{i^2} \tag{2.6}$$

$$J_x = 0.032 kgm^2 \tag{2.7}$$

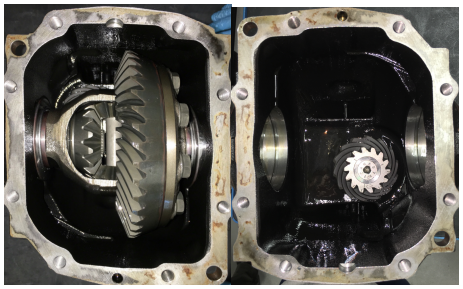

(a) Differential with cover removed

(b) Differential pinion

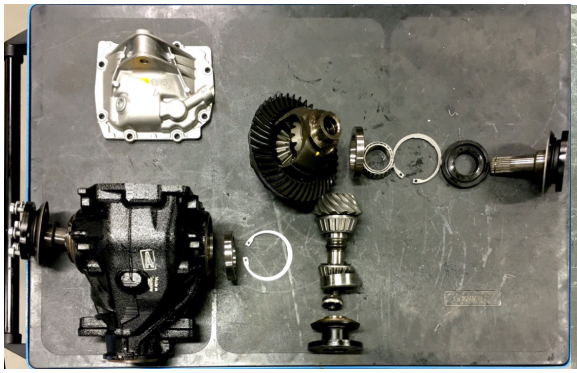

(c) Exploded view

(d) Differential case desmounted

Figure 2.10: Differential of a BMW E46 (320d)

assuming that the drive shafts will rotate at exactly the same speed J_y was calculated using equation (2.8).

$$J_y = J_2 + J_3 + J_5 + J_6 + J_4 + J_1 \times i^2 \tag{2.8}$$

Substituting the values in equation (2.8),

$$J_y = 0.054 kgm^2$$

2.5 Requirements definition

2.5.1 Tyre dimensions

Tyres have standardized dimensions that are presented in figure 2.12 [21].

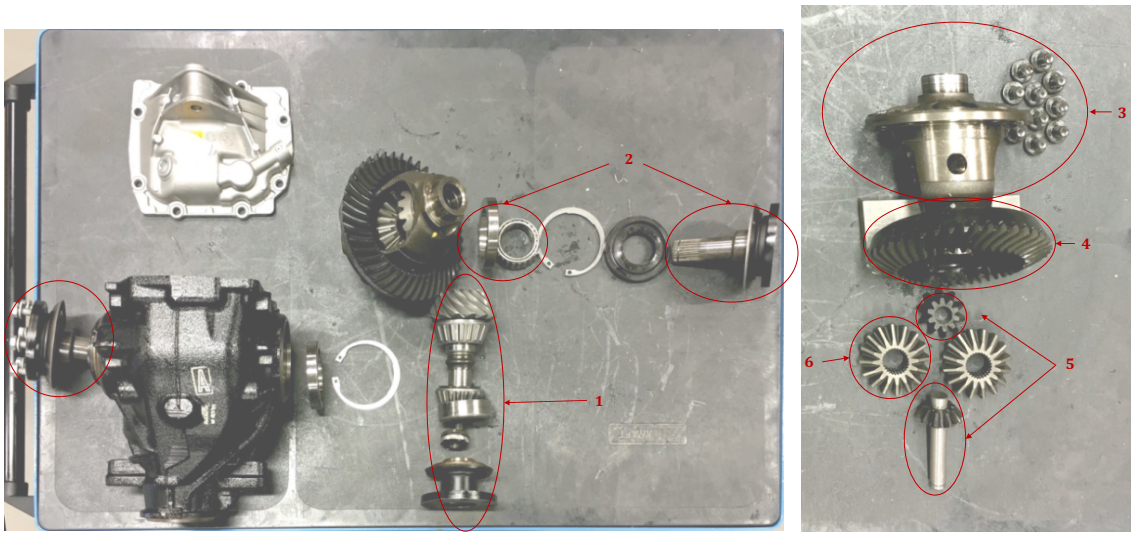

(a) (b)

Figure 2.11: Inertia scheme

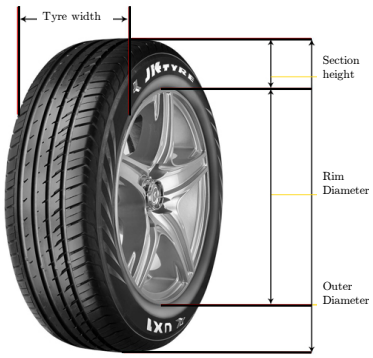

Figure 2.12: Tyres standardized dimensions

The vehicle under analysis has a 225/50 R17 tyre. Which means:

- 225 is the tyre width in mm;
- 50 is the height-to-width ratio as a percentage;
- R is the construction type (in this case, radial);
- 17 is the rim diameter in in ($1in = 25.4mm = 25.4 \times 10^{-3}m$).

The outer diameter of the tyre, D_{out}, is,

$$D_{out} = 2 \times 225 \times 50\% + 17 \times 25.4mm$$
$$D_{out} = 656.80mm$$

2.5.2 Power and torque requirements

Knowing the tyre dimensions, assuming a speed range from $20km/h$ to $140km/h$, and a 5% steepness of the path, using equations (1.2), (1.3), (1.4) and (1.5) it is possible to map the torque and power requirements for the test rig.

The torque that has to be applied in the propeller shaft, T_1 is defined as,

$$T_1 = \frac{F_x \frac{D_{out}}{2}}{i} \tag{2.9}$$

assuming an efficiency equal to 100% the correspondent torque in each drive shaft, T_2 and T_3 is calculated as,

$$T_2 = T_3 = \frac{F_x}{2}\frac{D_{out}}{2}$$

or

$$T_2 = T_3 = \frac{T_1}{2} \times i \tag{2.10}$$

To simulate the speed range selected with regard to the tire size, the angular velocity (when traveling through a straight line), n_2 and n_3, of the drive shafts must be calculated as,

$$n_2 = n_3 = \frac{60v}{\pi D_{out}} \tag{2.11}$$

and the correspondent angular velocity of the propeller shaft is,

$$n_1 = n_2 \times i = n_3 \times i \tag{2.12}$$

The power needed in the propeller shaft, P_{M1} is calculated as,

$$P_{M1} = T_1 \times \frac{2\pi\ n_1}{60} \tag{2.13}$$

The correspondent power in each drive shaft, P_{M2} and P_{M3} is defined as (when traveling through a straight line),

$$P_{M2} = T_2 \times \frac{2\pi n_2}{60} = T_3 \times \frac{2\pi n_3}{60} \tag{2.14}$$

Figure 2.13 shows the values mentioned above. However, when turning the power requirement for the outer wheel can be 25% higher than the inner.

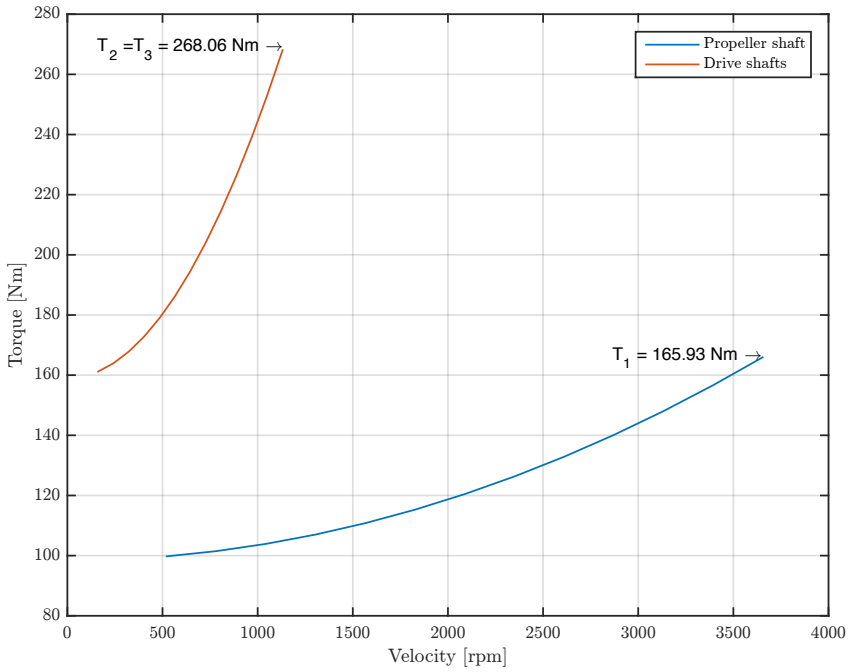

(a) Torque requirements

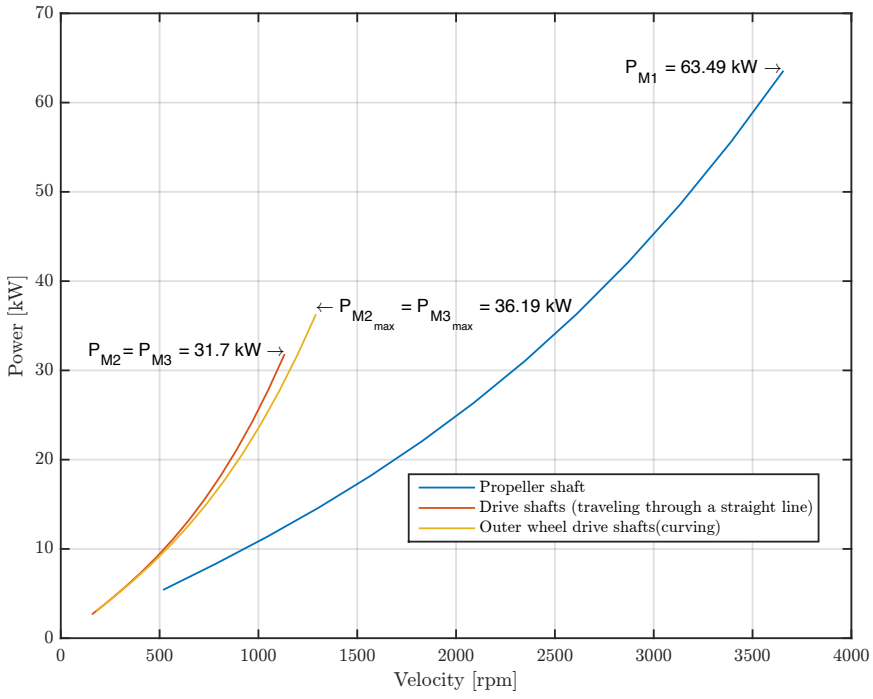

(b) Power requirements

Figure 2.13: Power and torque requirements for propeller shaft and drive shafts

As can be observed, the maximum torque for the drive shafts is about 270 Nm and for the propeller shaft, 170 Nm at 3700 rpm and 1200 rpm, respectively.

The maximum power for the drive shafts is about 35 kW and 65 kW at 3700 rpm and 1200 rpm, respectively also.

2.6 Measuring system

To quantify the power losses in the differential, the test bench must have tachometers in order to know the speed in each axle, n_1, n_2 and n_3. Moreover, a torque transducer has to be allocated in each axle (propeller and drive shafts) to measure T_1, T_2 and T_3.

Thus, the power loss, P_{loss} can be calculated as:

$$P_{loss} = P_{in} - P_{out} \tag{2.15}$$

where in case of accelerating,

$$P_{in} = T_1 \times \frac{\pi n_1}{30} \tag{2.16}$$

and

$$P_{out} = T_2 \times \frac{\pi n_2}{30} + T_3 \times \frac{\pi n_3}{30} \tag{2.17}$$

in case of decelerating,

$$P_{in} = T_2 \times \frac{\pi n_2}{30} + T_3 \times \frac{\pi n_3}{30} \tag{2.18}$$

and

$$P_{out} = T_1 \times \frac{\pi n_1}{30} \tag{2.19}$$

As shown before the speed range that the tachometers should cover is around 0 to 3700 rpm with a maximum uncertainty of less than ± 1 rpm.

The torque range that the torque transducers should cover is around 0 to 300 Nm with a maximum uncertainty of less than ± 0.5 Nm.

Finally, temperature sensors to monitoring the temperature have to be allocated in several positions:

- Lubricant temperature at pinion gear;
- Case wall;
- Lubricant temperature;
- Ambient temperature.

The requirements imposed by CETRIB was that the range of these measurements should be between 0 °C to 200 °C with a maximum uncertainty of less than ±1 °C.

These torque and speed transducers will be selected in chapter 4 and the temperature sensors in chapter 6.

Chapter 3

Power architecture

The global economy's growth results in a continuously expanding demand for energy. However, this causes an increasing rise in CO_2 emissions, resulting in climate change, whose progress and effects are not fully foreseeable at present. To preserve the future of our planet, it is necessary to eliminate the consequences of climate change [23].

Furthermore, as energy prices rise, increasing this cost factor will have a negative impact on production costs in the industrial sector.

Energy-efficiency is one of the solutions for industries who want to be competitive in the future. They can help to reduce manufacture costs, improve the return of their investment and lower CO_2 emissions [24].

The differential should be tested in several road conditions: different directions of travel (move back, forth and curve) and when simulating this kind of situations, the acceleration or deceleration modes should be defined. The power flux in this two last mentioned situations, changes.

In this chapter, the drive systems possibilities to execute these tests will be discussed.

3.1 Brake test bench vs test bench with energy recovery

Three machines (M1, M2 and M3), are necessary to simulate the propeller shaft (output of the driveline) and the wheels, figure 3.1.

The machine that plays the role of gearbox, M1, must be able to produce the correspondent speed and torque provided from it. Furthermore, machines M2 and M3, should simulate the load actually borne by the wheels of the vehicle.

These three machines must have the possibility to be speed or torque controlled.

To simulate corners, M2 and M3, which play the role of wheels must be speed controlled. Imposing this parameter, turns to the right side or to the left side can be simulated, by means of giving more or less speed to the driveshafts. A straight trajectory can be simulated, imposing the same speed in M2 and M3. On the other

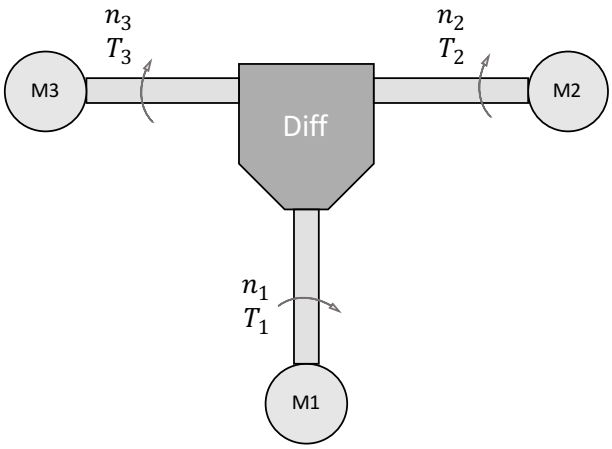

Figure 3.1: Power transmission's scheme

hand, machine M1, should be torque controlled.

As described in figure 2.13 presented on chapter 2.5, the maximum power required for the propeller shaft is $63.5kW$.

If this power was consumed by the two brake dynamometers represented by machines M2 and M3, all of this power could not be reused and will be converted into heat, figure 3.2. The numbers presented in this figure are examples of possible inefficiencies [25].

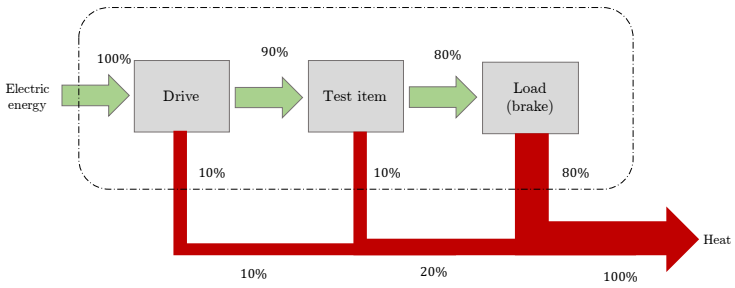

Figure 3.2: Brake test bench

Moreover, as the tests have a duration of 12 hours and nowadays the kWh price is around $0.3095€/kWh$ this solution is economically untenable [26]. Furthermore, implementing the solution with two, M2 and M3, dynamometers the differential deceleration test can not be executed. In this case, the load should be imposed by M1 and because of that the dynamometer should be allocated in there.

In order to provide a more economically viable and sustainable solution, a search of different systems types that can provide energy-saving in industrial sectors was made. Using this type of solution, the drive system only require to get 30% of

the required power from the electric network, figure 3.3. Once again, the numbers referred to in figure 3.3 are purely qualitative, since they are not based in the application of the present study.

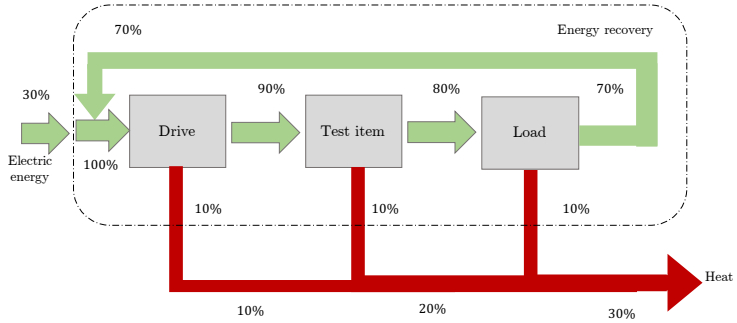

Figure 3.3: Test bench with energy recovery

In this test rig situation, the secondary control drive systems and the electrical drive systems can be noted as the most relevant.

3.2 Drive systems with energy recovery

3.2.1 Hydraulic secondary control drive systems

The secondary control drive systems have been developed and are marketed by Rexroth Bosch Group. The secondary control has high dynamics for setting up closed-loop speed, position or torque controls with energy recovery.

This kind of systems includes at least one hydraulic pump - the primary unit, an hydraulic accumulator and a consumer - the secondary unit that work at one supply network with constant pressure, figure 3.4. These machines are called axial piston variable pumps A4VSO. They are designed with a swash plate for hydrostatic drives. Its flow is proportional to the input drive speed and the plate displacement [27].

The hydraulic accumulator stores the energy fed by the consumer when working in reversed direction. When working under load, this accumulated energy is used to satisfy the consumption peaks [28].

To control the axial piston units there are digital controllers called HNC100-SEK. They are suitable for the closed-loop speed and torque control as well as the open-loop torque control [29].

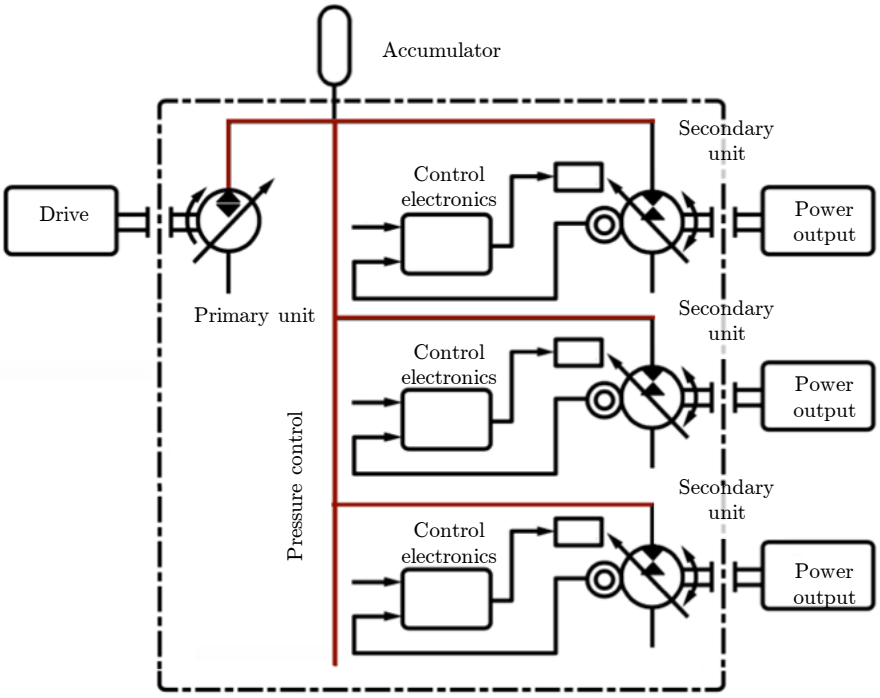

Figure 3.4: Configuration of secondary control drive systems

3.2.2 Electrical drive systems

As in secondary control systems, the electrical drive systems have a primary unit, an accumulator and consumers too.

The power supply is the power unit, the accumulator role is performed by the DC capacitors and the consumers are the motors working in motoring mode; when working in regenerative mode, the energy produced in each drive/motor module can be fed back to the DC link instead of being converted into heat in a brake resistor.

In this case, instead of taking energy from the grid there is a direct energy equalisation between several different drives in an interlinked system, figure 3.5 [23].

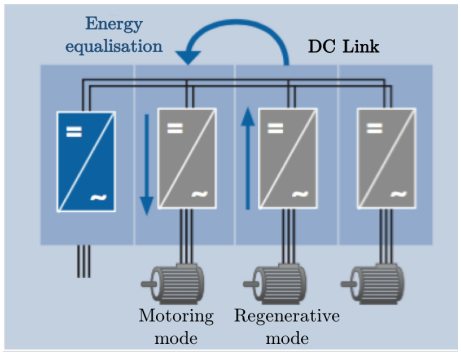

Figure 3.5: Energy equalisation between several drives

Siemens is a brand that has drives capable of providing this technology.

The Simotion Motion Control system provided by Siemens is combined with the Sinamics S120 drive systems and Simotics motors to create energy-efficient solutions which help to achieve considerable reductions in energy consumption. To allow efficient energy processes a previous energy management has to be done. This process involves three phases: identification, evaluation and implementing.

Identification provides the recognition of energy flows. After identification, the energy consumption has to be calculated - evaluation. Implementing involves the selection of the common DC link, which will save the energy, as well as power supply wich will fed the power losses in the process.

The Sinamics S120 drive system is a modular system for high-performance single-axis and multi-axis drives for a very broad range of applications. These units are capable of controlling in vector, servo and V/f modes. They also perform the speed and torque control functions.

The Sinamics S120 drive system is composed by power units and control units. The control unit is selected according to the number of drives to be controlled and the required performance level. On the other hand, the power unit must be rated to satisfy the energy requirements of the application.

A motor module integrates a voltage-source DC link and an inverter for supplying a motor. They are designed for multi-axis drive systems and are interconnected by a common DC busbar. Since they have a common DC link they can exchange energy with one another as shown in figure 3.5.

The voltage-source DC link is supplied with main voltage by a line module. Siemens provides three types of line modules: the basic, the smart and active line modules. The first is not capable of feeding regenerative energy back into the supply system. The smart line modules can supply energy and return regenerative energy. However, in case of power failure, a braking module and braking resistor are required if the drives have to be decelerated in a controlled manner. The active line modules have the same characteristics mentioned in the smart line modules but, they can

generate a regulated DC voltage which remains constant despite fluctuations in the line voltage is shown in figure 3.6 [30].

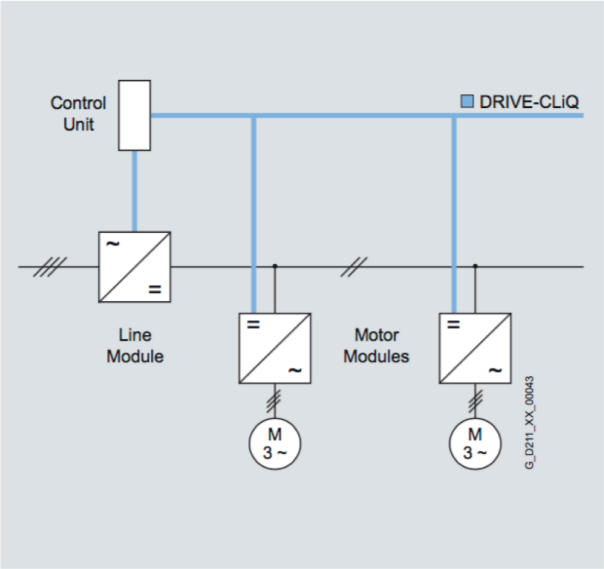

Figure 3.6: Sinamics S120 drive system overview

3.3 Power flow

The power flux is not defined until now, i.e., the machines that are working in motoring or regenerative mode have to change their function between each other, depending on what's being tested: acceleration or deceleration.

When testing the differential in acceleration mode, M1 has to work as motoring and the machines M2 and M3 in regenerative mode, see figure 3.7a.

In the other hand, in deceleration test, M2 and M3 should work in motoring mode and M1 as regenerative mode, figure 3.7b.

3.4 Electrical input power estimation

In order to select the most appropriated drive system solution for this application, an estimation of the electrical input power for both cases was made.

3.4.1 Hydraulic secondary control drive systems

Considering the differential in an acceleration test mode (with M2 and M3 at the same speed) and its efficiency equal to 100%, as described in previous section, M1

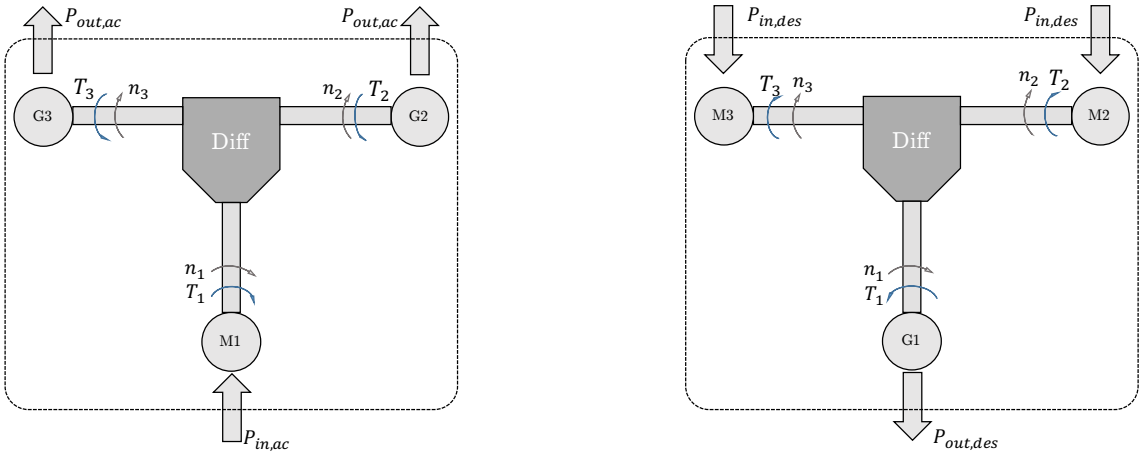

(a) Acceleration mode

(b) Deceleration mode

Figure 3.7: Electrical machines operating modes in acceleration and desaceleration

is working as motoring mode, M2 and M3 as regeneration mode.

In order to know the power that has to be supplied in this situation, the efficiency of the units for these power ranges must be known.

The efficiency of the primary and secondary unit can be calculated using the following equation,

$$\eta_t = \frac{q_v p}{P_{q_v max} \cdot 600} \tag{3.1}$$

where q_v is the secondary unit flow in [L/min], $P_{q_v max}$ is the drive power with maximum flow in [kW] and p is the operating pressure in [bar].

Using an A4VSO variable pump size 40, which characteristic is compatible with the requirements of machines M2 and M3 and is presented in figure 3.8, the total efficiency η_t can be calculated using equation (3.1) [31].

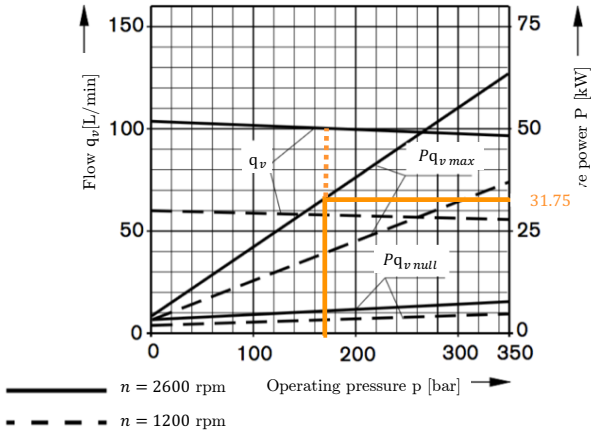

Figure 3.8: Drive power and flow characteristic of an A4VSO size 40 control unit

In view of the most critical situation and looking at figure 3.9, considering,

- P_{supp} as power supplied;
- P_{M1} as power required by M1;
- P_{M2} as power regenerated by M2;
- P_{M3} as power regenerated by M3.

The conversion's efficiency of electrical energy into mechanical energy η_2 it's around 98% [28]. Thus, the power that has to be supplied if a secondary control test bench was adopted, is calculated as,

$$P_{suppl} = \frac{P_{in}}{\eta_t \times \eta_2} \tag{3.2}$$

$$P_{in} = P_1 - (P_2 + P_3) \tag{3.3}$$

P_{M1} is the power required by M1 in the critical situation which it's equal to $63.5kW$. Thus, the power $P_{M2} = P_{M3}$ is $31.75kW$.

Using equation (3.1) and looking at figure 3.8, η_t is calculated. The efficiency of machine M1 was considered the same of M2 and M3.

$$\eta_t = \frac{100 \times 170}{31.75 \cdot 600}$$
$$\eta_t = 0.89$$

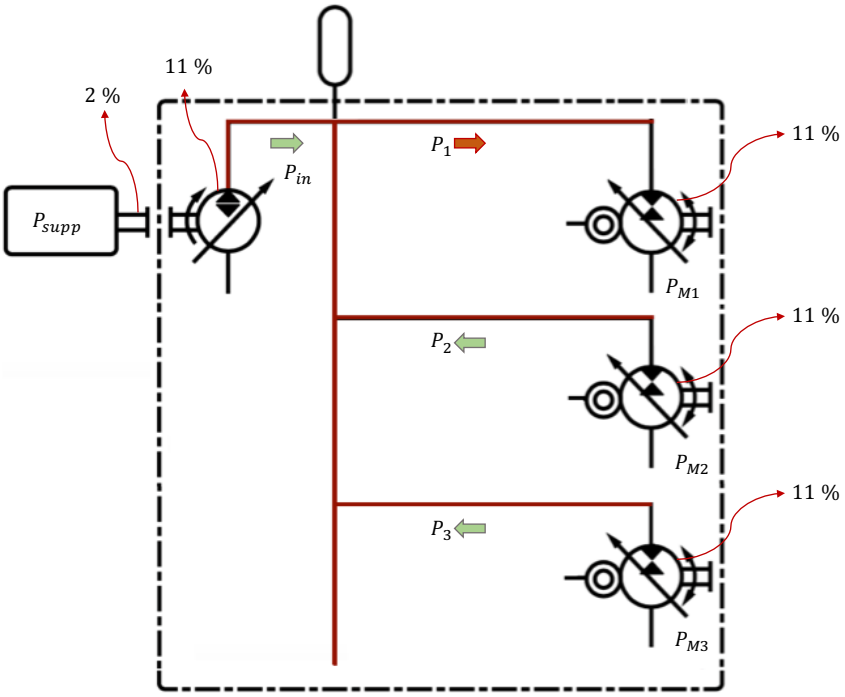

Figure 3.9: Secondary control drive systems power supplied estimation scheme

$$P_1 = \frac{P_{M1}}{\eta_t} \tag{3.4}$$

$$P_1 = \frac{P_{M1}}{0.89}$$

$$P_1 = 71.35kW$$

$$P_2 = P_{M2} \times \eta_t \tag{3.5}$$

$$P_2 = 28.3kW$$

$$P_3 = P_{M3} \times \eta_t \tag{3.6}$$

$$P_{M3} = P_{M2} \Rightarrow P_3 = P_2$$

$$P_{in} = 14.8kW$$

Thus, the power that as to be supplied in this application adopting a secondary control drive system is equal to,

$$P_{suppl} = \frac{14.8}{\eta_t \times \eta_2} \tag{3.7}$$
$$P_{suppl} = 17kW$$

3.4.2 Electrical drive systems

Considering the situation mentioned in previous subsection and same variables, an estimate of the power supplied can be done too, figure 3.10. The efficiency of the line modules, η_3 is equal to 95% and the drive + motor ensemble efficiency, η_4, it's around to 90% [30]. Thus,

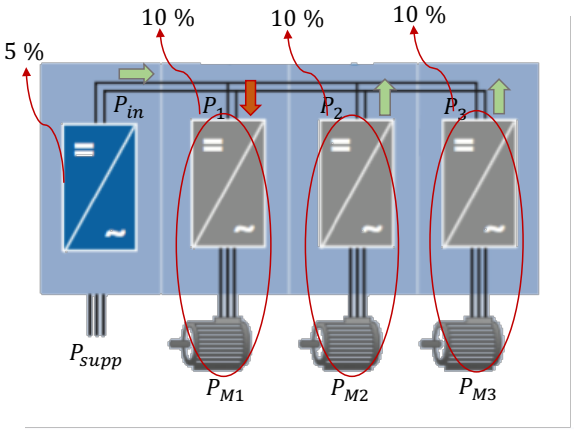

Figure 3.10: Electrical drive systems power supplied estimation scheme

$$P_{suppl} = \frac{P_{in}}{\eta_3} \tag{3.8}$$

$$P_{in} = P_1 - (P_2 + P_3) \tag{3.9}$$

$$P_1 = \frac{P_{M1}}{\eta_4} \tag{3.10}$$
$$P_1 = \frac{63.5}{0.90}$$
$$P_1 = 70.56kW$$

$$P_2 = P_{M2} \times \eta_4 \tag{3.11}$$

$$
\begin{aligned}
P_2 &= 31.75 \times 0.9 \\
P_2 &= 28.6kW \\
P_3 &= P_{M3} \times \eta_4 \\
P_{M3} &= P_{M2} \Rightarrow P_3 = P_2 \\
P_{in} &= P_1 - 2 \times P_2
\end{aligned}
\tag{3.12}
$$

$$
\begin{aligned}
P_{in} &= 13.41kW \\
P_{suppl} &= \frac{P_{in}}{\eta_3} \\
P_{suppl} &= 14.12kW
\end{aligned}
$$

The power that has to be provided by the power supply in case of using a hydraulic secondary control drive system is $P_{suppl_{sec}} = 17kW$. On the other hand, when using an electrical drive system this value decreases 20%.

Thus, the energy-efficient system chosen for this test bench was the electrical drive systems since they are modular, more compact than the hydraulic secondary control systems and even more important, the electrical machines and the drives of this systems are more efficient than the hydraulic machines which provides less power consumption.

Chapter

4 Components selection

Being the type of drive systems selected, in this chapter, the selection of torque transducers, couplings, electric motors and the correspondent drives and line module will be described.

As show in section 2.5.2 , increasing the drive shafts speed, a greater power and torque are necessary to allow to reproduce the real driving conditions.

To select all the components mentioned above the critical situation: maximum speed, presented on figure 2.13, will be considered.

Those values are resumed in table 4.1.

Table 4.1: Power and torque requirements

	n_{max}	$T_{@n_{max}}$	$P_{@n_{max}}$
	rpm	Nm	kW
M1	3660	170	63.5
M2	1300	270	36.20
M3	1300	270	36.20

4.1 Torque transducers

The differential has a torque efficiency ranging from 95 to 97%, thus, a high accuracy is required in order to minimize the errors in the measurements which may lead to the wrong conclusion that the differential has an efficiency equal to 100%. To measure the propeller and the drive shaft torques an HBM T40B torque transducer with a 500 Nm rated torque was chosen, figure 4.1.

Figure 4.1: HBM T40B torque transducers

The main characteristics of this HBM torque transducers are presented in table 4.2 [32].

Table 4.2: T40B HBM torque transducers characteristics

HBM T40B	500 Nm	
Accuracy class	0.05	
Nominal output signal	at positive nominal torque	at negative nominal torque
Voltage output	+10V	-10V
Nominal rotational speed	20 000 rpm	
Mass moment of inertia	0.0039 kgm^2	

4.2 Electric motors

M1, M2 and M3 should have a power and torque characteristic increased by the speed. As the tests will be performed on a steady state, the most critical situation will be maximum speed, and so is considered for dimensioning.

The electric motors available in Motion Control systems provided by Siemens are the Simotics servomotors and main motors, which are available in synchronous or induction/asynchronous versions.

The maximum power provided by Simotics servomotors is 34.2 kW, that does not satisfy the expected needs.

In turn, the asynchronous main motors have power ratings ranging from $2.8-1230$ kW, higher than the synchronous that presents a power range from $15-310$ kW.

However, the synchronous motors are more compact than induction, have a low rotor moment of inertia and therefore maximum dynamic response. The characteris-

tic speed/power curves of these motors are shown in figure 4.2. Here, the theoretical curve of the maximum permissible overload capacity is shown as a limit in the characteristic diagrams and corresponds to value P_{max} [30].

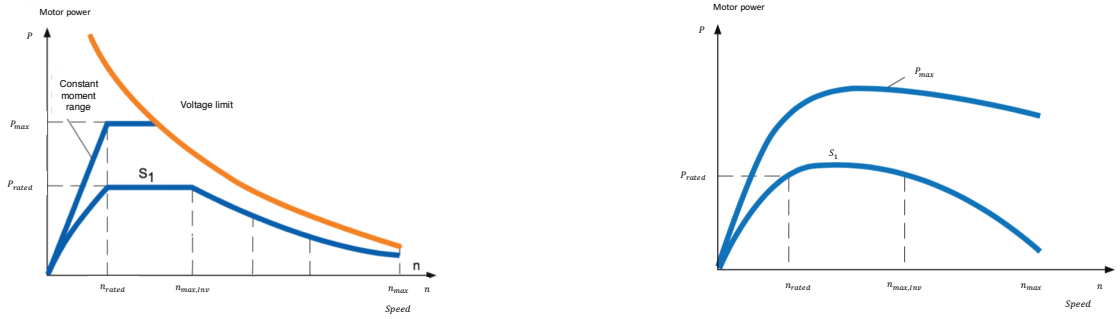

(a) 1PH8 asynchronous motors

(b) 1PH8 synchronous motors

Figure 4.2: Typical speed/power diagram for 1PH8 motors

The selected synchronous motors, figure 4.3, and their main characteristics are presented in table 4.3 as well as their power and torque characteristics curves, figures 4.4 and 4.5. The cooling system of these motors is forced ventilation.

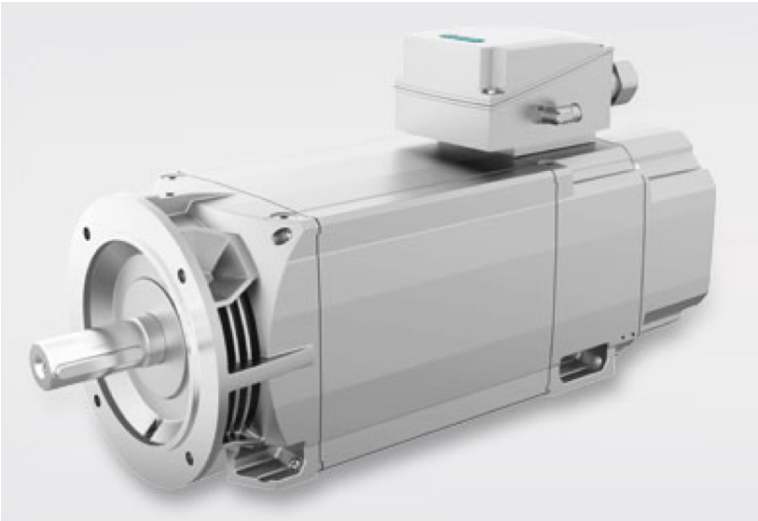

Figure 4.3: 1PH8 synchronous motors, forced ventilation

Table 4.3: Motors for M1, M2 and M3 specifications

		Shaft height	P_{rated} kw	M_{rated} Nm	I_{rated} A	V_{rated} V	f_{rated} Hz	$n_{max_{inv}}$ rpm	J kgm^2	Weight kg
M1	1PH8137	132	66.7	177	100	440	120	4500	0.0885	136
M2, M3	1PH8184	180	38	454	80	316	53	1450	0.46	330

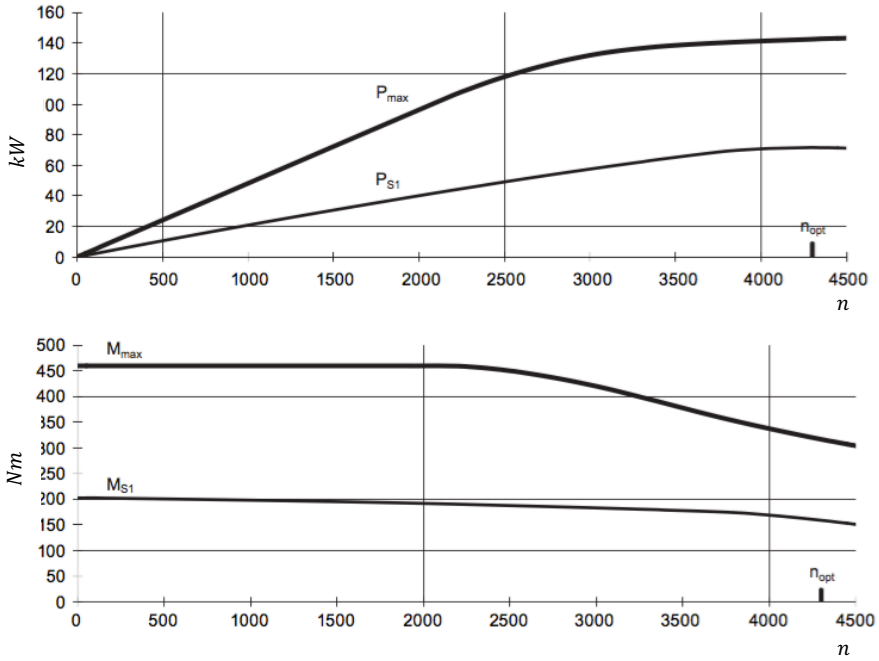

Figure 4.4: Power and torque characteristics curves of 1PH8137

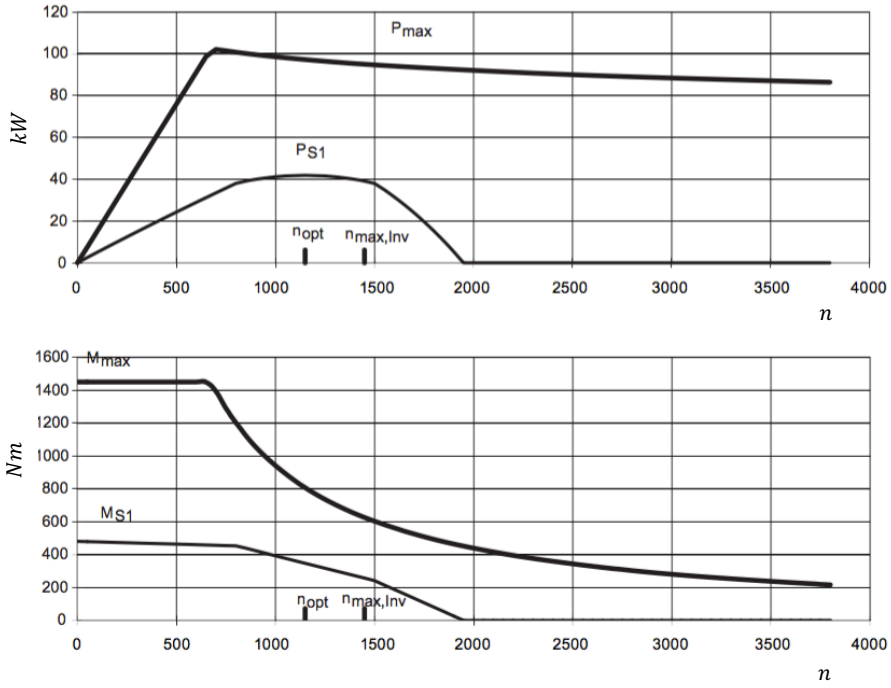

Figure 4.5: Power and torque characteristics curves of 1PH8184

4.2.1 Motor modules

Three motor modules are needed for supplying the three motors selected in the previous section. As referred in section 3.2.2, the motor modules are designed for multi-axis drive systems and are interconnected by means of a shared DC busbar. A connection example of a single motor module in booksize format with a current ranging from 45 to 200A is presented in figure 4.6 [30].

The main characteristics of the selected motor modules are presented in table 4.4. They were selected based on each motor rated current and power.

4.2.2 Line module

The voltage-source DC link is supplied with main line voltage by a Line Module. This component generates a DC voltage and supply motor modules with energy via the voltage source DC link [30].

In order to select a suitable power source, the worst situation was considered, i.e., when M2 and M3 are working in motoring mode and M1 is not regenerating energy, figure, 4.7.

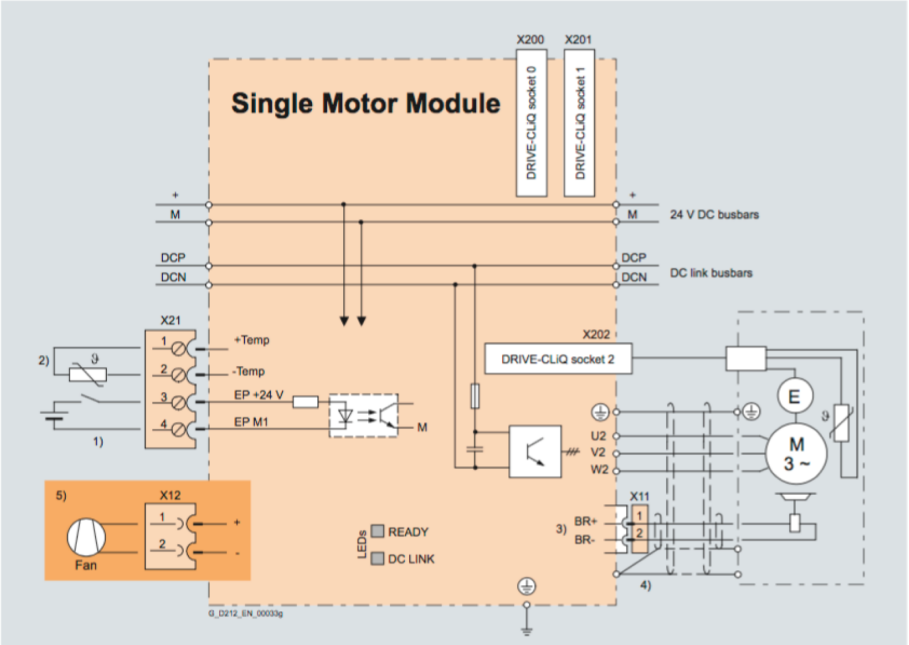

Figure 4.6: Connection example of a single motor module

When testing the differential at the maximum speed/load conditions, the power required in M2 and M3, P_{M2} and P_{M3}, respectively is equal to $31.75kW$.

Thus,

$$P_2 = \frac{P_{M2}}{\eta_4}$$

$$P_3 = \frac{P_{M3}}{\eta_4}$$

$$P_2 = P_3 = 35.3kW$$

As M1 is not regenerating energy, the power that has to be supplied by the line module, P_{in}, is calculated as,

$$P_{in} = P_2 + P_3 \tag{4.1}$$

$$P_{in} = 70.6kW \tag{4.2}$$

Looking at equation (4.2), the maximum power that can be required for the test bench is 70.6 kW. Thus, the rated power of the line module has to be , $P_{in} \geq 70.6$ kW.

An active line module was selected, figure 4.8. This component generates a reg-

Table 4.4: Technical specifications of motor modules

		M1	M2, M3
Ref.		6SL3120-1TE31-3AA3	6SL3120-1TE28-5AA3
Type of cooling		Internal air cooling	
	Units		
Output rated current	A	132	85
Type rating based on I_{rated}	kW	71	46
Current carrying capacity DC link busbars	A	200	200

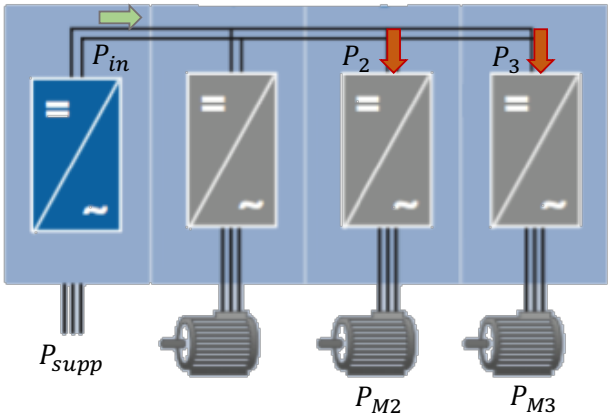

Figure 4.7: Line module selection scheme

ulated DC voltage which remains constant despite fluctuations in the line voltage. The main characteristics of the selected component are presented in table 4.5

Table 4.5: Active line module in booksize format

Ref.		6SL3130-7TE28-0AA3
Cooling		Internal air cooling
	Units	
Rated power @ 380V AC	kW	80
DC link current	A	134
Input current	A	128
Current carrying capacity DC link busbars	A	200

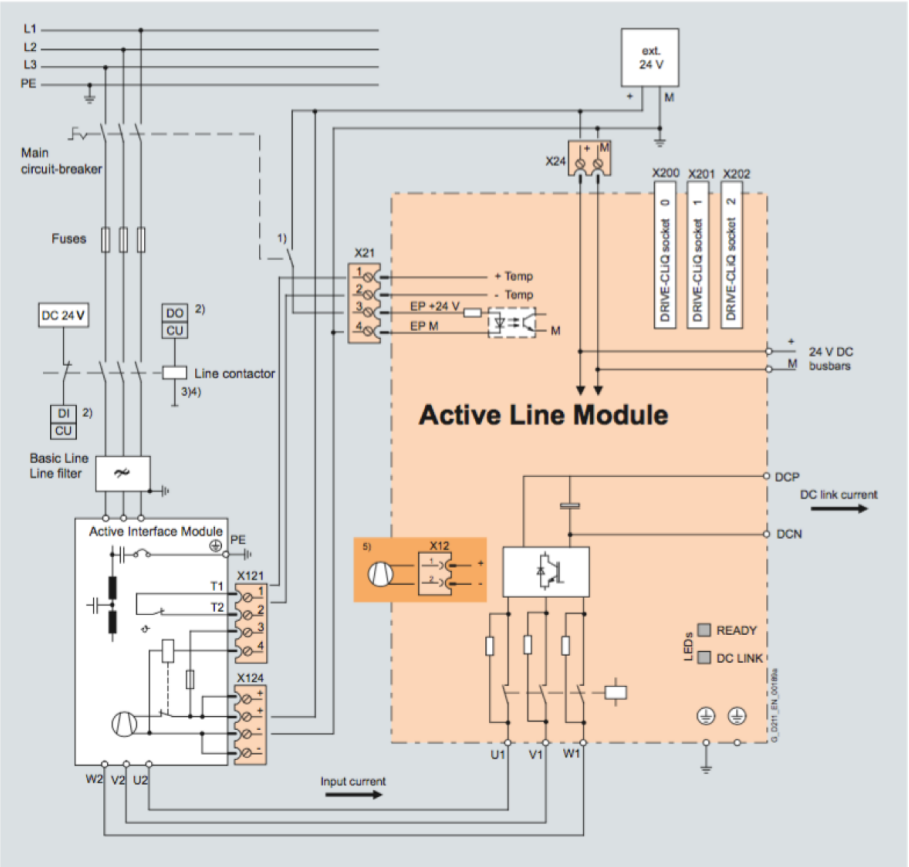

Figure 4.8: Line module selection scheme

4.2.3 Control unit

The control unit is selected according to the number of drives to be controlled and the required performance level.

A CU320-2 control unit was selected because it was designed to control multiple drives. In this application, the closed-loop control types that have to be available are the speed and torque control. Using synchronous motors, the servo control is the only way to control them ways.

This control unit is capable of controlling up to 6 drives in servo control function [30].

An overview of the control unit, line module and motor modules is presented in figure 4.9.

Figure 4.9: CU320-2 Control Unit, Line module and three motor modules in booksize format

4.3 Couplings

Flexible couplings are needed to connect the electric motors to the torque transducers. With them, misalignments can be compensated.

Thus, three ROBA®-DS couplings for HBM torque transducers marketed by mayr® were selected, figure 4.10. These shaft couplings are backlash-free and torsionally rigid. They compensate for axial, radial and angular shaft misalignments [33].

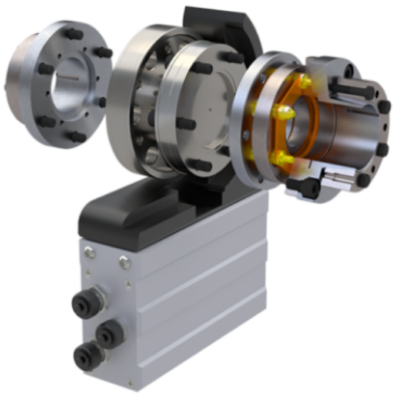

Figure 4.10: ROBA®-DS for HBM torque transducers

There are different construction designs available:

- Shrink disk hub external;
- Shrink disk hub internal;
- Sandwich construction.

The preferred type of construction is the shrink disk hub external, shown in figure 4.11 because it provides a compact and low mass moment of inertia design, a quick installation and external clamping and the shortest design [33].

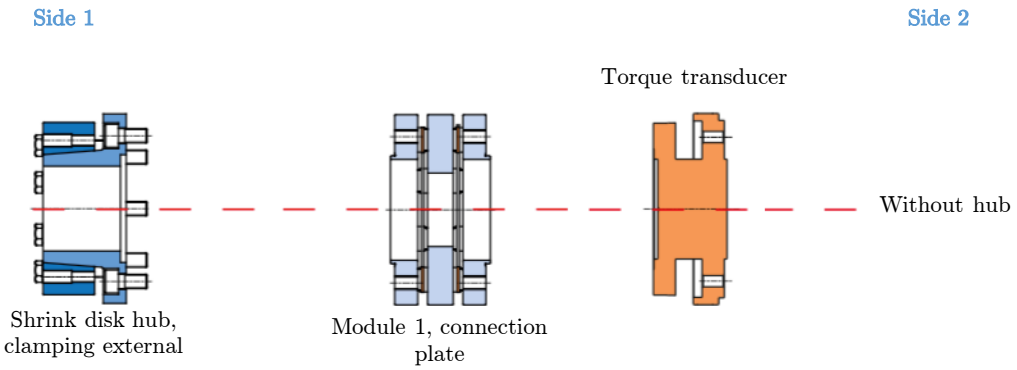

Figure 4.11: Preferred type of construction (shrink disk hub external)

The ROBA®-DS size for torque transducers selected in previous section was 64 for 500 Nm T40B torque ranging, respectively.

The technical data of this couplings is presented on table 4.6.

Table 4.6: Technical data of ROBA®-DS 64 size

ROBA-DS size			64
Nominal torque		Nm	1100
Peak torque		Nm	1650
Outer diameter		mm	132
Minimum hub bore		mm	45H6
Maximum hub bore		mm	70H6
Maximum speed		rpm	15 000
Permitted misalignments	angular	°	0.6
	axial	mm	1.1
	radial	mm	0.25
Mass moments of inertia	Shrink disk hub, clamping external	kgm^2	0.00849
	Connection plate	kgm^2	10.78

4.4 System inertia

To obtain a robust speed control of the electrical machines by the drives, it is necessary to ensure that the relation between the mass moment of inertia exerted by the motor load and its own mass moment of inertia smaller than 3:1. In this context, similarly of what was done in section 2.4, the correspondent mass moment of inertia seen by each electric machine, $J_{1,eq}$, $J_{2,eq}$ and $J_{3,eq}$ respectively, was calculated, see figure 2.11.

$$J_{1,eq} = J_{ROBA} + J_{T,500} + J_{Part_1} + \frac{J_{M_2} + J_{M_3}}{i^2} \tag{4.3}$$

Substituting the values in equation (4.3),

$$J_{1,eq} = 0.133811 kgm^2 < 3 \times J_{M_1}$$

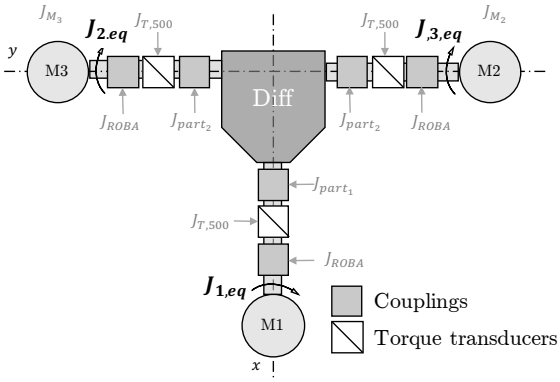

Figure 4.12: Inertia scheme

Assuming that the electrical machine M_2 will rotates at exactly the same speed as electrical machine M_3, $J_{2,eq} = J_{3,eq}$ was calculated using equation (4.4).

$$J_{2,eq} = J_{ROBA} + J_{T,500} + J_{Part_2} + (J_{Part_1} + J_{T,500} + J_{ROBA}) \times i^2 + J_{M_1} \times i^2 \tag{4.4}$$

$$J_{2,eq} = J_{3,eq}$$

Substituting the values in equation (4.4),

$$J_{2,eq} = 1.094 kgm^2 < 3 \times J_{M_2}$$

Chapter

5 Mechanical design

In this chapter, the mechanical design will be described according to the following order: first of all, will be presented the test bench specifications and a summary of the Bosch Rexroth structural profiles; an overview of the mechanical structure will be presented; next, as the structure have 3 main parts, each assembly will be explained in section 5.3; in section 5.4 will be presented the final mechanical solution implemented.

5.1 Test bench structural specifications

To bring together all the components mentioned in previous chapter, a mechanical structure was designed. Additional parts were also designed to fix the electric motors, the torque transducers and the differential to the structure.

The structure of the test bench was designed following several specifications:

- Versatile connection elements;
- Rapid manufacturing acquisition;
- Few parts obtained by machining processes;
- Modular structure;
- Reusable and durable.

Rexroth Bosch Group offers many types of structural profiles complying with these criteria allowing high static and dynamic loads.

The profiles are slotted with 6 mm, 8 mm and 10 mm modular width. All of them within one profile range have the same slot dimensions and spacing to ensure perfect coordination during construction, figure 5.1 [34].

The modular dimensions available for 10 mm width slot are: 40 mm, 45 mm, 50 mm and 60 mm, figure 5.2. The 10 mm slotted profiles are suitable for applications

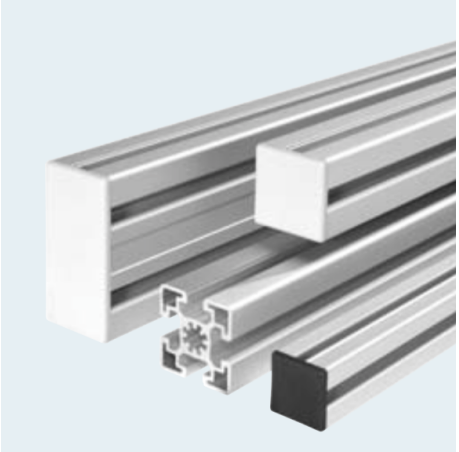

Figure 5.1: Bosch profiles with different slot dimensions

with high loads. Due to its very sturdy design and consequently high degree of robustness, this slot allows maximum strength connections and because of that was the slot dimension selected.

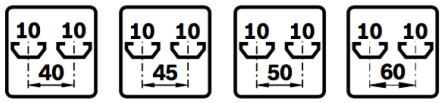

Figure 5.2: Modular dimensions for profile with slot 10mm with

The main dimensions of the electric motors M1, M2 and M3, figure 5.3 are presented in table 5.1 [30].

Table 5.1: M1, M2 and M3 principal dimensions

		$\varnothing D$ [mm]	L [mm]	H [mm]	A [mm]
M1	1PH8137	48	679	317.1	260
M2, M3	1PH8184	65	1047	490	364

The 90 mm was the height dimension chosen for this application (with a 10 mm width slot) because the 90 mm height dimension profiles offers the largest width. Therefore, as the electric motors are very wide ($A = 364$mm), they can seat in the profiles without an exaggerated number of connections.

The material of these structural profiles is AlMgSi 0,5 F25, which corresponds a 6000 series aluminum alloy, the 6063 T6. This material is alloyed with magnesium and silicon and is easy to machine and weldable.

The main properties of this material are presented in table 5.2.

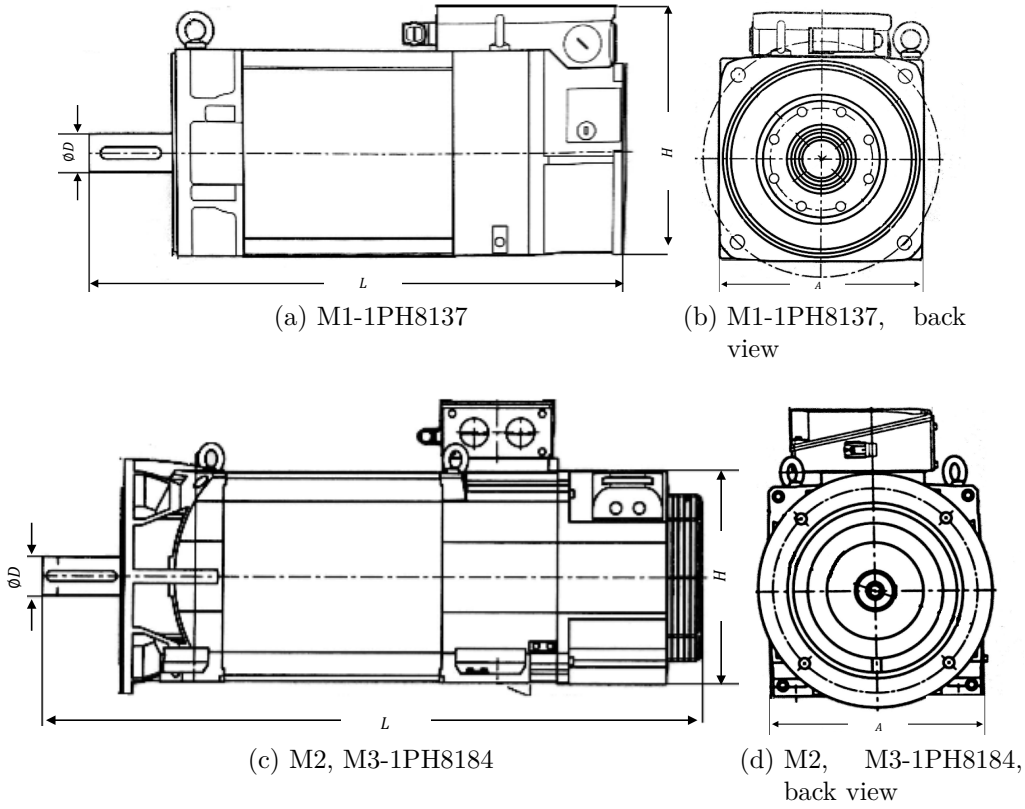

(a) M1-1PH8137

(b) M1-1PH8137, back view

(c) M2, M3-1PH8184

(d) M2, M3-1PH8184, back view

Figure 5.3: M1, M2 and M3 main dimensions

Table 5.2: 6064 Aluminum alloy material properties

Elastic Modulus	E	Pa	6.9×10^{10}
Poisson's ratio	ν		0.33
Shear Modulos	G	Pa	2.58×10^{10}
Mass density	ρ	kg/m^3	2700
Tensile strength	σ_r	Pa	17×10^7
Yield strength	σ_y	Pa	9×10^7
Thermal conductivity	k	$\frac{J}{kg°C}$	900

The profiles that were used are shown in figure 5.4 and their technical data are presented in table 5.3.

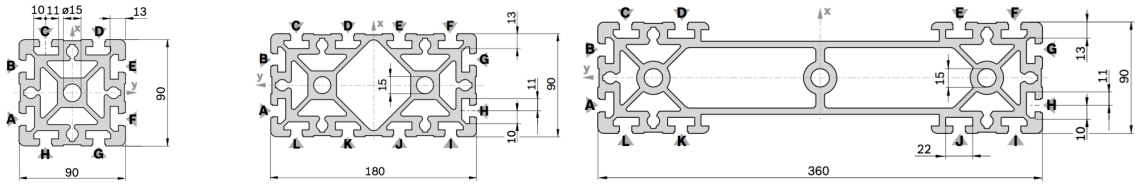

(a) (b) (c)

Figure 5.4: Rexroth profile with 90mm of modular dimension with 10mm slot

Table 5.3: Profiles technical data

	Profile surface $[cm^2]$	Moment of Inertia $[cm^4]$		Torsion Index$[cm^4]$	Mass $[kg/m]$
		I_x	I_y	$I_t = K$	
90×90	38.4	299.8	299.8	118.60	10.4
90×180	63.6	2138.3	544.3	429.00	17.2
90×360	90.2	14 065.0	710.0	937.10	24.4

5.2 Structure overview

An overview of the mechanical structure of this test bench is presented in figure 5.5.

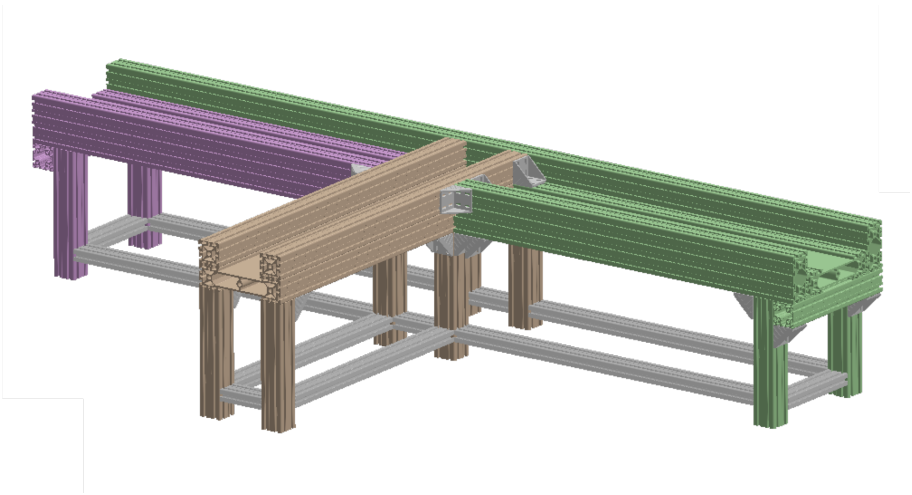

Figure 5.5: Test bench mechanical structure

As shown, the structure is mainly composed by three parts:

- Part 1 - in orange;

- Part 2 - in green;
- Part 3 - in rose.

Parts 1 is composed by 6 legs of 90×90 profile and 3 main profiles: two 90×90 profiles over a 90×360 profile presented in figure 5.6. All of the mentioned profiles, except the legs, are 1500 mm long.

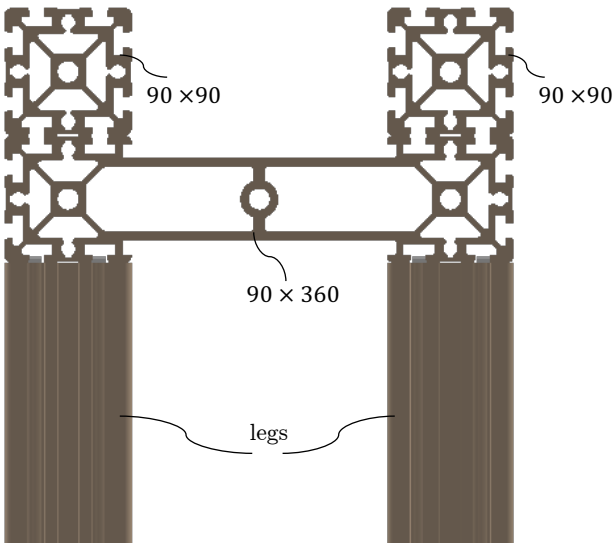

Figure 5.6: Profiles used in part 1

In a similar manner, part 2 is composed by 2 legs and 4 principal profiles, too: 2 90×180 profiles alongside a 90×360 profile. These three profiles are fix to the above of a 90×90 profile, figure 5.7. Part 3 is formed by the same components as the part 2 and they are placed in exactly same way and symmetric. As in part 1, all of the profiles have $1500mm$ long, except the 90×180 profile, placed in the right side of part 2, that has a $3360mm$ and the 90×90 profile ($360 + 2 \times 90 = 540$mm).

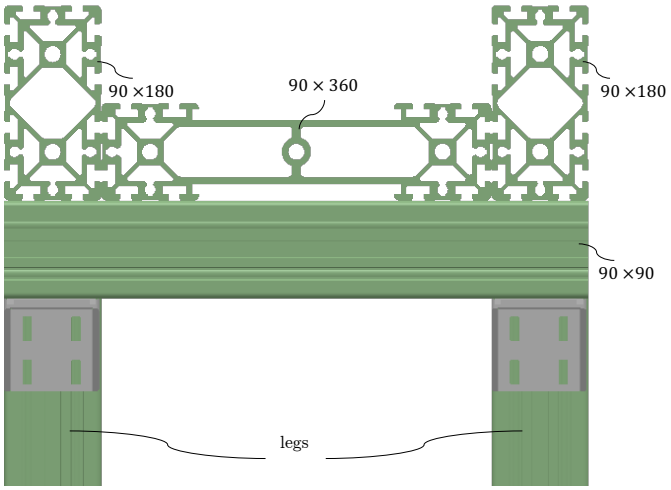

Figure 5.7: Profiles used in part 2

5.3 Assembly

In this subsection the assembly of the mechanical structure will be described, as well as will be mentioned all the components required for this.

5.3.1 Feet for support legs

First of all, 10 base plates have to be fixated into the 10 support legs, figure 5.8 .

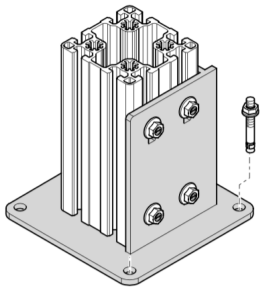

Figure 5.8: Base plate, steel

To fasten these components, for each leg, 4 T-bolts M8 × 20 (no. 3 842 528 715) are needed with the correspondent flange nuts (4 × 3 842 345 082). Finally, to fasten the base plates into the floor, 4 floor dowel are required (4 × 3 842 526 560).

5.3.2 Part 1

Assembly of legs and 90×360

To fasten the legs with 90×360 profile, 6 90/90 brackets (no. 3 842 523 575) are necessary (with this ordering number the fastening components are already included).

(a) (b)

Figure 5.9: Brackets with centering lugs

Connection between 90×360 **and 2** 90×90 **profiles**

To provide a connection between these 3 profiles, 16 $\times$ 2 parallel connector are needed. The corresponding ordering number is 3 842 542 736.

An example of this type of connection is presented in figure 5.10.

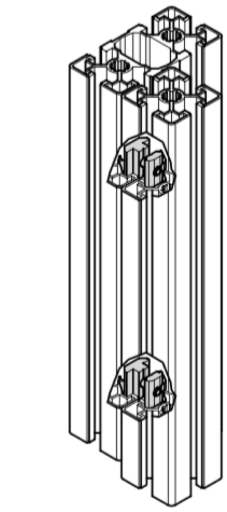

Figure 5.10: Parallel connector for a gap-free connection between two strut profiles

5.3.3 Part 2 and 3

The assembly of part 2 components and part 3 components is done in the same way because these parts are composed by the same components and because of that, only the assembly of part 2 will be explained.

90×180 and 90×360 fixation

To provide the connection between the 90×180 profile and 90×360, 4 90/90 $\times 2$ brackets (no. 3 842 523 575) are required. In addition to this joining, a steel plate was designed, figure 5.11. To fix this plate into both profiles, 8×4 T-nuts (no. 3 842 536 603) and 8×4 EN ISO 4762 M8 $\times$ 25 are necessary.

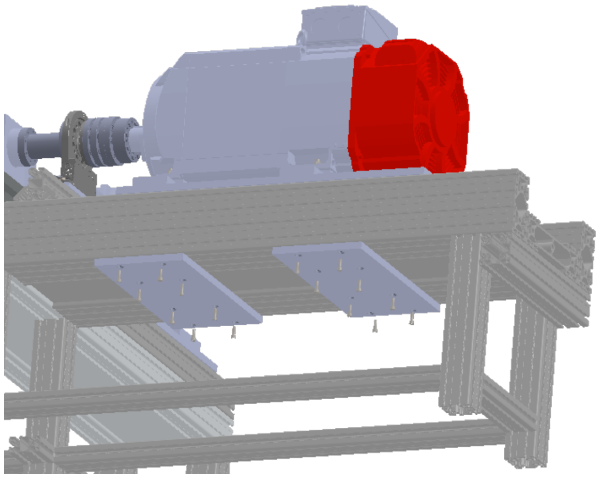

Figure 5.11: Steel plates to connect Bosch profiles

90×180, 90×360 and 90×90 assembly

In order to provide a rigid structure, a 90×90 profile was selected to connect 90×180 and 90×360 profiles at the beginning of part 2 and part 3.

This connection is provided by 4 parallel connectors (4 × 3 842 542 736), using the assembly principle explained in figure 5.12.

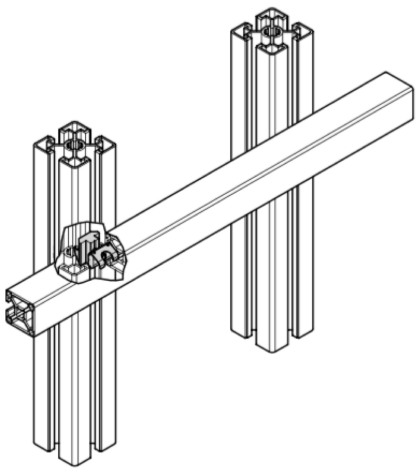

Figure 5.12: Parallel connector for a connection between two perpendicular strut profiles

The connection between this module and the legs of part 2 is made using 4 brackets (no. 3 842 523 575).

5.3.4 Connection between part 1, 2 and 3

To fasten parts 2 and 3 to part 1, 6 brackets (figure 5.9) are needed (no. 3 842 523 575), figures 5.13 and 5.14.

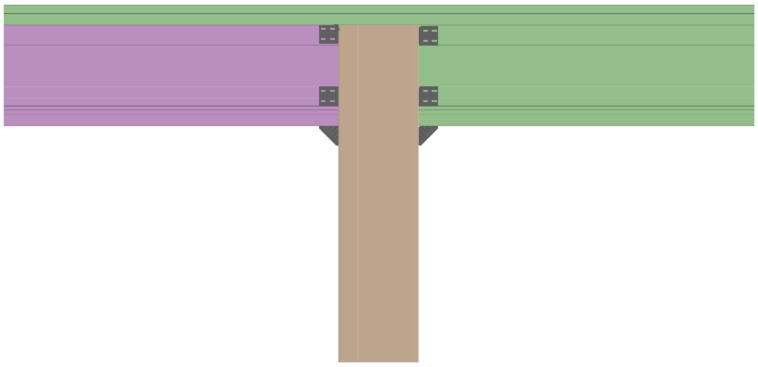

Figure 5.13: Brackets for connection between parts 1, 2 and 3 on the upper side

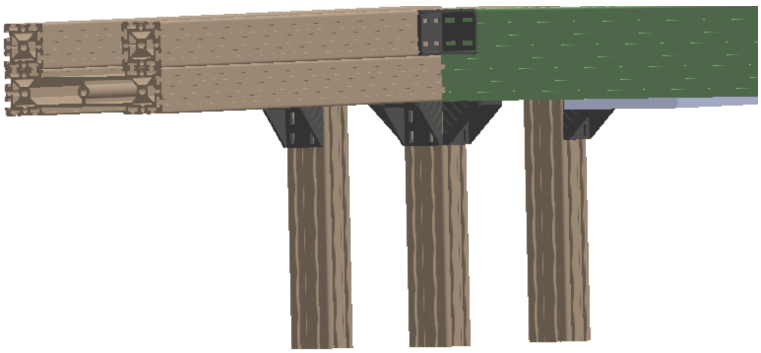

Figure 5.14: Brackets for connection between parts 1, 2 and 3 on the bottom side

5.4 Kinematic chain and assembly

Taking into account the purpose of this test bench - testing rear axles - in this section will be presented the final mechanical solution implemented.

Figure 5.15 presents an overview of the test rig, where all the numbered components are part of the kinematic chain and are referred in table 5.4.

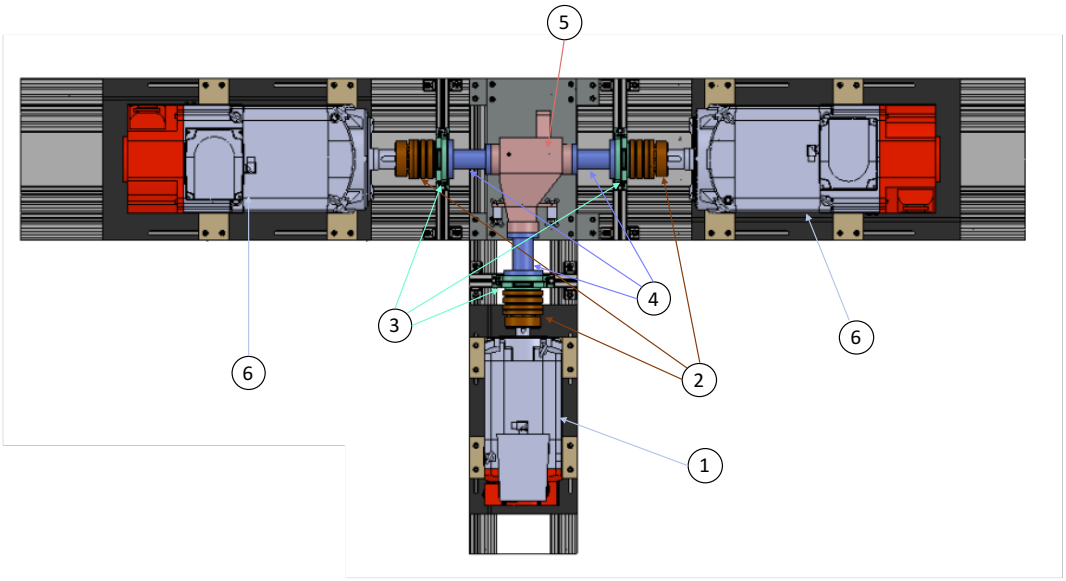

Figure 5.15: Brackets for connection between parts 1, 2 and 3 on the bottom side

Table 5.4: Components of kinematic chain

Kinematic chain	Component	Number of components
1	Electric motor 1PH8137	1
2	ROBA couplings	3
3	T40B torque transducer	3
4	Coupling designed	3
5	Differential	1
6	Electric motor 1PH8184	2

In this section, only the assembly sequence of part 1 will be described because the mounting sequence and the components of all the main structure parts are similar.

Finally, the design of the differential support will be described.

5.4.1 Electric motor support

The selected mounting position of M1, M2 and M3 electric motors was IMB3, i.e., horizontal shaft and "feet on floor", figure 5.16. With this mounting position the alignment is easily obtained.

To fix the electric motors to a metal plate (that is fasten in Bosch profiles) a foot was designed, figure 5.17.

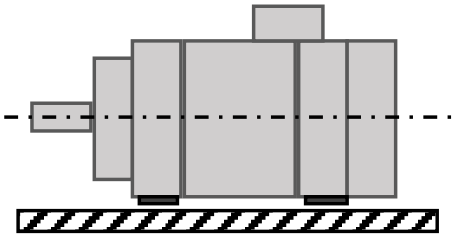

Figure 5.16: Type of M1, M2 and M3 mounting position

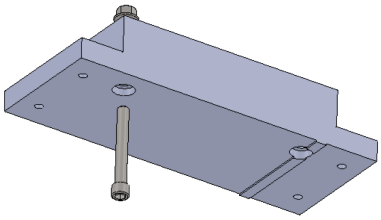

Figure 5.17: Foot for M1

To make the electric motor M1 and feet connection, 4 screws: M12 × 90 EN ISO 4762 - 36N5 and as well as 4 flange nuts DIN 6923-M12-N5 are required.

To allow faster assembly and minimize the risk of damage the Bosch profiles during that operation, a steel plate was also designed, figure 5.18.

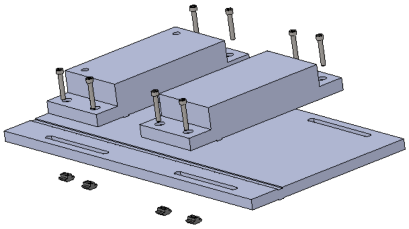

Figure 5.18: M1 metal board with T-nut and screws

The feet are fixed to the metal plate, and the last, in time, will fix in Bosch profiles, using 2 × 4 T-nut (no. 3 842 536 603) and 2 × 4 EN ISO 4762 M8 × 50 screws.

To provide an easier alignment between the electric motors and the profiles it was designed a metal plate and two feet. The metal plate is situated between the Bosch profile and the feet. The face that slights on the Bosch profile should have low roughness and the plain tolerance should be around 0.05 mm. In the machining process of this face, a longitudinal rule should be also machined. This rule will guide

the metal board through the Bosch profile. In the opposite side, a parallel slot was designed to align the feet and the motor it self. All the horizontal faces that are parallel to the Bosch profile must have plain and parallelism tolerances of 0.05mm and 0.1mm, respectively. This way, the parallelism between the motor axis and the horizontal plan are improved. This will be important to do not create external loads that deteriorate the transducer measurement.

5.4.2 Connection between electric motor and ROBA® coupling

The electric motors M1, M2 and M3 have a feather key as shaft extension.

To connect the motors shafts to the torque transducers it is necessary a coupling, already mentioned in section 4.3.

5.4.3 Connection between ROBA® coupling and torque transducer

ROBA couplings are specially designed for T40B HBM torque transducers.

To connect the coupling to the rotor of the transducer 8 × M10 × 25 screws are needed, figure 5.19.

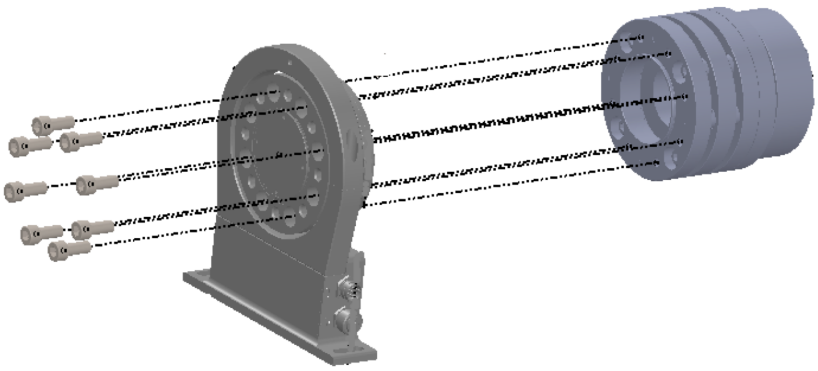

Figure 5.19: Connection between Roba coupling and torque transducer

Finally, another component was required to install the stator of the transducer. This part is fasten in a 45 × 90 Bosch (no. 3 842 548 756) profile with 300 mm long in part 1 and 540 mm long in parts 2 and 3.

5.4.4 Connection between torque transducer and propeller shaft flange

A component was designed to provide the connection between the torque transducer and the propeller shaft, shown in figure 5.20

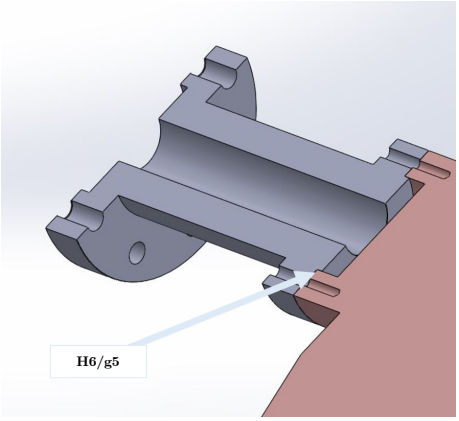

Figure 5.20: Modeled part for flanges connection

The guide between the differential flange and the part modeled has a tolerance H6/g5 that provides an accurate mechanical guidance. However, ROBA coupling is abble to absorve an angular misalignement of 0.6°. Those two parts are fixed by 4 × M8 and 4 × M6 fasteners.

5.4.5 Differential support

The BMW E46 differential has 3 machined faces for supports: 2 of them have screws M8. To align and provide the differential stabilization 3 shims are needed. To fix the shims, a steel block was designed. These components described were designed and are presented in figure 5.21

The differential shown in figure 5.21, is a sketch of the real one, with the same outside dimensions.

To provide easier assembly, the steel plate has pockets to allocate the shims. These connection as a H8/g8 tolerance, which gives an assembly that can be done by hand, see the row of figure 5.21. Finally, to fix the steel plate on the Bosch profiles, 4 feet were also modulated.

To fasten the feet to the steel plate, 8 EN ISO 4762 M8 × 35 screws are required and to fasten the feet in bosch profiles, 8 T-nuts (no. 3 842 536 603) and 8 EN ISO 4762 M8 × 35 screws are required, too.

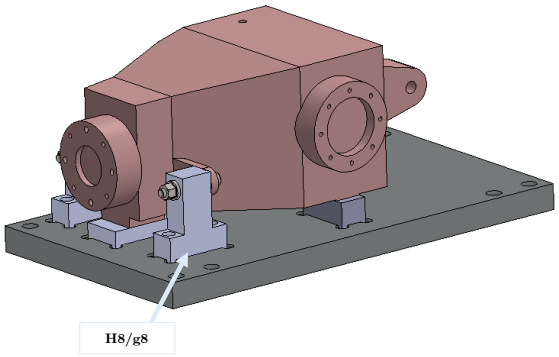

Figure 5.21: Differential with shims screwed

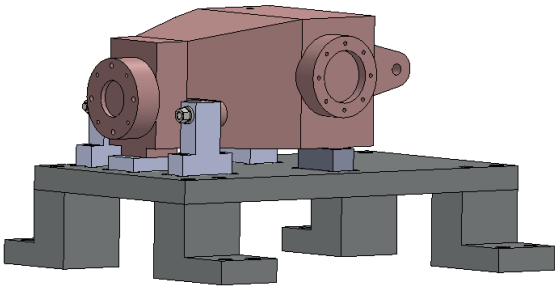

Figure 5.22: Differential with shims screwed

5.5 Mechanical solution validation

Once found an appropriated mechanical solution it is necessary to validate it considering the stresses applying by the component's supports (motor, torque transducers and differential). The structure will face mainly torsion efforts, i. e., the external loads are twisting moments. As these applied efforts are simple a model was created and the correspondent analytical solution will be presented.

Straight bars of uniform circular section under pure torsion

Consider a straight bar with an uniform circular section of an homogeneous isotropic material. Applying a twist couples at its ends in plane normal to its axis, the bar will twists, each section will rotates about its torsional center, figure 5.23.

If θ were the angle of twist, M_t were the twisting moment, l the length of the member, J the polar moment of the section and G the shear modulus, the θ can be calculated as,

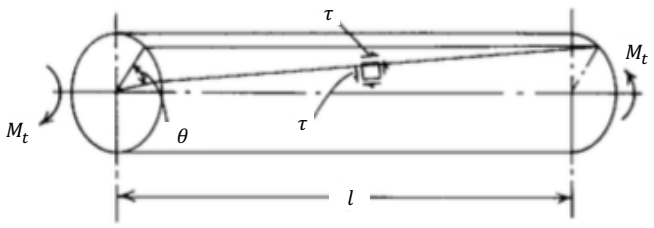

Figure 5.23: Deformation and stresses of a circular bar twisting

$$\theta = \frac{M_t l}{JG} \tag{5.1}$$

Bars of noncircular uniform section under pure torsion

Considering a noncircular cross section of a bar, and considering all the assumptions of the previous subsection, θ can be expressed as,

$$\theta = \frac{M_t l}{KG} \tag{5.2}$$

where K is a factor dependent on the form and dimensions of the cross section. For a circular section K is the polar moment of inertia J, equation (5.1), for other sections K is less than J and may be only a very small fraction of J.

As mentioned before, a model was created in order to know the maximum twisting angle of each basis cross section and these values should be compared to the maximum angle of twisting recommended in the literature for an equivalent material, in order to verify the structural criteria.

As presented in previous sections, the structure is basically composed by three parts, figure, 5.24.

To calculate the twisting angle suffered by each cross section part, θ_1, θ_2 and θ_3, respectively, the connection between part 1 and part 2 was considered rigid, and the connection between part 1 and part 3 was considering rigid too.

As shown before, K is a fraction of J; J, the polar moment of a cross section, is the sum of the moments of inertia I_x and I_y. Thus, the J of each profiles was calculated and is presented in table 5.5.

θ_1,θ_2 and θ_3 are calculated from the torsion center which coincides with the geometric center, G_1 and $G_2 = G_3$, of each part cross section, figures 5.25 and 5.26. Using equations (5.3) and (5.4), y_{G_1} and $y_{G_2} = y_{G_3}$ were determined.

$$A_A \cdot y_A + A_B \cdot y_B + A_C \cdot y_C + A_D \cdot y_D = (\sum A_i) \cdot y_{G_1} \tag{5.3}$$

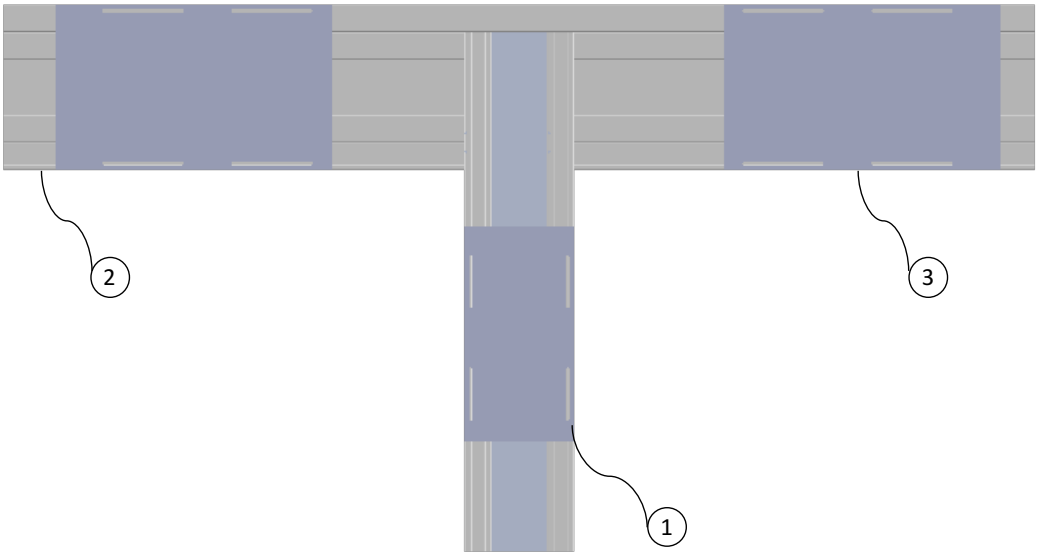

Figure 5.24: Main parts of the mechanical structure

Table 5.5: Polar moment of the Bosch profiles section

Profile	J cm^4
90×90	599.6
90×180	2682.6
90×360	14 775

$$y_{G_1} = 11.07cm$$
$$A_E \cdot y_E + A_F \cdot y_F + A_G \cdot y_G + A_H \cdot y_H = (\sum A_i) \cdot y_{G_2} \tag{5.4}$$
$$y_{G_2} = y_{G_3} = 11.76cm$$

The areas of profiles A, B, C, E, F and G are presented in table 5.3. The area of parts D and H are $A_D = 54 \times 2cm^2 = 108cm^2$ and $A_G = 36 \times 2mm^2 = 72cm^2$.

Looking at equation (5.2), it can be noticed that K, the fraction of the polar moment of each part cross section, must be calculated at geometric centers. In order to calculate, $K_A^{G_1} = K_B^{G_1}$, $K_C^{G_1}$, $K_D^{G_1}$, $K_E^{G_2} = K_F^{G_2}$, $K_G^{G_2}$ and $K_H^{G_2}$ it was assumed that,

$$\frac{K_i}{J_i} = \frac{K_i^{G_j}}{J_i + A_i \times d_i^2} \tag{5.5}$$

where d_i, is the distance between the geometric center of the total cross section and

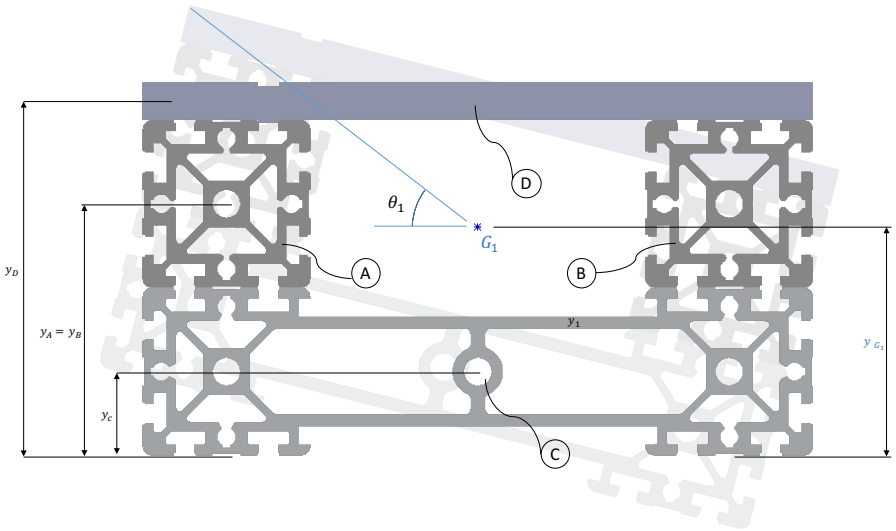

Figure 5.25: Part 1 cross section

the geometric center of each component for the total cross section, $i = A, B, C...H$ and $j = 1, 2$, respectively.

K_D and K_H were calculated using equation 5.6 [35],

$$K = ab^3 \left[\frac{16}{3} - 3.36 \frac{b}{a} \left(1 - \frac{b^4}{12a^4} \right) \right] \tag{5.6}$$

where a and b dimensions, figure 5.27 are $a = 18$cm, $b = 1$cm in part D and $a = 27$cm, $b = 1$cm in part G.

Figure 5.27: Solid rectangular section

Using equation (5.5), each $K_i^{G_j}$ was calculated and the correspondent values are presented in table 5.6.

The maximum twisting moment felt by part 1 is $Mt = 170$Nm.Using equation (5.7), θ_1 was calculated.

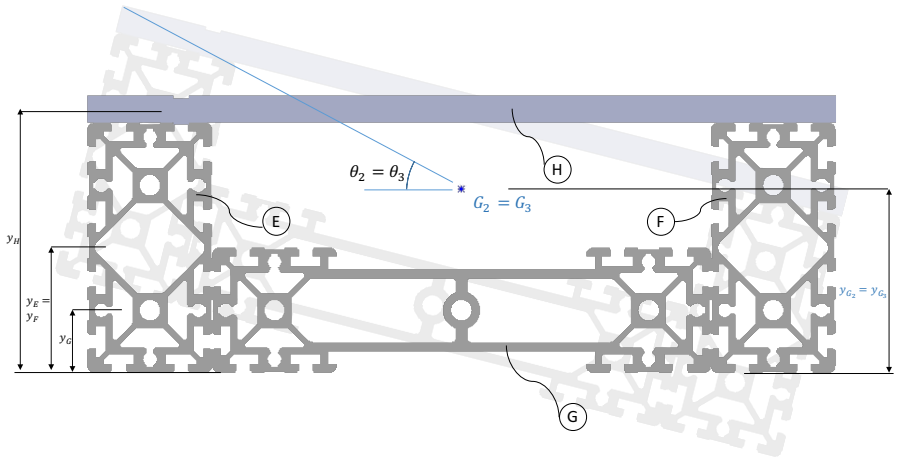

Figure 5.26: Part 2 cross section

Table 5.6: K's of the component parts cross sections at the center of torsion

$K_i^{G_j}$	cm^4
$K_A^{G_1} = K_B^{G_1}$	1525.87
$K_C^{G_1}$	1238.64
$K_D^{G_1}$	136.841
$K_E^{G_2} = K_F^{G_2}$	5622.24
$K_G^{G_2}$	1184.04
$K_H^{G_2}$	176.986

$$\theta_1 = \frac{M_t l}{K_{G_1} G} \tag{5.7}$$

where

$$K_{G_1} = K_A^{G_1} + K_B^{G_1} + K_C^{G_1} + K_D^{G_1} \tag{5.8}$$

$$\theta_1 = \frac{170 \times 1.5}{K_{G_1} G}$$

$$\theta_1 = 0.0128°$$

Applying the same principle θ_2 was calculated too, but M_t in time is equal to 270Nm.

$$\theta_2 = \frac{M_t l}{K_{G_2} G} \tag{5.9}$$

where

$$K_{G_2} = K_E^{G_2} + K_F^{G_2} + K_G^{G_2} + K_H^{G_2} \tag{5.10}$$

$$\theta_2 = 0.00714^\circ$$

The maximum twisting angles, θ_1 and θ_2 are both less than $0.15^\circ/foot$, that is equivalent a $\theta = 0.7^\circ$ for the same length ($l = 1500$mm) [36].

Chapter 6

Automation project design

LabView is a graphic programming system from National Instruments that CETRIB uses in all of their bench tests. Thus, this software was selected to make the test rig automation and data acquisition.

LabView programs are called Virtual Instruments (VIs) and comprise two components:

- The front panel that accommodates the user interface;
- The block diagram that shows the graphic program code.

Using a network connection there are two main architectures that can be adopted: use LabView as graphical interface and use a Siemens PLC or using LabView as graphical interface and controller.

In this chapter these possibilities will be discussed.

6.1 Speed acquisition

In order to obtain measurements that allow the analysis of the axle efficiency, the velocity of the drive shafts and the propeller shaft has to be known. The electric motors M1, M2 and M3 have two types of encoders: incremental and absolute.

As the variable to control is not position but speed, an absolute encoder is not needed for this application. Thus, an incremental encoder with $22bit$ was chosen, which means that, if this incremental encoder has 2^{22} pulses per revolution (ppr), the resolution of it is equal to,

$$Res_{enc} = \frac{360^\circ}{2^{22}} \tag{6.1}$$

$$Res_{enc} = 0.00008583^\circ$$

The internal acquisition time of the drive speed, T, is 0.667ms, which corresponds to a speed resolution of

$$Res_{speed} = \frac{\frac{1}{2^{22}}}{T} \tag{6.2}$$

$$Res_{speed} = 0.02rpm$$

The speed data acquisition should be at $f = 1$ Hz. At the same acquisition frequency, three analog outputs from the torque transducers have to be read and saved, too. As mentioned before, the output range of them is ±10V.

6.2 Temperature acquisition

The efficiency of lubricants depends strongly on the friction properties of the lubricant employed. For the design of modern highly efficient lubricants it is thus essential to understand the influence of the components of the lubricating fluid in terms of film formation and consequent friction which strongly depends on lubricant temperatures.

Thus, five temperatures have to be registered at a frequency of $f = 0.5$ Hz.

The maximum permissible error for this measurement is $\pm 1°C$.

6.3 Measurement of temperature

Temperature is one of the most frequently measured physical quantities. Several techniques can be used in temperature measurement: thermometers whose sensor element is a resistance or measurement based on the use of thermocouples [37].

6.3.1 Resistance thermometers

Resistance thermometers cover a range from -250 to $+850°C$, with excellent accuracy and very good stability. Moreover, they provide an electric output signal which is a very important feature.

Resistance thermometers are based on sensor elements that present a resistance change with temperature variation. The sensor elements first used were of metallic type and were usually called Resistance Temperature Detectors (RTDs).

The most popular metal alloy for this sensors is platinum. Platinum is a noble metal, non-reactive across a wide temperature range, and presents a very linear response, figure 6.1 [37].

The strong points of RTD's are:

- Great accuracy;

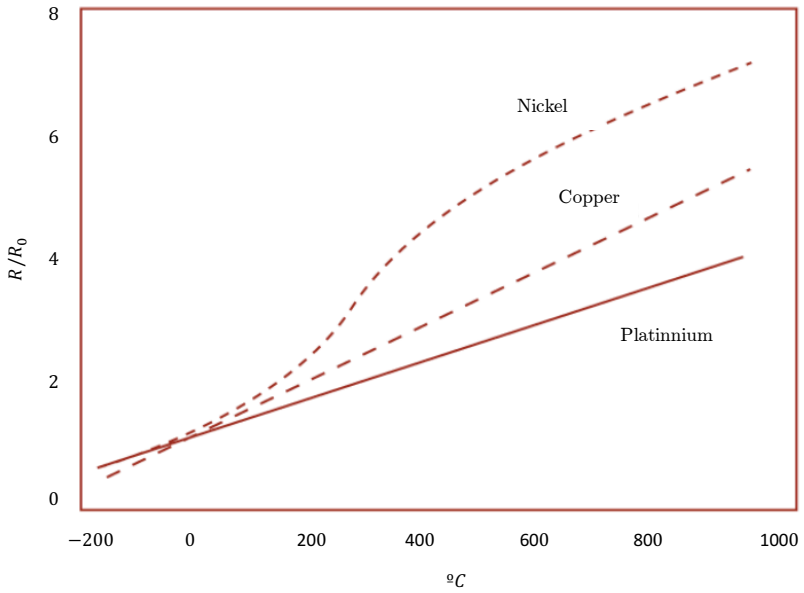

Figure 6.1: Variation of resistance with temperature for platinum, copper and nickel

- Great stability;
- Good linearity;
- Absolute measurement of temperature (without needing a reference temperature).

On the other hand, the weak points of RTD's are:

- Expensive;
- Large response time;
- Power supply requirement;
- Self-heating.

6.3.2 Thermocouples

One of the techniques employed in the measurement of temperature is based on the use of thermocouples.

Thermocouples are robust, versatile and wide in range, reading temperatures from -200 to $2000°C$. They present an important feature: their output is an electrical voltage [37].

Operating principle

The operating principle of thermocouples is based on Seebeck effect, i.e., if two metallic conductors A and B (pure metals or alloys) form an open circuit with two AB junctions (Y_1, Y_2) at different temperatures T_1 and T_2, a thermal electromotive force, ε, will appear on their terminals. The value of this greatness depends on the materials A and B and on the junction temperatures T_1 and T_2, figure 6.2 [37].

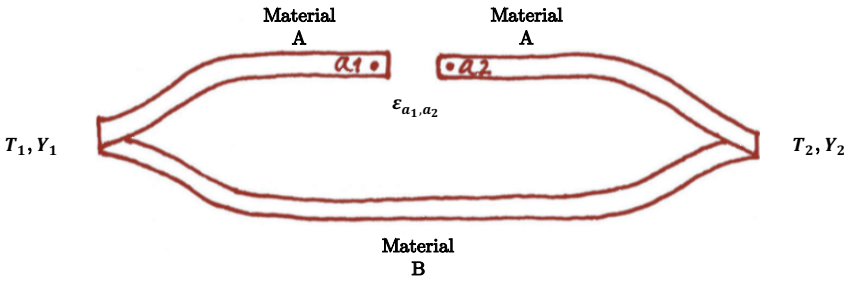

Figure 6.2: Seebeck effect

This set of two associated material A and B with two junctions is called thermocouple [37].

If one of the junctions is maintained at a known constant temperature T_1, the other junction temperature may be calculated by measuring the thermoelectric force value generated by the thermocouple. A thermocouple therefore allows differential measurement of temperature [37].

Types of thermocouples

Combinations of different materials A and B correspond to different thermocouples. Some material combinations have been defined as standard and named T, J, K, E, etc.

For each type of standard thermocouple there is a standard table that gives the temperature of the "hot junction" (or measuring junction) corresponding to the thermoelectric electromotive force produced by the thermocouple, assuming the "cold junction" is at a reference temperature, $0°C$ [37].

This type of temperature transducers produces a rather low signal, in general not exceeding some dozen of mV for the extreme temperatures of the range. Table 6.1 presents several standard thermocouples, indicating for each one the respective operation range and the corresponding electromotive force amplitude [37].

The relation between temperature and the thermocouple thermoelectric electromotive force is called the Seebeck coefficient or sensitivity. This greatness throughout the respective measurement ranges is, frequently, a highly nonlinear function.

Table 6.1: Standard thermocouples

Thermocouple	$°C$	$\varepsilon[mV]$
Copper/Constantan (T-type)	-164 to 350	-5.602 to 17.816
Iron/Constantan (J-type)	0 to 749	0 to 42.283
Cromel/Constantan (E-type)	-164 to 885	-8.824 to 68.783
Cromel/Alumel (K-type)	-164 to 1250	-5.973 to 50.633

The K-type thermocouple is an exception to this characteristic. This thermocouple type presents a nearly constant sensitivity, around 40 $\mu V/°C$ between 0 and 1000$°C$, corresponding to a nearly linear relation between temperature and thermoelectric electromotive force, figure 6.3 [37].

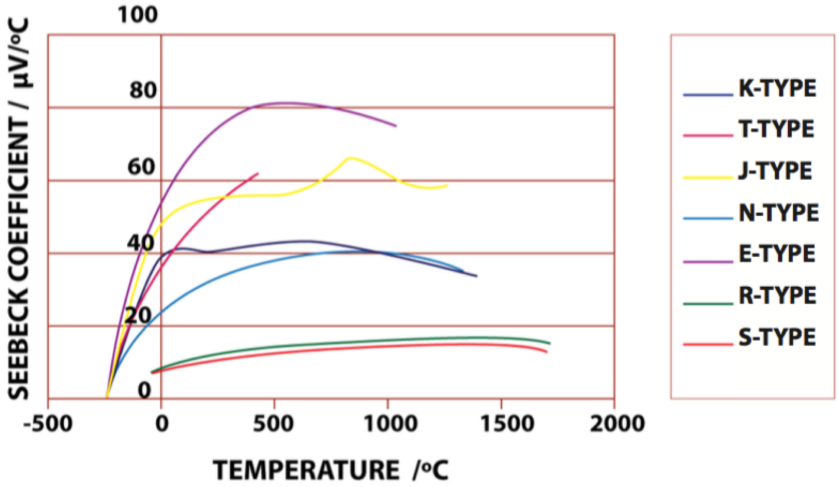

Figure 6.3: Sensitivity of different thermocouple types

The strong points of thermocouples are:

- Strong points;
- Self-powered;
- Wide variety;
- Inexpensive;
- Wide temperature range: $-200°C$ to 2000$°C$;
- Robust and simple;
- No self-heating problems.

On the other hand, the weak points are:

- Non-linear;
- Requires a well known temperature reference;
- Low level voltages.

As the maximum permissible error of temperature measurement is $\pm 1°C$ the thermocouple that was chosen was the T-type, Class 1. The main characteristics of these sensors are presented in table 6.2, the reference temperature is $0°C$ [38].

Table 6.2: Tolerance classes for thermocouples according to the IEC 60 584-2:1995

Thermocouple	Class 1
Temperature	$-40°C \leq T \leq 125°C$
Tolerance	± 0.5
Temperature	$125°C \leq T \leq 350°C$
Tolerance	$\pm 0.004 \cdot T$

6.4 PROFIBUS vs PROFINET

To make the communication between the field devices and the controllers it has be found an architecture. There are two possibilities available for making this connection: using a data acquisition board (DAQ) or using a network communication.

As the brand selected for drive system was SIEMENS and it already has standard solutions using a network connection, the network communication was the architecture selected.

The two main networks that Siemens offers to make the communication between the field devices and the controllers are PROFIBUS and PROFINET.

PROFIBUS DP (Decentralized Peripherals) is a network that is made up of two types of devices connected to the bus: master devices and slave devices. It is a bidirectional network, meaning that one device, a master, sends a request to a slave, and the slave responds to that request. With PROFIBUS each port has to be individually configured, in the other hand [39].

Based on Industrial Ethernet, PROFINET enables direct communication of field devices (IO Devices) with controllers (IO Controllers).

Nowadays, PROFINET is the industrial network that provides higher transmission speeds and shorter port configuration times. In PROFINET the IP address can be automatically assigned. Base on these advantages, the communication protocol that was selected was the PROFINET [30].

6.5 LabView as PROFINET controller

In order to integrate real hardware (Sinamics S120 converters), with the measurement system, it is necessary that this hardware is directly connected to LabView, figure 6.4.

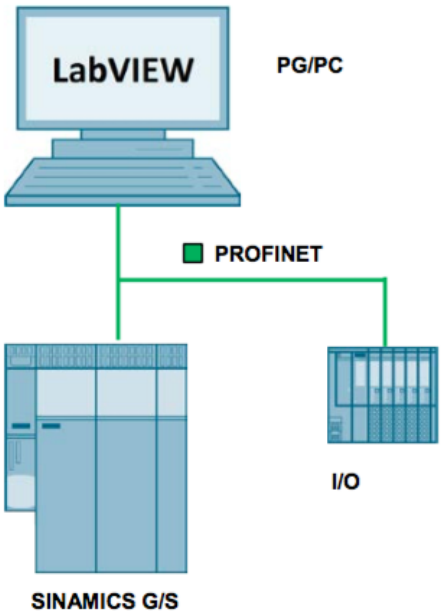

Figure 6.4: Labview as PROFINET controller

PROFINET is available for establishing a connection between Sinamics drivers, PROFINET I/O devices and LabView via a standard Ethernet interface.

The application comprises a PROFINET communication driver for controllers, a DLL (dynamic link library), which is integrated in LabView and which is executed there,i.e., it serves as the interface between the LabView user program and the PROFINET IO devices. It provides functions, which control the communication and allow cyclic IO data to be transferred. This provides functions for communication with PROFINET I/O devices directly from *LabView*.

This solution has many advantages such as:

- Shorter time and lower costs when implementing the solution;
- Simple integration of the communication driver;
- Simple control of SINAMICS drives from LabView;
- Integration of additional PROFINET IO devices in LabView;

Figure 6.5: Flowchart

- Connection via standard Ethernet interface.

However, as a limit: using this architecture, high demands on real-time communication are not assured and therefore, this is not a viable option [40].

6.6 Controller-based

Siemens provides basic and advanced controllers. The S7-1200 is a family of basic controllers with compact design for simple automation tasks [41].

The S7-1500 is a advanced controller projected for complex plants with high demands in terms of speed and deterministic response. Furthermore, this controllers don't have integral I/O, they have to be purchased separately, which configures to it a final price much higher than the basic controllers.

This application doesn't require high demands in terms of speed and deterministic response, thus, the most appropriated family of controllers is the basic one [41].

After contact Siemens, the basic controller more appropriated for this application is the S7-1214, figure 6.6.

Figure 6.6: Simatic S7-1214 basic controller

This component has 16 inputs:

- 14 digital;

- 2 analog ranging from 0 to 10V.

The outputs available are:

- 10 digital.

The HMI role keeps to be played by LabView, which continues to communicate with the other field devices by PROFINET.

6.6.1 Analog module for torque transducers

As the output signal of the torque transducers ranging between −10V and 10V, the analog input integrated on the PLC S7-1214 cannot be used. Thus, one I/O module was selected to read the values provid by the three HBM T40B which reference is 6ES7231-4HD32-0XB0. The characteristics of these I/O module are presented on table 6.3 [41].

Table 6.3: 6ES7231-4HD32-0XB0 main characteristics

Analog inputs	4; current or voltage differential inputs
Input ranges	
Voltage	$10; 5; 2.5$
Current	4 to 20mA; 0 to 20mA
Analog value creation	
Resolution with overrange	12 bit;+sign

As referred before, the output signal of the torque transducers is $\pm 10V$, thus, using this voltage input range, the resolution of torque measure will be,

$$R_{torque} = \frac{500Nm}{2^{12}}$$

$$R_{torque} = 0.1221Nm \tag{6.3}$$

The torque resolution is 12 times smaller than the accuracy of the transducer which doesn't commits the measure according to its accuracy class.

6.6.2 Analog module for thermocouples

Another I/O module was selected to read the values provide by the five thermocouples which reference is 6ES7231-5QF32-0XB0, figure 6.7 [41].

The characteristics of these I/O module are presented on table 6.3.

Figure 6.7: Analog Input, SM 1231 TC, 8 AI Thermocouple for Simatic S7-1200

Table 6.4: 6ES7231-5QF32-0XB0 main characteristics

Analog inputs	8; Thermocouples
Technical unit for temperature measurement adjustable	Degrees celsius/Degrees fahrneit
Input ranges	$10; 5; 2.5$
Thermocouple	Type J, K, T, E, R, S, N, C, TXK/XK(L); voltage range: $\pm 80mV$
Resolution with overrange	15 bit;+sign

The resolution of the analog module is:

$$R_{voltage} = \frac{80mV}{2^{15}}$$

$$R_{voltage} = 0.00244mV \tag{6.4}$$

By looking at figure 6.3 and the temperature measurement range (20° C - 120° C), the worst sensitivity was considering to calculate the correspondent temperature resolution.

$$S_{@20°C} \approx 40\mu V/°C$$

$$R_{temperature} = \frac{R_{voltage}}{S_{@20°C}}$$

$$R_{temperature} = 0.052°C \tag{6.5}$$

Comparing the value obtained in equation (6.5) and the maximum error provided by the thermocouple, the analogue module is adequate for this application.

Chapter 7

Conclusions and future work

7.1 Conclusions

The aim of this project was to design the mechanical and automatic project for a rear axle transmission test rig.

After do the review of the state of the art, it was noted that instead of using a brake test bench where all the power provided for the electric machines, working as motor modes, would be consumed by the two brake dynamometers and could not be reused, it would be interesting to use a drive system where energy recovery was available. Using this architecture, the drive system just has to get the energy from the network who lost in system power losses.

Two different drive systems with energy recovery where compared. As the electrical drive system has machines that have an efficiency around 93%-95% and hydraulic machines around 89%, when doing a test with positive torque flux, for example, it can be saved 20% in system losses, when using an electrical drive system. Due to that, the hydraulic secondary control drive system was stayed out.

After searching the laboratory tests for measuring the vehicle's CO_2 emissions and taking as a start-point the BMW 318d, the power and torque requirements for the test bench drive system were defined. For the machine that plays the role of gearbox, M1, it is necessary to have 170Nm at 3660rpm ($P_{M1} = 63.5$kW). For the machines that plays the role of the wheels's load, M2 and M3, it is necessary to have 270Nm at 1300rpm($P_{M2,M3} = 37$kW). With these requirements, the electric machines were chosen as well as the correspondents drives and a compatible power supply.

In order to test the several situations whereby the differential is normally subjected, the power flow of the test bench for simulating acceleration, braking and curves was also defined.

To provide an accurate measurement of the torque applied in each differential shaft, three torque transducers were selected, as well as couplings that ensures a correct connection between the electric motors and the transducers. With ROBA couplings the misalignment and assembly errors can be compensated.

The final kinematic chain solution chosen permits the torque losses measurements in the differential transmission. With the mechanical structure all of the kinematic chain components can be positioned. The correspondent assembly and exploded drawings are presented in the present report.

Finally, a PLC and the correspondent necessary analog modules was chosen as a command solution, using LabView as a graphical interface. The analog modules selected for measuring the output of the torque transducers has 13-bits which provides a compatible resolution according to the torque transducers accuracy class. Additionally, thermocouples where selected which provide a $\pm 1^{\circ}$ of maximum error. The analog module for measuring these data where selected and the correspondent resolution is compatible with the maximum permissible error.

7.2 Future works

As future works, it will be interesting to design a control system for controlling the differential temperatures, using a fan and a heater.

To provide the electric power, to do the signal conditioning, protection and cutting functions an electric box should be also designed.

Finally, in order to join all the information and making the command function, the PLC has to be programmed as well as LabView interface.

References

[1] European Automobile Manufacturers Association. Passenger cars. http://www.acea.be/automobile-industry/passenger-cars, 2016. *[visited on 2016-05].*

[2] European Automobile Manufacturers Association. Economic and market report eu automotive industry quarter 1 2016. http://www.acea.be/uploads/statistic_documents/Economic-and-Market-Report-Q1-2016.pdf, 2016. *[visited on 2016-05].*

[3] European Automobile Manufacturers Association. New passenger car registrations by engine capacity and power. http://www.acea.be/statistics/tag/category/cubic-capacity-average-power, 2016. *[visited on 2016-05].*

[4] European Automobile Manufacturers Association. New passenger car registrations by manufacturer. http://www.acea.be/uploads/press_releases_files/20160513_PRPC_1604_FINAL.PDF, 2016. *[visited on 2016-08].*

[5] Rear Wheel Drive Association. List of new rear wheel drive cars. http://www.rearwheeldrive.org/rwd/rwdlist.html, 2016. [*[visited on 2016-04].*

[6] BMW. The BMW 3 series saloon, 2015.

[7] S. Evans. Delivering axle efficiency and fuel economy through optimised fluid design. *SAE techincal paper*, 2014.

[8] European Automobile Manufacturers Association. Alternative powertrains. http://www.acea.be/industry-topics/tag/category/alternative-powertrains, 2016. *[visited on 2016-03].*

[9] European Automobile Manufacturers Association. Emissions testing, laboratory tests. http://www.acea.be/industry-topics/tag/category/laboratory-test, 2016. *[visited on 2016-02].*

[10] T. J. Barlow, S. Latham, I. S. McCrae, and P. G. Boulter. *A reference book of driving cycles for use in the measurement of road vehicle emissions.* Published Project Report, 2009.

[11] The international council on clean transportation. The wltp: How a new test procedure for cars will affect fuel consumption values in the eu. http://www.theicct.org/sites/default/files/publications/ICCT_WLTP_EffectEU_20141029.pdf, 2016. *[visited on 2016-02].*

[12] DieselNet. Emission test cycles common artemis driving cycles. https://www.dieselnet.com/standards/cycles/artemis.php, 2016. *[visited on 2016-03].*

[13] V.A.W. Hillier and P. Coombes. *Hillier's Fundamentals of Motor Vehicle Technology.* Number liv. 1 in Hillier's Fundamentals of Motor Vehicle Technology. Nelson Thornes, 2004.

[14] J.Y. Wong. *Theory of Ground Vehicles.* Wiley-Interscience. Wiley, 2001.

[15] S. Day, G. Lechner, and H. Naunheimer. *Automotive Transmissions: Fundamentals, Selection, Design and Application.* Springer Berlin Heidelberg, 1999.

[16] B.E. MR. Anant Shivaji Kolekar. *Lubrication & efficiency of rear wheel drive axles in road vehicles.* PhD thesis, Imperial college London, 2013.

[17] D. Porrett, S. Miles, E. Werderits, and D. Powell. Development of a laboratory axle efficiency test. *SAE techincal paper*, 1980.

[18] K. Bjornen, H. Chambers, and D. DeGonia. Development of a fuel efficient multipurpose 75w-90 gear lubricant. *SAE techincal paper*, 2003.

[19] H. Heisler. *Vehicle and Engine Technology.* SAI (Engineering Society for Advancing Mobility Land Sea Air and Space International), 1999.

[20] B. Heißing and M. Ersoy. *Chassis Handbook: Fundamentals, Driving Dynamics, Components, Mechatronics, Perspectives.* ATZ/MTZ-Fachbuch. Vieweg+Teubner Verlag, 2010.

[21] D.A. Crolla. *Automotive Engineering: Powertrain, Chassis System and Vehicle Body.* Butterworth Heinemann. Butterworth-Heinemann, 2009.

[22] BMW blog. Dct transmission: How they work and why we use them. http://www.bmwblog.com/2015/07/09/dct-transmission-how-they-work-and-why-we-use-them/, 2015. *[visited on 2016-08].*

[23] European committee of manufacturers of electrical machines and power electronics. Energy-ef ciency with electric drive systems, 2015.

[24] SIEMENS. Energy-efficient drives, 2009.

[25] Bosch Rexroth Group. Secondary control technology. `http://fluidpowerjournal.com/wp-content/uploads/2012/12/secondary-control-pp.pdf`, 2012. *[visited on 2016-04].*

[26] Energias de Portugal. Tarifas e horários, 2016.

[27] Bosch Rexroth. Axial piston variable pump a4vso, 2009.

[28] Bosch Rexroth Group. Secondary control with a4vso axial piston units, 2016.

[29] Bosch Rexroth. Digital controller assembly hnc100-sek for the secondary control of axial piston units, 2011.

[30] SIEMENS. Simotion, sinamics s120 & simotics equipment for production machines, 2013.

[31] Bosch Rexroth. A4vso series 10, 11 and 30, re 92050/04.09, 2009.

[32] Hbm. T40b data sheet, 2016.

[33] Mayr. Roba®-ds 9110 / 9210, 2016.

[34] Bosch Rexroth Group. Basic mechanic elements, 2015.

[35] C. Young Warrem and Richard G. Budynas. *Roark's Formulas for Stress and Strain.* Seventh Edition. McGraw-Hill, 2002.

[36] J.M. Gere and B.J. Goodno. *Mechanics of Materials.* Cengage Learning, 2012.

[37] M. T. Restivo, F. Gomes de Almeida, M. F. Chouzal, J. Gabrial Mendes, and A. Mendes Lopes. *Laboraories of instrumentation for measurement.* UP, 2008.

[38] Pentronic. Tolerance classes for thermocouples according to the iec 60 584-2:1995. `http://www.pentronic.se/media/26434/IEC_60584_TC_060210.pdf`, 2012. *[visited on 2016-05].*

[39] National Instruments. Profibus overview. `http://www.ni.com/white-paper/6958/en/`, 2010. *[visited on 2016-05].*

[40] Siemens. Sinamics g/s: Profinet connection with labview. `http://support.automation.siemens.com/WW/view/en/99684399`, 2015. *[visited on 2016-05].*

[41] Siemens. Products for totally integrated automation, simatic, 2015.

Appendix

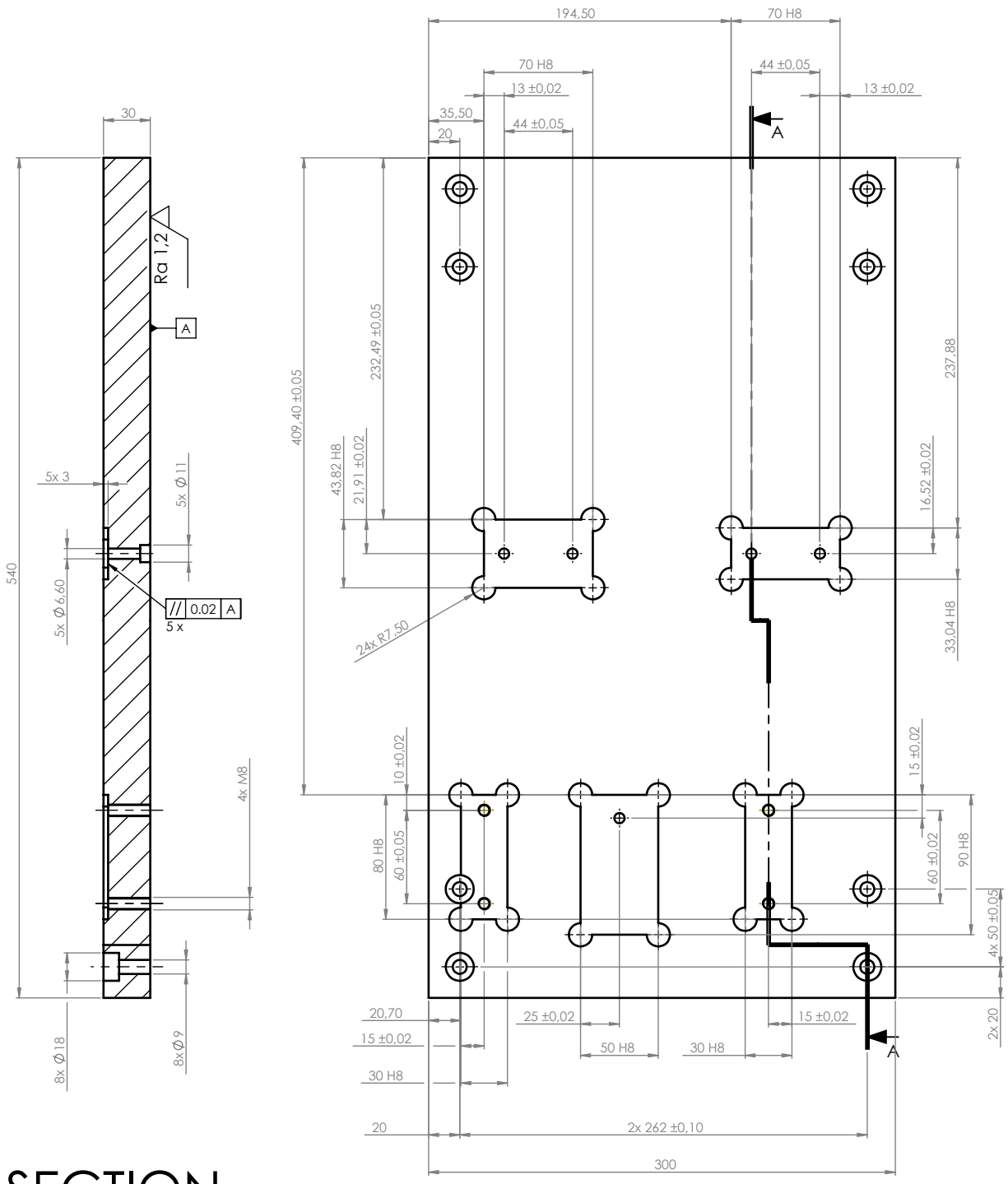

SECTION A-A

SCALE 1 : 4

Toleranciamento / Tolerances ISO 2768-m	Revisão / Revision	Data / Date	Nome / Name	Tol. lineares / Tol. of lenght					Tol. angulares / Tol. of angle				
Rugosidades / Surface roughness	1			±0,1	±0,1	±0,2	±0,3	±0,5	±1°	±0°30'	±0°20'	±0°10'	±0°5'
	2			Dimensões nominais / Nominal dimensions					Lado menor do ângulo / Short angle side				
	3			> 0,5 ≤ 3	> 3 ≤ 6	> 6 ≤ 30	> 30 ≤ 120	> 120 ≤ 400	≤ 10	> 10 ≤ 50	> 50 ≤ 120	> 120 ≤ 400	> 400
	4			Designação / Designation					Material / Material				
	5			Base diferencial									
	6			Número / number									
		Data / Date	Nome / Name										
	Desenhado / Designed			Escala / Scale	Desenho de definição / Technical drawing				Tam. / Size	Folha / Sheet	Rev.		
	Verificado / Checked			1:4					A4	1/1			
	Aprovado / Approved												

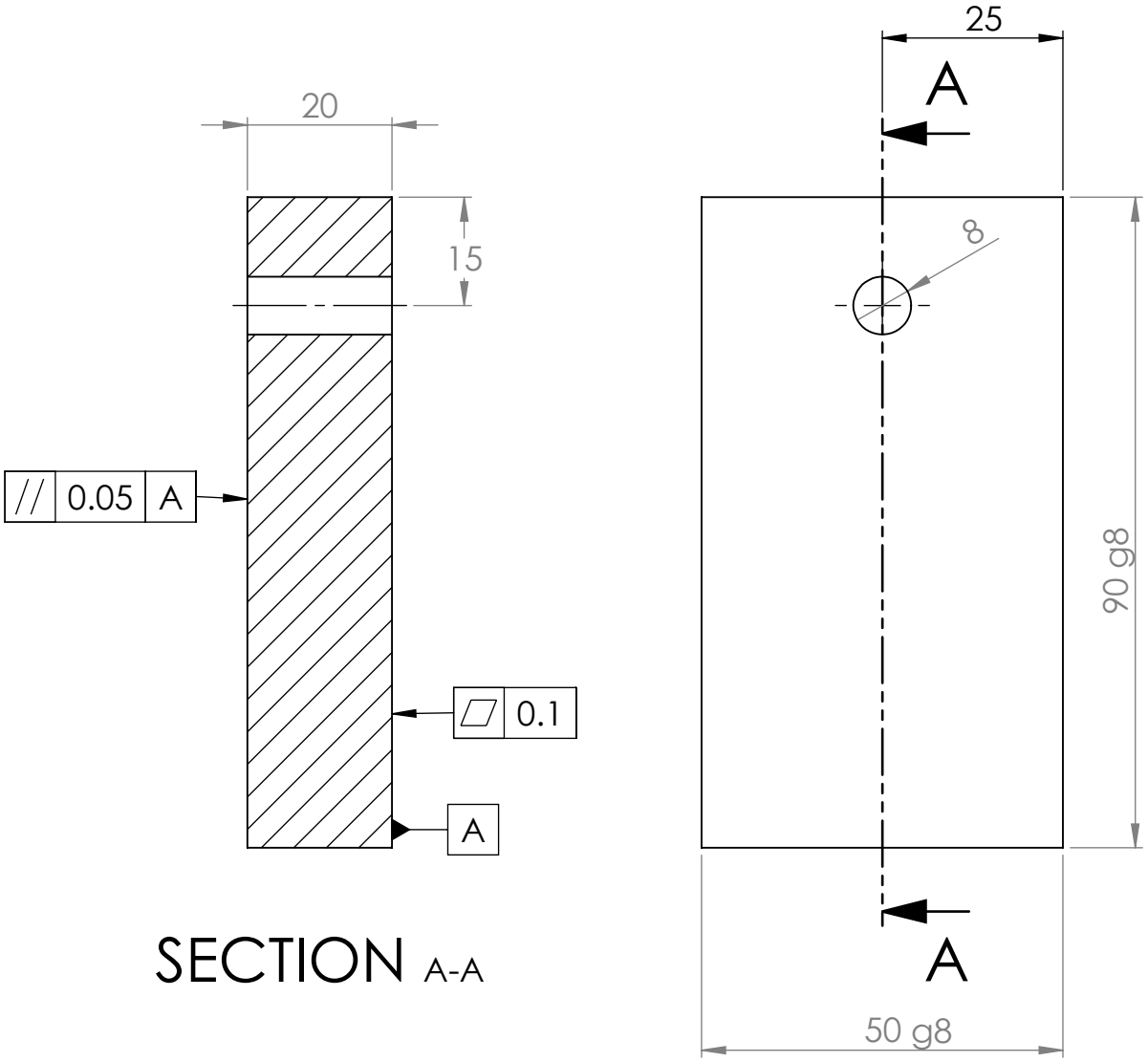

SECTION A-A

Toleranciamento / Tolerances ISO 2768-m	Revisão / Revision	Data / Date	Nome / Name
Rugosidades / Surface roughness	1		
	2		
	3		
	4		
	5		
	6		

Tol. lineares / Tol. of lenght					Tol. angulares / Tol. of angle				
±0,1	±0,1	±0,2	±0,3	±0,5	±1°	±0°30'	±0°20'	±0°10'	±0°5'

Dimensões nominais / Nominal dimensions					Lado menor do ângulo / Short angle side				
> 0,5 ≤ 3	> 3 ≤ 6	> 6 ≤ 30	> 30 ≤ 120	> 120 ≤ 400	≤ 10	> 10 ≤ 50	> 50 ≤ 120	> 120 ≤ 400	> 400

Designação / Designation	Material / Material
Calço diff frente	

SOLIDWORKS Educational Product. For Instructional Use Only

Número / number

	Data / Date	Nome / Name
Desenhado / Designed		
Verificado / Checked		
Aprovado / Approved		

Escala / Scale		Tam. / Size	Folha / Sheet	Rev.
1:1	Desenho de definição / Technical drawing	A4	1/1	

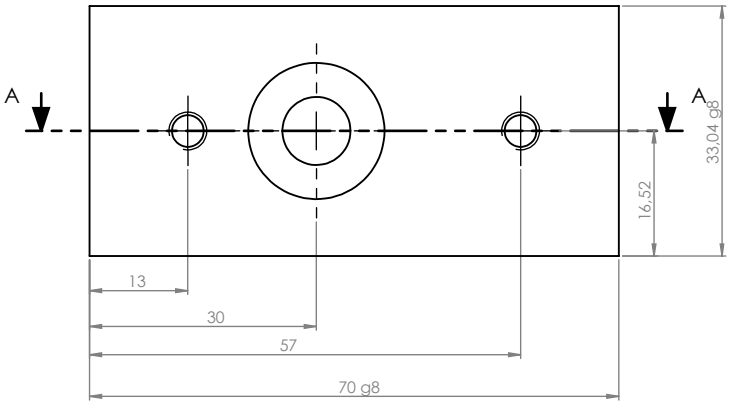

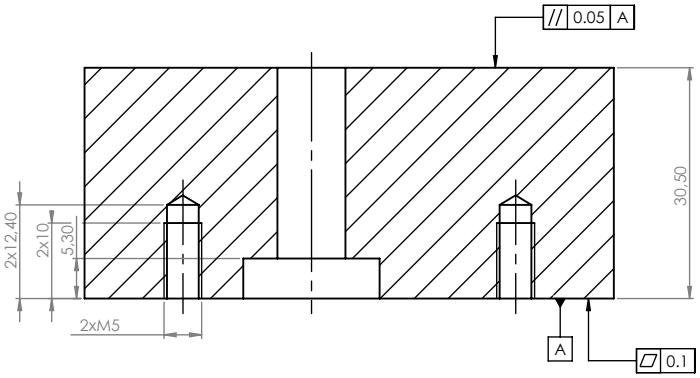

SECTION A-A

Toleranciamento / Tolerances ISO 2768-m	Revisão / Revision	Data / Date	Nome / Name	Tol. lineares / Tol. of lenght					Tol. angulares / Tol. of angle				
Rugosidades / Surface roughness	1			±0,1	±0,1	±0,2	±0,3	±0,5	±1°	±0°30'	±0°20'	±0°10'	±0°5'
	2			Dimensões nominais / Nominal dimensions					Lado menor do ângulo / Short angle side				
	3			> 0,5 ≤ 3	> 3 ≤ 6	> 6 ≤ 30	> 30 ≤ 120	> 120 ≤ 400	≤ 10	> 10 ≤ 50	> 50 ≤ 120	> 120 ≤ 400	> 400
	4			Designação / Designation					Material / Material				
	5			Calço diff trás direita									
SOLIDWORKS Educational Product. For Instructional Use Only	6			Número / number									
		Data / Date	Nome / Name										
	Desenhado / Designed			Escala / Scale	Desenho de definição / Technical drawing				Tam. / Size	Folha / Sheet	Rev.		
	Verificado / Checked			1:1					A4	1/1			
	Aprovado / Approved												

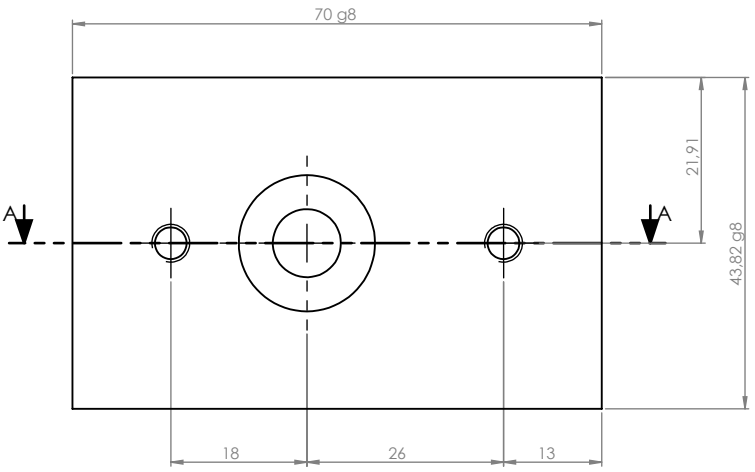

SECTION A-A

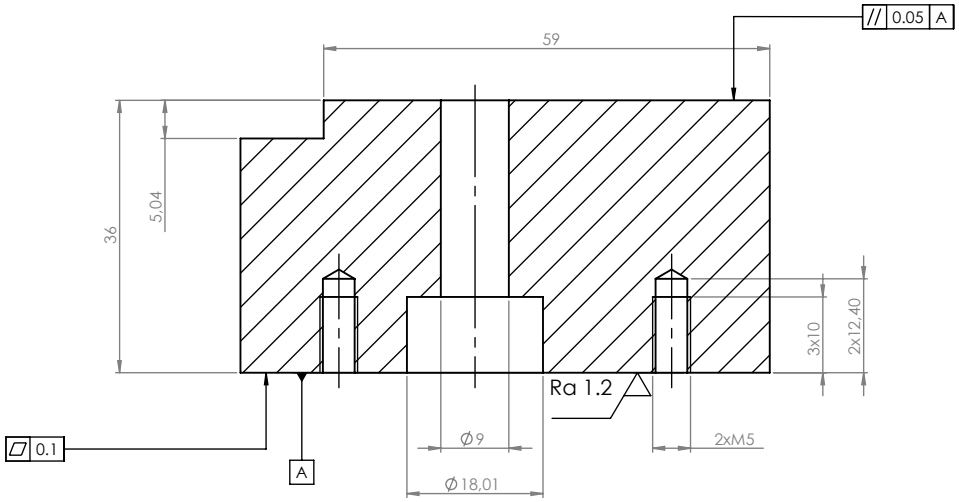

Toleranciamento / Tolerances ISO 2768-m	Revisão / Revision	Data / Date	Nome / Name	Tol. lineares / Tol. of lenght					Tol. angulares / Tol. of angle				
Rugosidades / Surface roughness	1			±0,1	±0,1	±0,2	±0,3	±0,5	±1°	±0°30'	±0°20'	±0°10'	±0°5'
	2			Dimensões nominais / Nominal dimensions					Lado menor do ângulo / Short angle side				
	3			> 0,5 ≤ 3	> 3 ≤ 6	> 6 ≤ 30	> 30 ≤ 120	> 120 ≤ 400	≤ 10	> 10 ≤ 50	> 50 ≤ 120	> 120 ≤ 400	> 400
	4			Designação / Designation					Material / Material				
	5			Calço diferencial trás esquerda									
SOLIDWORKS Educational Product. For Instructional Use Only	6			Número / number									
		Data / Date	Nome / Name										
	Desenhado / Designed			Escala / Scale	Desenho de definição / Technical drawing				Tam. / Size	Folha / Sheet		Rev.	
	Verificado / Checked			1:1					A4	1/1			
	Aprovado / Approved												

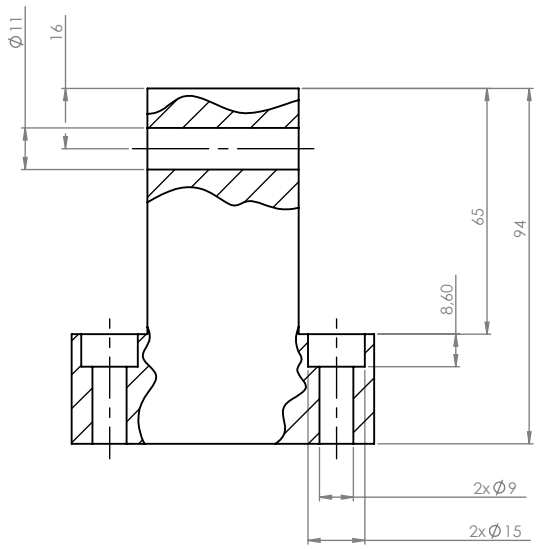

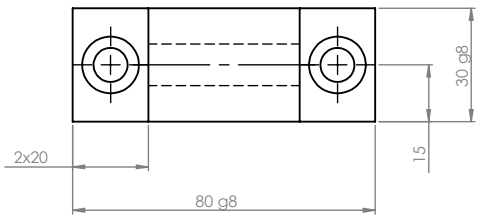

Toleranciamento / Tolerances ISO 2768-m		Revisão / Revision	Data / Date	Nome / Name	Tol. lineares / Tol. of lenght					Tol. angulares / Tol. of angle				
Rugosidades / Surface roughness					±0,1	±0,1	±0,2	±0,3	±0,5	±1°	±0°30'	±0°20'	±0°10'	±0°5'
	1				Dimensões nominais / Nominal dimensions					Lado menor do ângulo / Short angle side				
	2				> 0,5 ≤ 3	> 3 ≤ 6	> 6 ≤ 30	> 30 ≤ 120	> 120 ≤ 400	≤ 10	> 10 ≤ 50	> 50 ≤ 120	> 120 ≤ 400	> 400
	3				Designação / Designation					Material / Material				
	4				Calco diff 1_3									
	5													
	6				Número / number									
			Data / Date	Nome / Name										
		Desenhado / Designed			Escala / Scale 1:2	Desenho de definição / Technical drawing				Tam. / Size A4	Folha / Sheet 1/1		Rev.	
		Verificado / Checked												
		Aprovado / Approved												

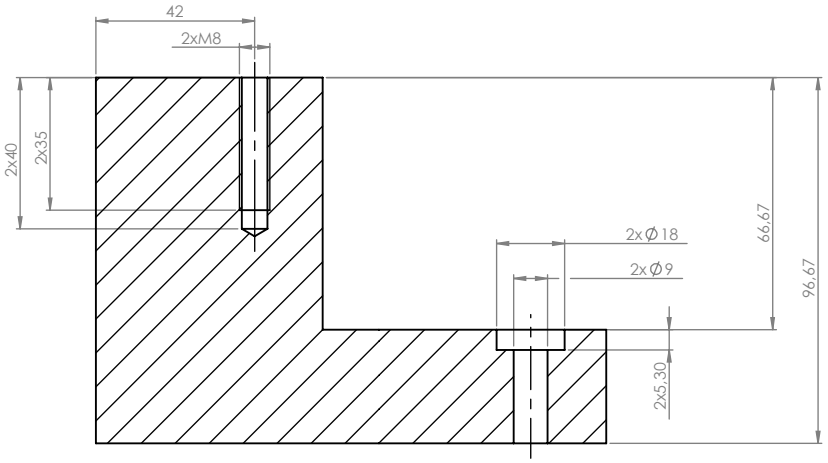

SECTION A-A

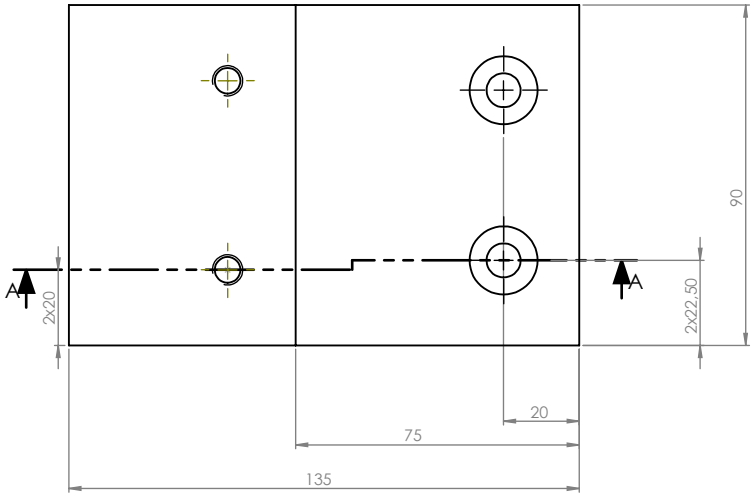

Toleranciamento / Tolerances ISO 2768-m		Revisão / Revision	Data / Date	Nome / Name	Tol. lineares / Tol. of lenght					Tol. angulares / Tol. of angle				
Rugosidades / Surface roughness					±0,1	±0,1	±0,2	±0,3	±0,5	±1°	±0°30'	±0°20'	±0°10'	±0°5'
	1				Dimensões nominais / Nominal dimensions					Lado menor do ângulo / Short angle side				
	2				> 0,5 ≤ 3	> 3 ≤ 6	> 6 ≤ 30	> 30 ≤ 120	> 120 ≤ 400	≤ 10	> 10 ≤ 50	> 50 ≤ 120	> 120 ≤ 400	> 400
	3				Designação / Designation					Material / Material				
	4				Pata diff									
	5													
	6				Número / number									
			Data / Date	Nome / Name										
		Desenhado / Designed			Escala / Scale 1:5	Desenho de definição / Technical drawing				Tam. / Size A4	Folha / Sheet 1/1		Rev.	
		Verificado / Checked												
		Aprovado / Approved												

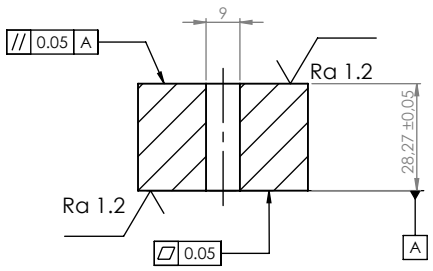

SECTION A-A

SCALE 1 : 2

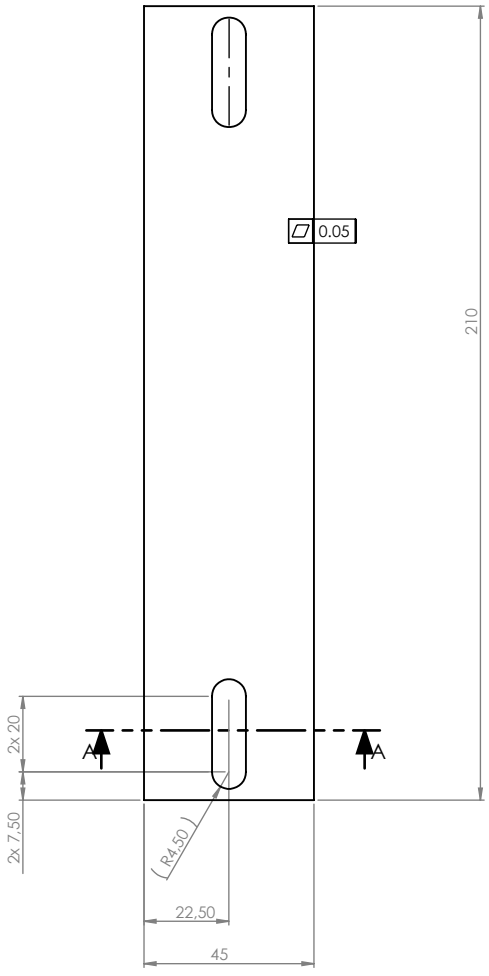

Toleranciamento / Tolerances ISO 2768-m	Revisão / Revision	Data / Date	Nome / Name	Tol. lineares / Tol. of lenght					Tol. angulares / Tol. of angle				
Rugosidades / Surface roughness	1			±0,1	±0,1	±0,2	±0,3	±0,5	±1°	±0°30'	±0°20'	±0°10'	±0°5'
	2			Dimensões nominais / Nominal dimensions					Lado menor do ângulo / Short angle side				
	3			> 0,5 ≤ 3	> 3 ≤ 6	> 6 ≤ 30	> 30 ≤ 120	> 120 ≤ 400	≤ 10	> 10 ≤ 50	> 50 ≤ 120	> 120 ≤ 400	> 400
	4			Designação / Designation					Material / Material				
	5			Calco trans in									
	6			Número / number									
		Data / Date	Nome / Name										
	Desenhado / Designed			Escala / Scale	Desenho de definição / Technical drawing				Tam. / Size	Folha / Sheet	Rev.		
	Verificado / Checked			1:2					A4	1/1			
	Aprovado / Approved												

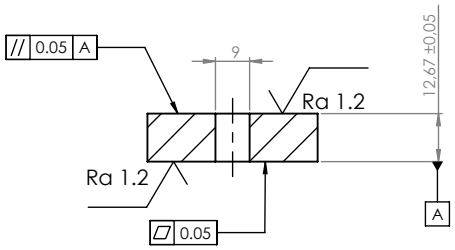

SECTION A-A

SCALE 1 : 2

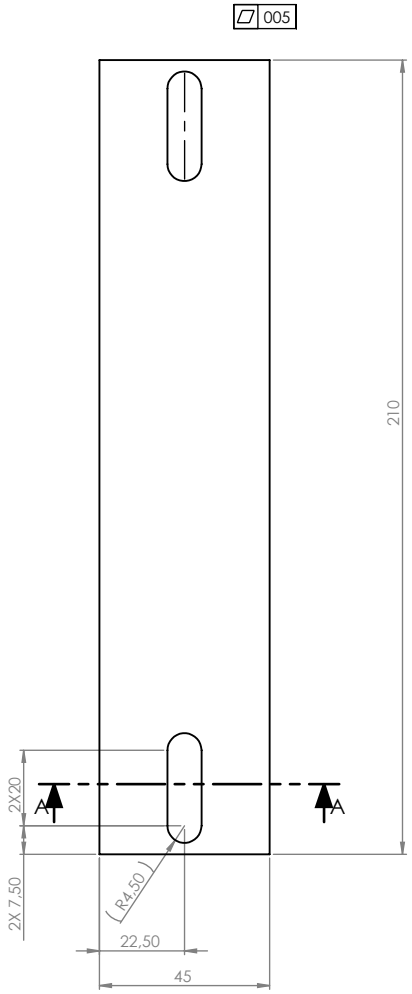

Toleranciamento / Tolerances ISO 2768-m	Revisão / Revision	Data / Date	Nome / Name	Tol. lineares / Tol. of lenght					Tol. angulares / Tol. of angle				
Rugosidades / Surface roughness	1			±0,1	±0,1	±0,2	±0,3	±0,5	±1°	±0°30'	±0°20'	±0°10'	±0°5'
	2			Dimensões nominais / Nominal dimensions					Lado menor do ângulo / Short angle side				
	3			> 0,5 ≤ 3	> 3 ≤ 6	> 6 ≤ 30	> 30 ≤ 120	> 120 ≤ 400	≤ 10	> 10 ≤ 50	> 50 ≤ 120	> 120 ≤ 400	> 400
	4			Designação / Designation					Material / Material				
	5			Calco trans out									
	6			Número / number									
		Data / Date	Nome / Name										
	Desenhado / Designed			Escala / Scale	Desenho de definição / Technical drawing				Tam. / Size	Folha / Sheet	Rev.		
	Verificado / Checked			1:2					A4	1/1			
	Aprovado / Approved												

SECTION A-A

SCALE 1 : 4

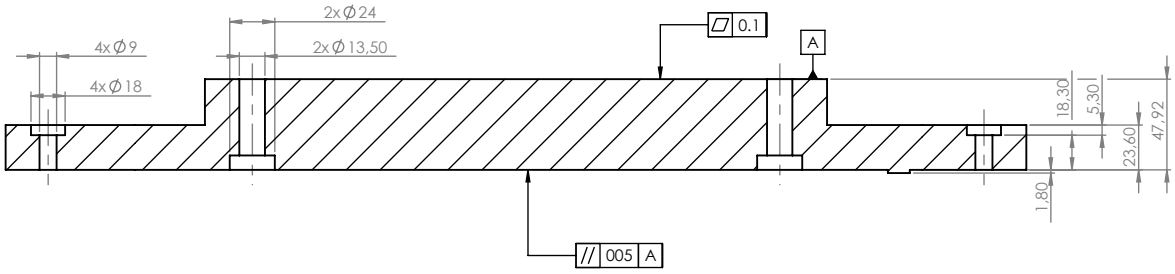

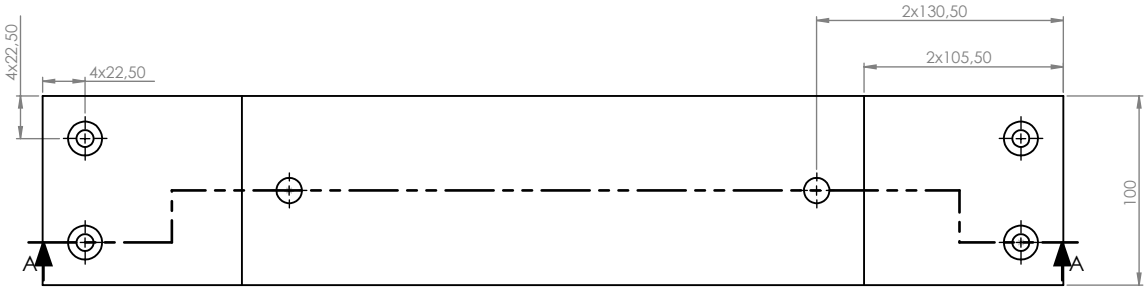

Toleranciamento / Tolerances ISO 2768-m	Revisão / Revision	Data / Date	Nome / Name	Tol. lineares / Tol. of lenght					Tol. angulares / Tol. of angle				
Rugosidades / Surface roughness	1			±0,1	±0,1	±0,2	±0,3	±0,5	±1°	±0°30'	±0°20'	±0°10'	±0°5'
	2			Dimensões nominais / Nominal dimensions					Lado menor do ângulo / Short angle side				
	3			> 0,5 ≤ 3	> 3 ≤ 6	> 6 ≤ 30	> 30 ≤ 120	> 120 ≤ 400	≤ 10	> 10 ≤ 50	> 50 ≤ 120	> 120 ≤ 400	> 400
	4			Designação / Designation					Material / Material				
	5			Patas motor saída									
SOLIDWORKS Educational Product. For Instructional Use Only	6			Número / number									
		Data / Date	Nome / Name										
	Desenhado / Designed			Escala / Scale	Desenho de definição / Technical drawing				Tam. / Size	Folha / Sheet		Rev.	
	Verificado / Checked			1:4					A4	1/1			
	Aprovado / Approved												

SECTION A-A

SCALE 1 : 6

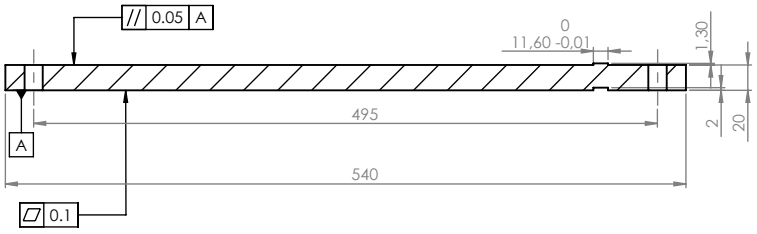

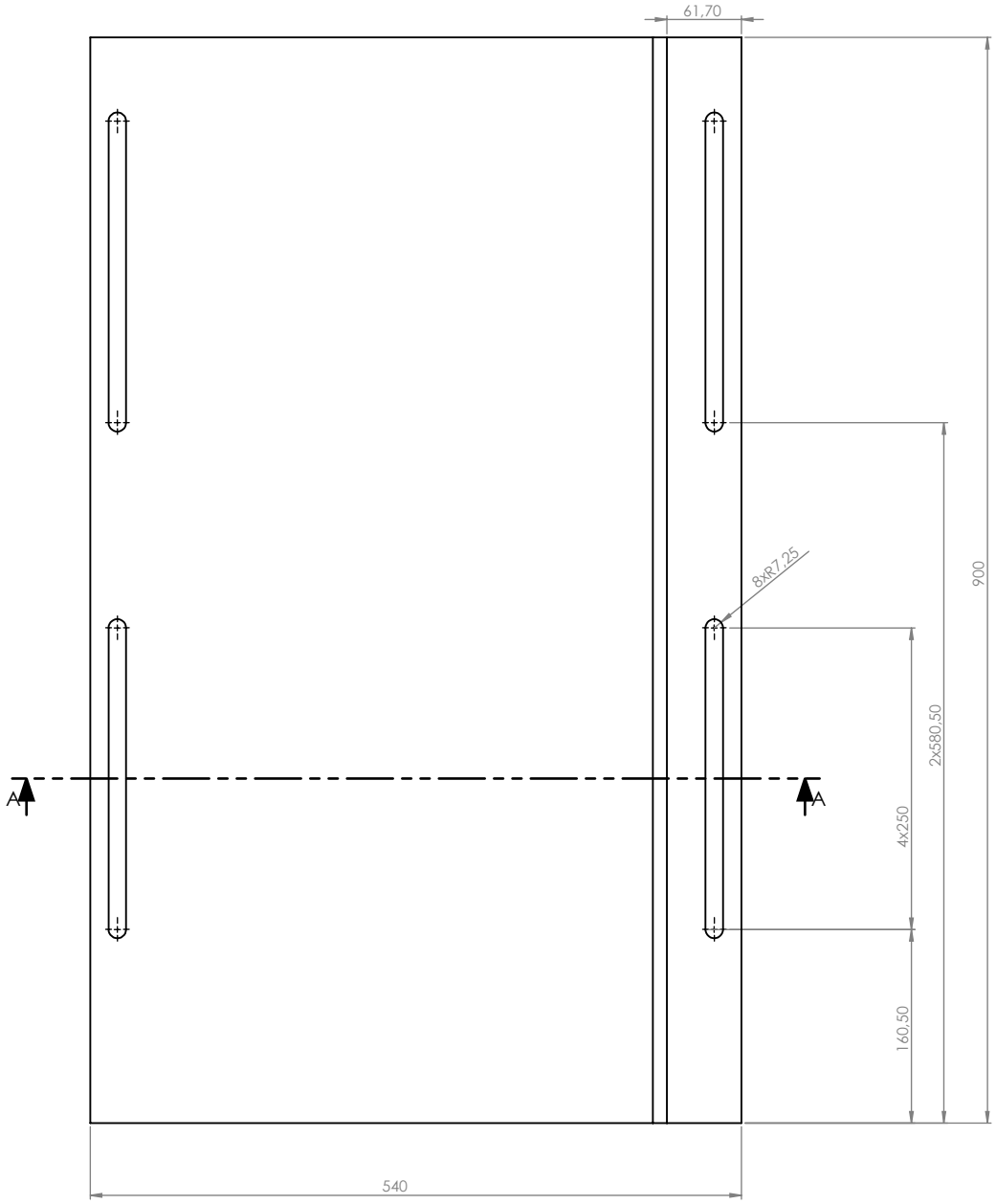

Toleranciamento / Tolerances ISO 2768-m	Revisão / Revision	Data / Date	Nome / Name
Rugosidades / Surface roughness	1		
	2		
	3		
	4		
	5		
	6		

SOLIDWORKS Educational Product. For Instructional Use Only

	Data / Date	Nome / Name
Desenhado / Designed		
Verificado / Checked		
Aprovado / Approved		

Tol. lineares / Tol. of lenght					Tol. angulares / Tol. of angle				
±0,1	±0,1	±0,2	±0,3	±0,5	±1°	±0°30'	±0°20'	±0°10'	±0°5'

Dimensões nominais / Nominal dimensions					Lado menor do ângulo / Short angle side				
> 0,5 ≤ 3	> 3 ≤ 6	> 6 ≤ 30	> 30 ≤ 120	> 120 ≤ 400	≤ 10	> 10 ≤ 50	> 50 ≤ 120	> 120 ≤ 400	> 400

Designação / Designation	Material / Material
Chapa saída	

Número / number

Escala / Scale		Tam. / Size	Folha / Sheet	Rev.
1:5	Desenho de definição / Technical drawing	A4	1/1	

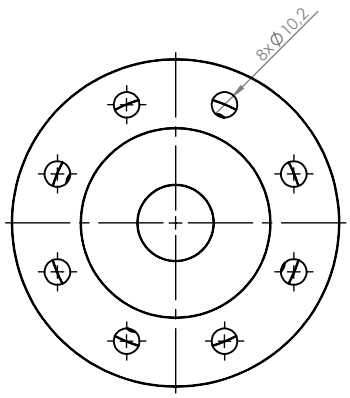

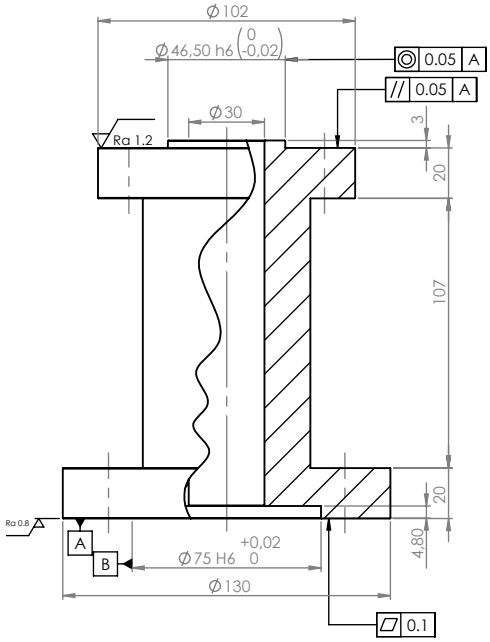

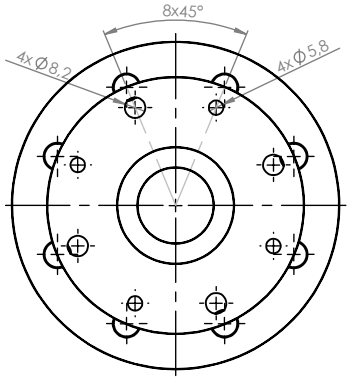

All edges chanfered with 0.2x45°

Toleranciamento / Tolerances ISO 2768-m	Revisão / Revision	Data / Date	Nome / Name
Rugosidades / Surface roughness	1		
	2		
	3		
	4		
	5		
	6		

Tol. lineares / Tol. of lenght					Tol. angulares / Tol. of angle				
±0,1	±0,1	±0,2	±0,3	±0,5	±1°	±0°30'	±0°20'	±0°10'	±0°5'

Dimensões nominais / Nominal dimensions					Lado menor do ângulo / Short angle side				
> 0,5 ≤ 3	> 3 ≤ 6	> 6 ≤ 30	> 30 ≤ 120	> 120 ≤ 400	≤ 10	> 10 ≤ 50	> 50 ≤ 120	> 120 ≤ 400	> 400

Designação / Designation	Material / Material
Acoplamento propeller shaft e transdutor	

SOLIDWORKS Educational Product. For Instructional Use Only

Número / number

	Data / Date	Nome / Name
Desenhado / Designed		
Verificado / Checked		
Aprovado / Approved		

Escala / Scale	Desenho de definição / Technical drawing	Tam. / Size	Folha / Sheet	Rev.
1:5		A4	1/1	

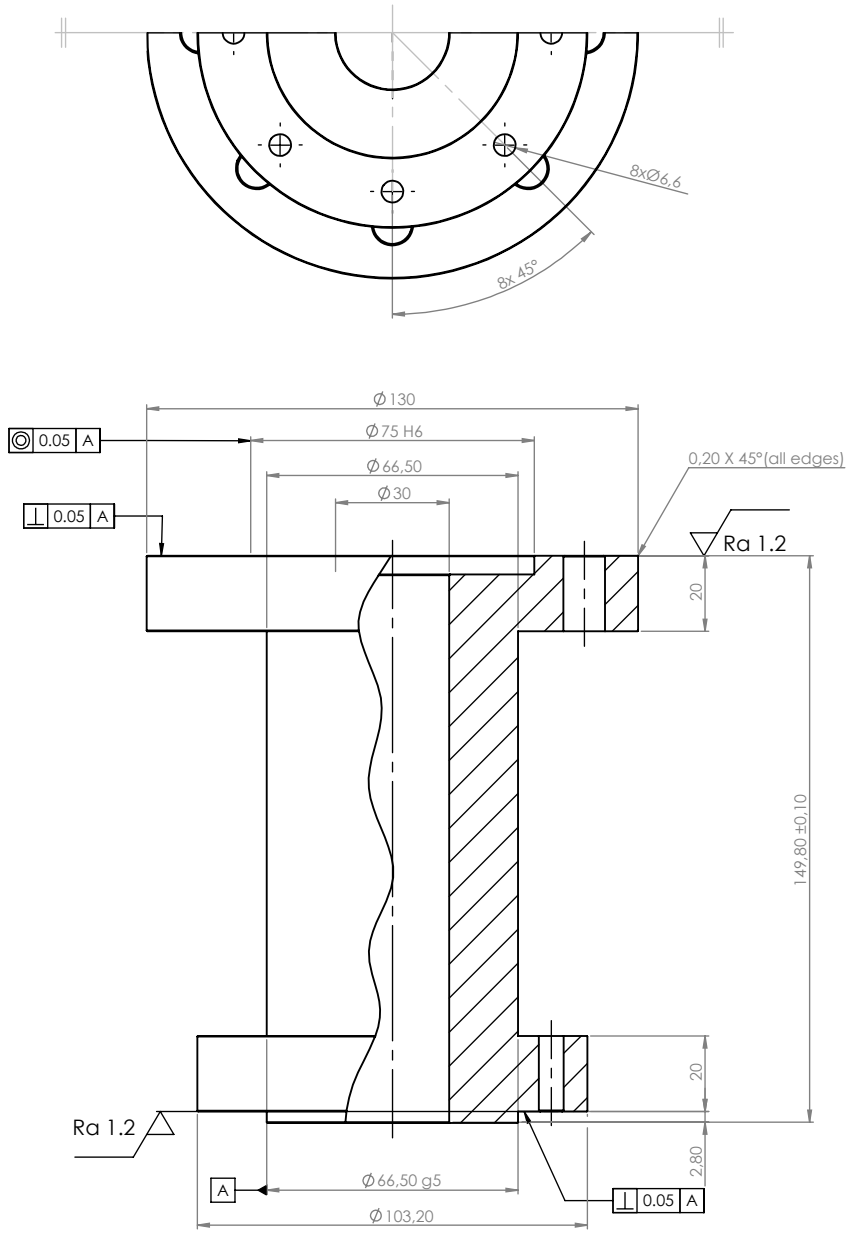

Toleranciamento / Tolerances: ISO 2768-m	Revisão / Revision	Data / Date	Nome / Name
Rugosidades / Surface roughness	1		
	2		
	3		
	4		
	5		
	6		
		Data / Date	Nome / Name
	Desenhado / Designed		
	Verificado / Checked		
	Aprovado / Approved		

Tol. lineares / Tol. of lenght					Tol. angulares / Tol. of angle				
±0,1	±0,1	±0,2	±0,3	±0,5	±1°	±0°30'	±0°20'	±0°10'	±0°5'
Dimensões nominais / Nominal dimensions					Lado menor do ângulo / Short angle side				
> 0,5 ≤ 3	> 3 ≤ 6	> 6 ≤ 30	> 30 ≤ 120	> 120 ≤ 400	≤ 10	> 10 ≤ 50	> 50 ≤ 120	> 120 ≤ 400	> 400

Designação / Designation: Acoplamento dif trans out

Material / Material:

Número / number:

Escala / Scale	Desenho de definição / Technical drawing	Tam. / Size	Folha / Sheet	Rev.
1:2		A4	1/1	

SECTION A-A

SCALE 1 : 3

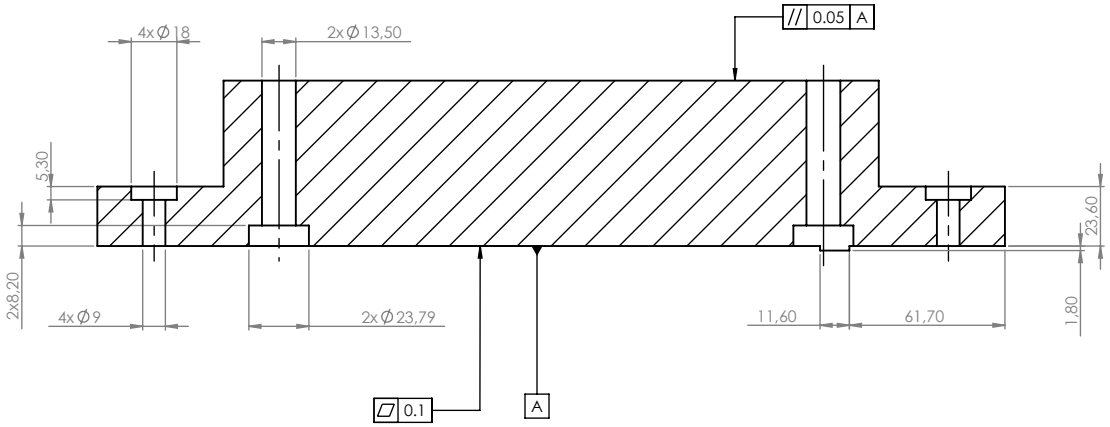

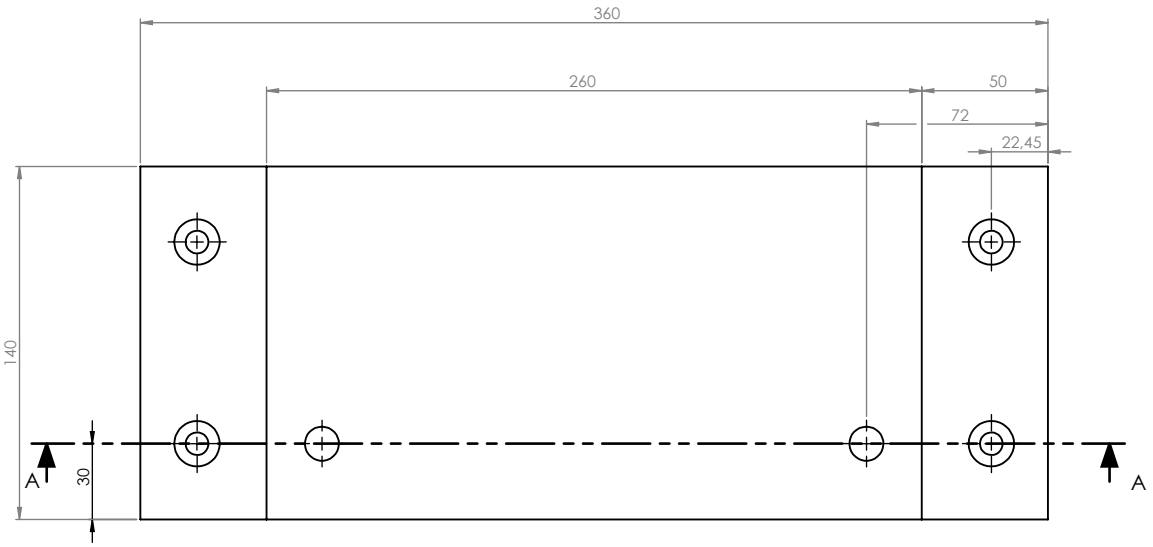

Toleranciamento / Tolerances ISO 2768-m	Revisão / Revision	Data / Date	Nome / Name	Tol. lineares / Tol. of lenght					Tol. angulares / Tol. of angle				
Rugosidades / Surface roughness	1			±0,1	±0,1	±0,2	±0,3	±0,5	±1°	±0°30'	±0°20'	±0°10'	±0°5'
	2			Dimensões nominais / Nominal dimensions					Lado menor do ângulo / Short angle side				
	3			> 0,5 ≤ 3	> 3 ≤ 6	> 6 ≤ 30	> 30 ≤ 120	> 120 ≤ 400	≤ 10	> 10 ≤ 50	> 50 ≤ 120	> 120 ≤ 400	> 400
	4			Designação / Designation					Material / Material				
	5			Pata entrada frente									
SOLIDWORKS Educational Product. For Instructional Use Only	6			Número / number									
		Data / Date	Nome / Name										
	Desenhado / Designed			Escala / Scale	Desenho de definição / Technical drawing				Tam. / Size	Folha / Sheet		Rev.	
	Verificado / Checked			1:3					A4	1/1			
	Aprovado / Approved												

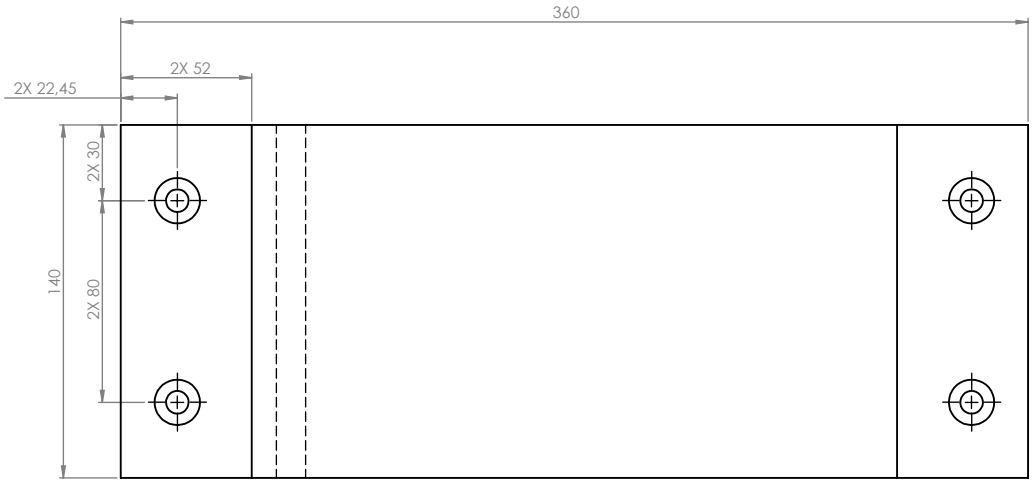

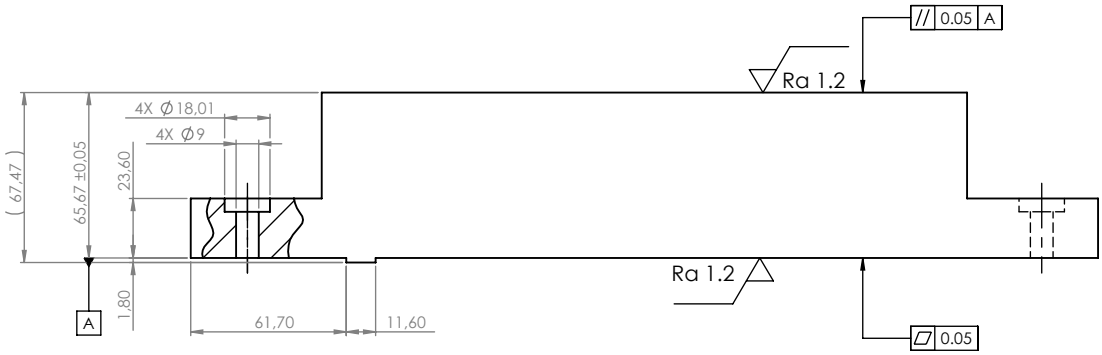

Toleranciamento / Tolerances ISO 2768-m	Revisão / Revision	Data / Date	Nome / Name	Tol. lineares / Tol. of lenght					Tol. angulares / Tol. of angle				
Rugosidades / Surface roughness	1			±0,1	±0,1	±0,2	±0,3	±0,5	±1°	±0°30'	±0°20'	±0°10'	±0°5'
	2 0.05			Dimensões nominais / Nominal dimensions					Lado menor do ângulo / Short angle side				
	3			> 0,5 ≤ 3	> 3 ≤ 6	> 6 ≤ 30	> 30 ≤ 120	> 120 ≤ 400	≤ 10	> 10 ≤ 50	> 50 ≤ 120	> 120 ≤ 400	> 400
	4			Designação / Designation					Material / Material				
	5			PATA 2 1 5									
	6			Número / number									
		Data / Date	Nome / Name										
	Desenhado / Designed			Escala / Scale	Desenho de definição / Technical drawing				Tam. / Size	Folha / Sheet	Rev.		
	Verificado / Checked			1:3					A4	1/1			
	Aprovado / Approved												

SECTION A-A

SCALE 1 : 5

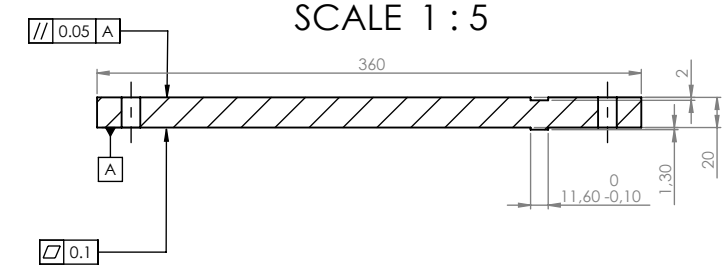

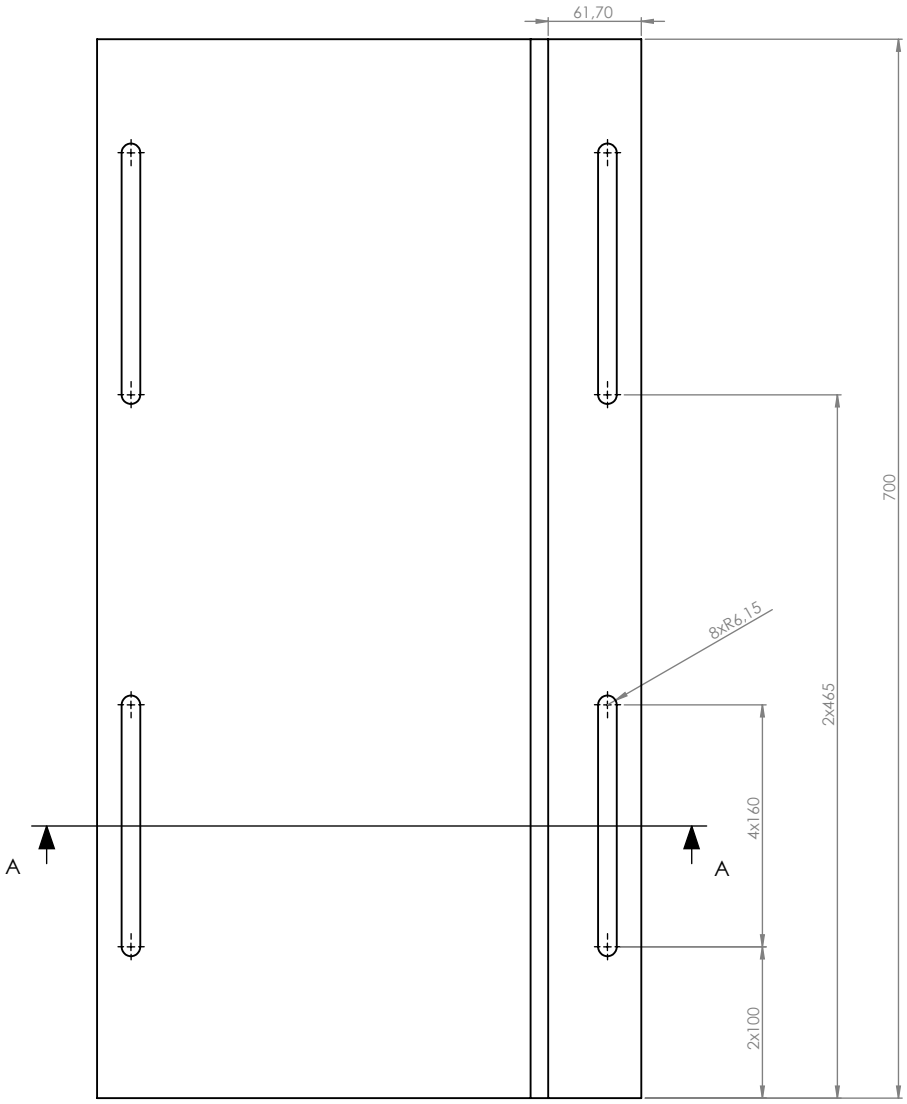

Toleranciamento / Tolerances: ISO 2768-m	Revisão / Revision	Data / Date	Nome / Name
Rugosidades / Surface roughness	1		
	2		
	3		
	4		
	5		
	6		

Tol. lineares / Tol. of lenght					Tol. angulares / Tol. of angle				
±0,1	±0,1	±0,2	±0,3	±0,5	±1°	±0°30'	±0°20'	±0°10'	±0°5'

Dimensões nominais / Nominal dimensions					Lado menor do ângulo / Short angle side				
> 0,5 ≤ 3	> 3 ≤ 6	> 6 ≤ 30	> 30 ≤ 120	> 120 ≤ 400	≤ 10	> 10 ≤ 50	> 50 ≤ 120	> 120 ≤ 400	> 400

Designação / Designation: Chapa entrada

Material / Material:

Número / number:

SOLIDWORKS Educational Product. For Instructional Use Only

	Data / Date	Nome / Name
Desenhado / Designed		
Verificado / Checked		
Aprovado / Approved		

Escala / Scale	Desenho de definição / Technical drawing	Tam. / Size	Folha / Sheet	Rev.
1:5		A4	1/1	

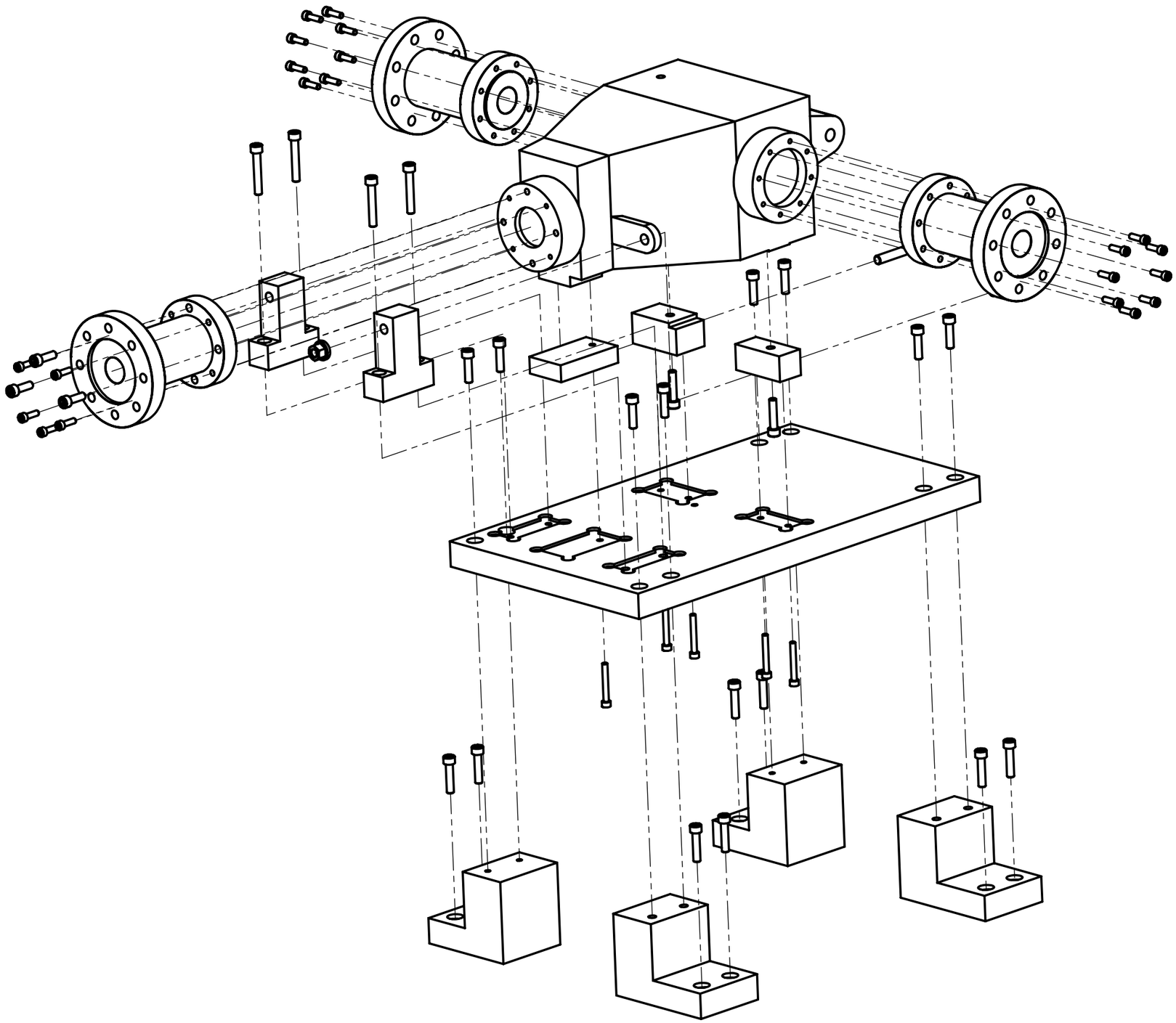

AUTHOR: FILIPA BRANDÃO	DATE: 19-06-2016
TITLE: DIFFERENTIAL_EXPLODE	
SCALE:1:50	SHEET 1 OF 1

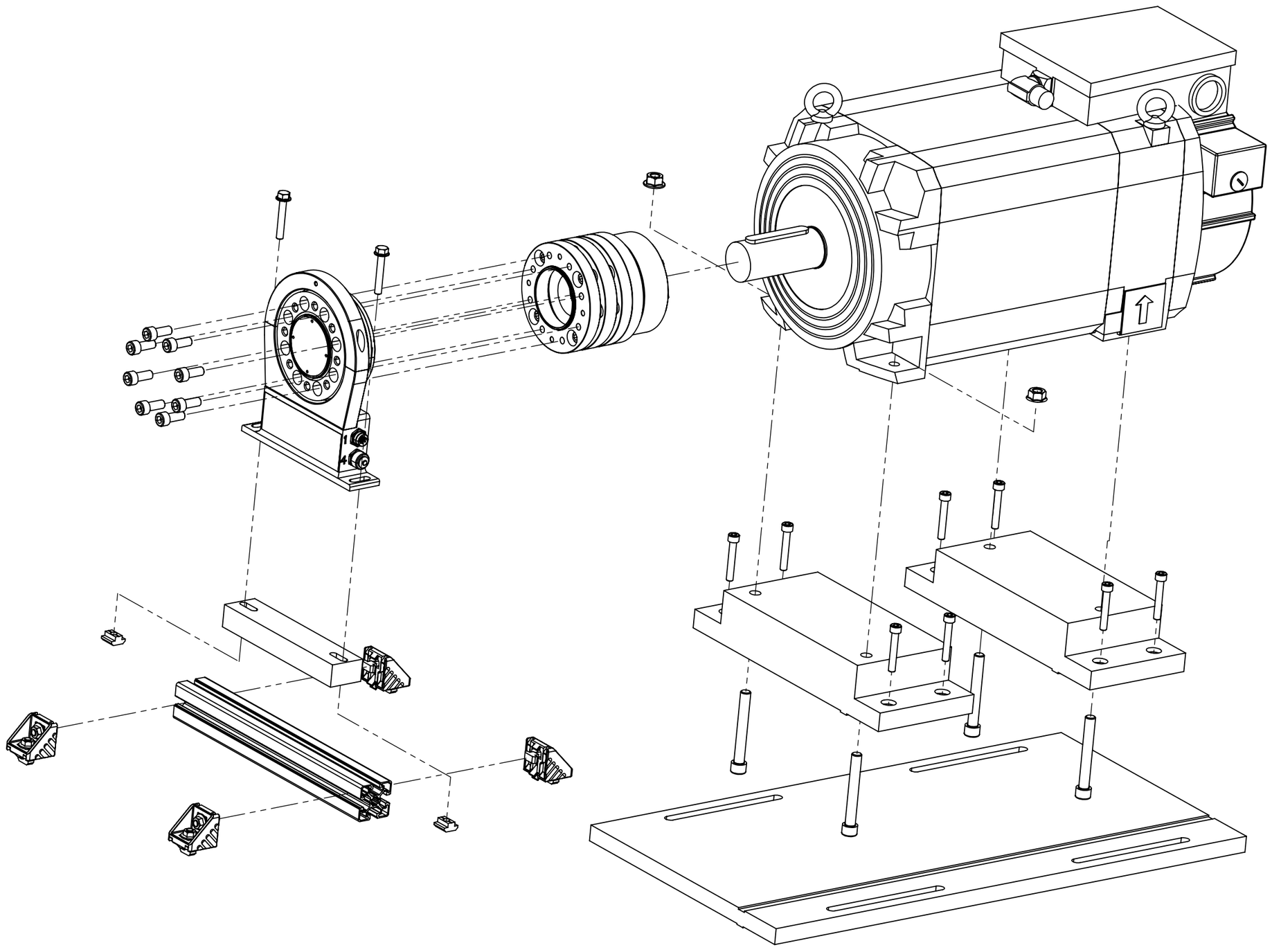

AUTHOR: FILIPA BRANDÃO	DATE: 19-06-2016
TITLE: 1PH8137_EXPLODE	
SCALE:1:50	SHEET 1 OF 1

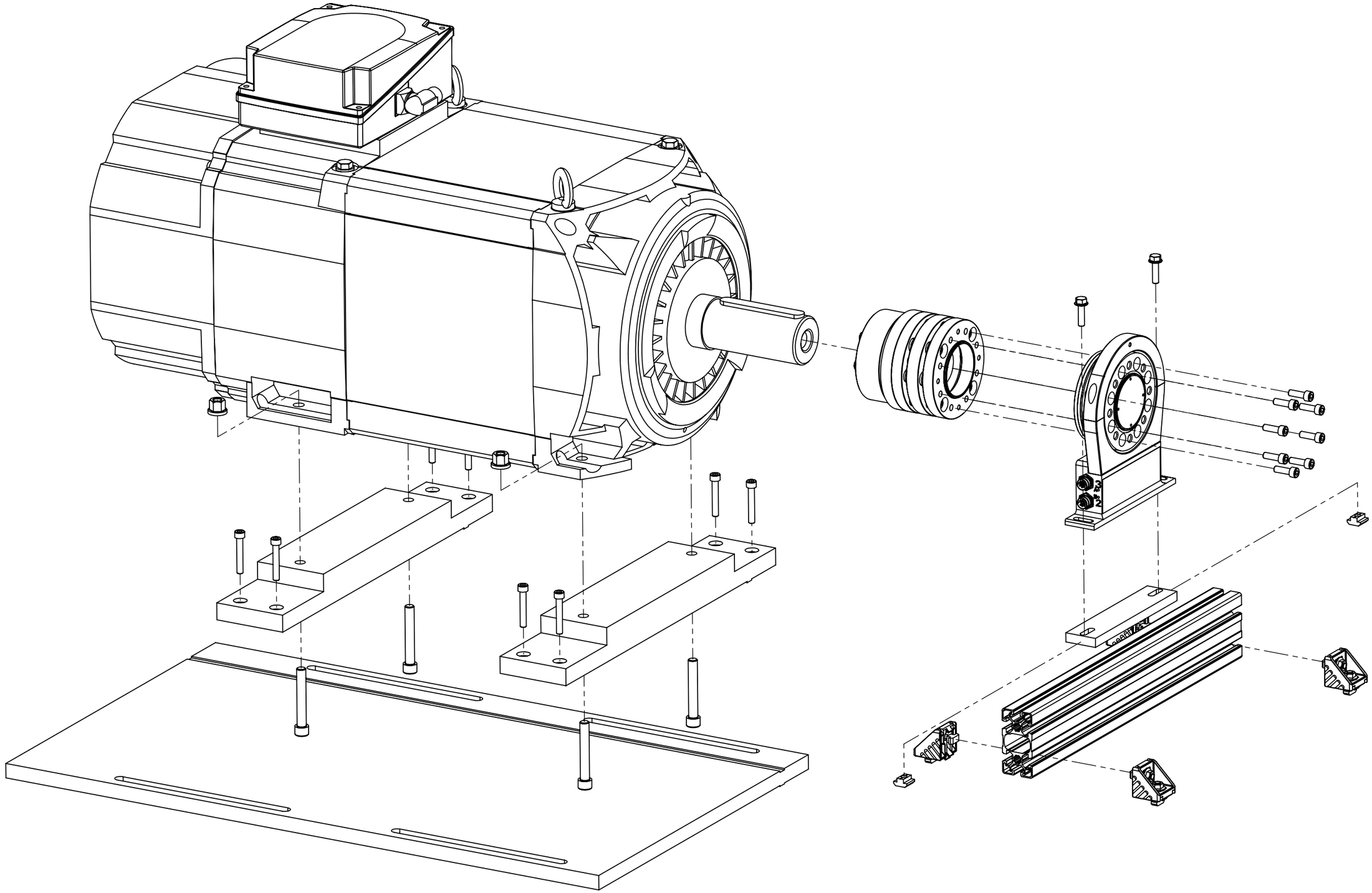

AUTHOR: FILIPA BRANDÃO	DATE: 19-06-2016
TITLE: 1PH8184_EXPLODE	
SCALE:1:50	SHEET 1 OF 1

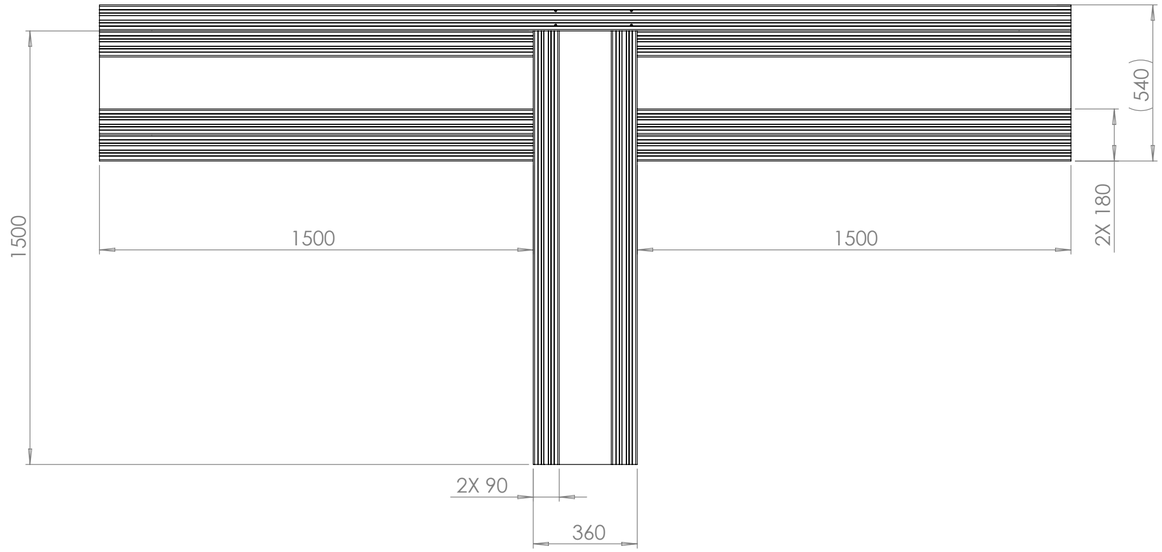

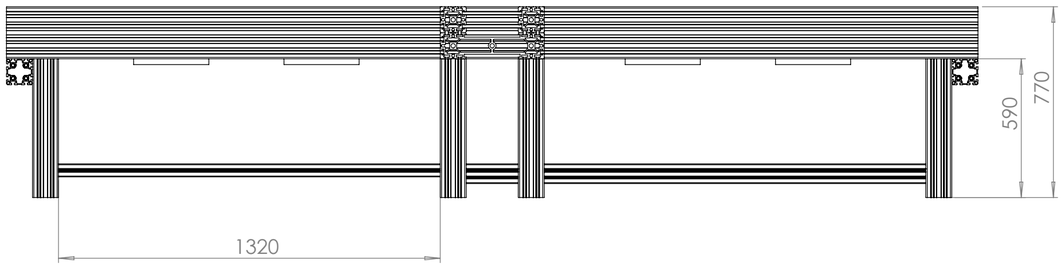

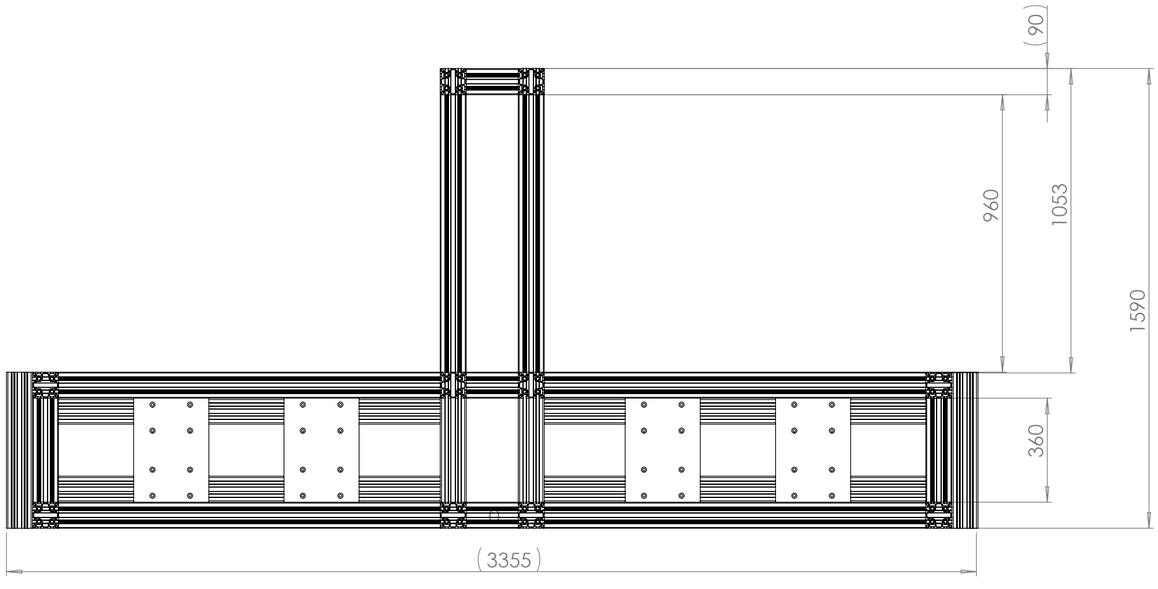

AUTHOR: FILIPA BRANDÃO	DATE: 19-06-2016
TITLE: REAR AXLE TEST RIG	
SCALE:1:50	SHEET 1 OF 1

Shrink disk hub, clamping external

Type 9110.10000

Size	16 F	16	64	300	500	850
a	6x M8		8x M10	8x M12	8x M14	8x M16
b_1	9,6		14,6	21	20	21,6
d_2	77		120	164	198	234
f_1	3,5		4	5	4	4
k	3,5		5,3	5,3	6,4	7,5
l_1	38		58	70	80	98
D_1	102		132	167	193	240
T_K	84		101,5	130	155,5	196
Z_i	57 H6		75 H6	90 H6	110 H6	140 H6

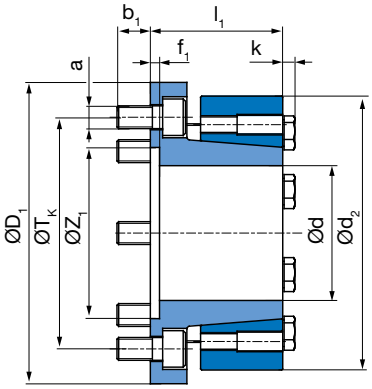

Shrink disk hub, clamping internal

Type 9110.20000

Size	16 F	16	64	300	500	850
a	6x M8		8x M10	8x M12	8x M14	8x M16
b_2	13		16	21	25	30
d_2	77		120	164	198	234
f_2	3		3	3	2,5	3
l_2	41		61	72	82,5	101
D_1	102		132	167	193	240
T_K	84		101,5	130	155,5	196
Z_A	57 g6		75 g6	90 g6	110 g6	140 g6

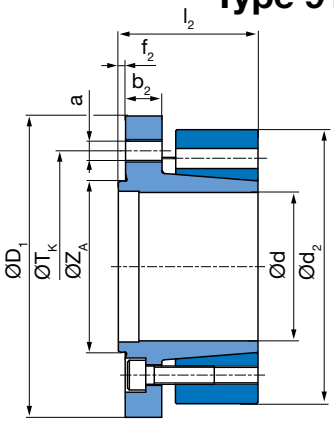

Module 1, connection plate*

Type 9110._ _100

* Does not correspond to the former HBM ID. number 1-4411._ _ _ _ (see page 11)

Size	16 F	16	64	300	500	850
a	6x M8	6x M8	8x M10	8x M12	8x M14	8x M16
f	3	3	3	2,5	2,5	3
D	99	99	132	178	210	252
L_2	46,2	41,2	63,4	88	100	116
S	7,1	4,6	6,8	11,2	12	14
T_K	84	84	101,5	130	155,5	196
U_2	10	10	16	22	25,5	29
U_1	26,2	21,2	31.4	44	49	58
Z_A	57 g6	57 g6	75 g6	90 g6	110 g6	140 g6

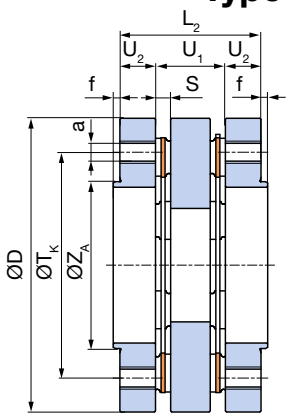

Module 1, sleeve

Type 9110._ _200

Size	16 F	16	64	300	500	850
a	6x M8	6x M8	8x M10	8x M12	8x M14	8x M16
f	3	3	3	2,5	2,5	3
D	99	99	132	178	210	252
L_1	90,2	85,2	142,6	204,4	221	278
S	7,1	4,6	6,8	11,2	12	14
T_K	84	84	101,5	130	155,5	196
H_1	70,2	65,2	110,6	160,4	170	220
U_2	10	10	16	22	25,5	29
Z_A	57 g6	57 g6	75 g6	90 g6	110 g6	140 g6

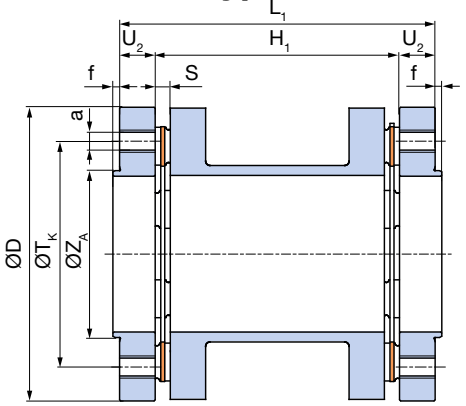

Dimensions of T40B 500 Nm - 1 kNm without rotational speed measurement

Dimensions in mm (1 mm = 0.03937 inches)

Dimensions without tolerances, per DIN ISO 2768-mk

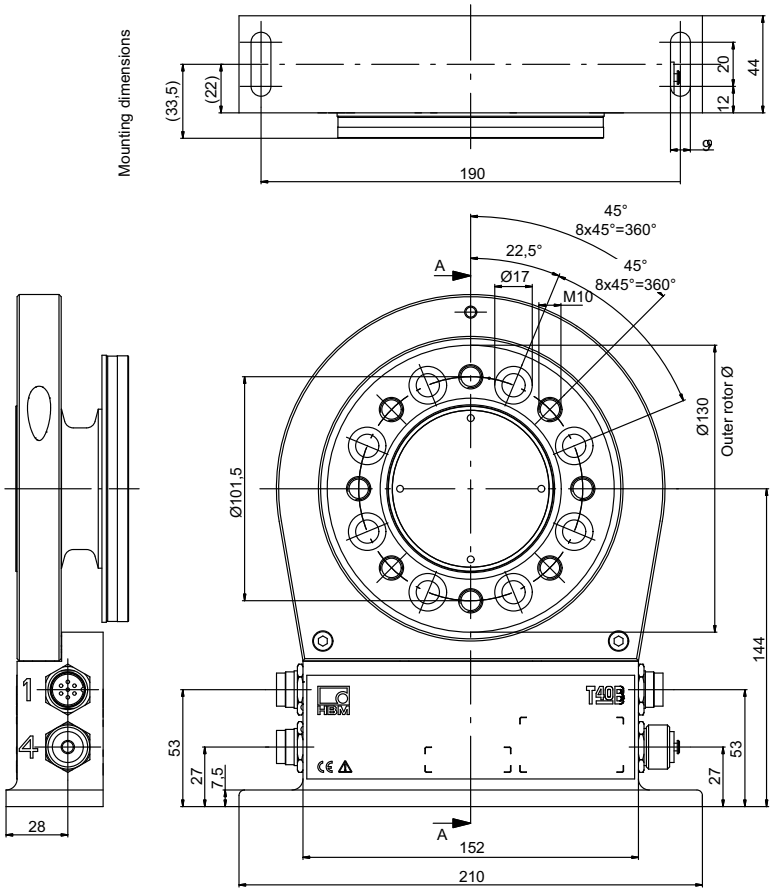

Dimensions of T40B 500 Nm - 1 kNm without rotational speed measurement, continued

Dimensions in mm (1 mm = 0.03937 inches)

Dimensions without tolerances, per DIN ISO 2768-mk

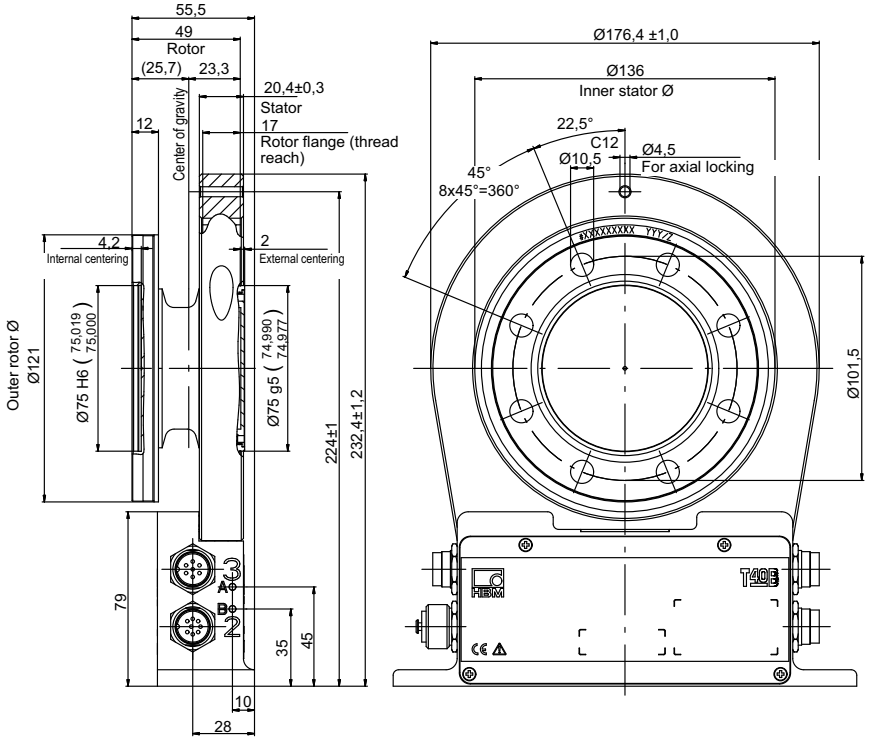

Partial sections cut A-A